NASA CR-135024
FR-7436

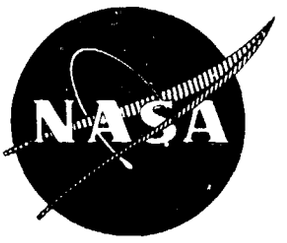

EFFECT OF SWIRLING FLOW ON AUGMENTOR PERFORMANCE

PHASE II

FINAL REPORT

By
T. R. Clements

PRATT & WHITNEY AIRCRAFT GROUP
GOVERMENT PRODUCTS DIVISION

Prepared For
NATIONAL AERONAUTICS AND SPACE ADMINISTRATION

NASA Lewis Research Center
Contract NAS3-19413

1 Report No	2 Government Accession No	3. Recipient's Catalog No
CR-135024		

4 Title and Subtitle	5 Report Date
EFFECT OF SWIRLING FLOW ON AUGMENTOR PERFORMANCE - PHASE II	June 1976
	6. Performing Organization Code
7. Author(s) T. R. Clements Approved: J. H. Shadowen	8. Performing Organization Report No FR-7436
	10. Work Unit No.
9. Performing Organization Name and Address Pratt & Whitney Aircraft Group United Technologies Corporation Government Products Division West Palm Beach, Florida 33402	11. Contract or Grant No NAS3-19413
	13. Type of Report and Period Covered Contractor December 1974 - December 1975
12 Sponsoring Agency Name and Address National Aeronautics and Space Administration Washington, D. C. 20546	14 Sponsoring Agency Code

15. Supplementary Notes

Project Manager; A. J. Juhasz, Air Breathing Engines Division,
NASA-Lewis Research Center, Cleveland, Ohio

16. Abstract

A test program has been conducted with an augmentor that employed swirling flow as a means of promoting rapid flame propagation. The program measured the trajectory and dispersion of JP-5-type kerosene sprayed into a strongly swirling flowfield. Using the data obtained, a set of sprayrings was designed and evaluated in the augmentor at conditions simulating those typical of augmented turbojet engines. At the inlet test temperature of 649°C (1200°F) the swirling flowfield nad no effect on the radial position of the fuel spray. The augmentor demonstrated combustion efficiencies greater than 95% over most of the operating range, which extended from an equivalence ratio of 0.2 to over 1.0.

17. Key Words (Suggested by Author(s))	18. Distribution Statement
Augmentor, Swirl, Swirling Flow, Afterburner, Turbojet, Exhaust Emissions, Combustion Efficiency, Pressure Loss, Exhaust Air Angle	Unclassified - Unlimited

19. Security Classif. (of this report)	20. Security Classif. (of this page)	21. No. of Pages	22 Price
Unclassified	Unclassified	77	

*For sale by the National Technical Information Service, Springfield, Virginia 22151

CONTENTS

CONTENTS (Continued)

ILLUSTRATIONS

ILLUSTRATIONS (Continued)

ILLUSTRATIONS (Continued)

SUMMARY

A test program has been conducted with an experimental augmentor that employed swirling flow to promote rapid flame propagation. The program included measurement of the trajectory and dispersion of JP-5-type kerosene injected into a strongly swirling flowfield. Based on the results of these tests, a set of fuel injectors was designed and fabricated. Using these fuel injectors, the performance of the augmentor was determined by hot testing over a wide range of equivalence ratios.

The trajectory and dispersion of the fuel sprays were determined through an enthalpy balance based on the measured drop in air temperature brought about by fuel evaporation. Temperature traverses were made at four axial positions downstream of the fuel injection plane, using a multipoint probe. Traverses were made with four different injector fuel flows, as well as an isothermal baseline at each of the four axial positions. The test temperature was nominally 649°C (1200°F), and the pressure was near ambient. Tests were conducted with fuel injectors installed at four radial locations. Results showed the swirling flowfield had no effect on the radial trajectory of the fuel spray. This was due to the rapid evaporation of the fuel at the high test temperatures. The evaporation of the fuel reduced the density difference between the fuel and air such that the centrifugal forces were not able to separate them. Circumferentially, the fuel was displaced in accordance with the swirl angle.

A concentric sprayring-type fuel injector design was selected on the basis of these results. The main criterion for the location and diameter of each sprayring design was the requirement of a reasonably uniform fuel distribution across the augmentor flamefront.

Using these sprayrings, hot tests were conducted at a nominal inlet temperature of 649°C (1200°F) and at a 2-atmosphere pressure level. Two combustion cases were used, giving augmentor length-to-diameter ratios (L/D) of 0.87 and 1.37. With the longer case (L/D = 1.37), combustion efficiency was greater than 95% over most of the operating range, which extended from an equivalence ratio of 0.2 to over 1.0. The combustion efficiency obtained with the shorter case (L/D = 0.87) was lower but was above 80% at all equivalence ratios.

Air angle measurements were made during the fuel dispersion tests at three locations downstream of the fuel injection plane. The data show the air angle to be equal to the vane angle except near the outer wall and the rig centerline.

To initiate and maintain combustion, a swirling flow augmentor has an annular pilot burner surrounding the outer wall of the combustion zone. Lean blowout of the augmentor is defined by the lean blowout of the pilot. As long as the pilot is operating, the augmentor can be ignited. The lean blowout of the pilot, and hence the augmentor, was found to occur at an augmentor fuel-air ratio of 0.0018.

INTRODUCTION

The work described herein is the second phase of an effort undertaken by the NASA Lewis Research Center and the Pratt & Whitney Aircraft Florida Research and Development Center (FRDC) to determine the effects of swirling flow on augmentor performance. It has been demonstrated that swirling flow enhances the combustion process by greatly increasing the flame speed. The mechanism by which this is accomplished is the buoyancy of the hot burned gases relative to the cold unreacted gases. In a strongly swirling flowfield, the hot gases will accelerate toward the centerline of swirl and the cold gases toward the outer wall due to the centrifugal forces created by the flowfield. In such an augmentor, combustion is initiated at the outer wall by a suitable pilot burner. The flame then rapidly spreads toward the rig centerline until combustion is complete. Data obtained in a combustion centrifuge (Reference 1) show that the flame propagation velocity in a strongly swirling flowfield can be as high as three times the normal turbulent flame velocity. This high rate of flame spreading can be utilized to increase the combustion efficiency of augmentors and/or to reduce the augmentor length without sacrificing efficiency.

Since the flame is stabilized by the pilot burner and the flame propagation rate is much faster than normal, the swirling flow augmentor requires no additional flame stabilizing devices, such as "vee gutter" type flameholders. This makes possible considerable reduction in augmentor total pressure losses.

An earlier program (Reference 2) demonstrated the ability of the swirling flow augmentor to provide near 100% combustion efficiency in a short length (augmentor L/D = 1.37), with pressure losses typical of current augmentors. However, sufficient data were not generated for the confident design of future swirling flow augmentors. Of immediate interest is information describing the behavior of JP-type fuels injected into the swirling flowfield. An obvious question is, do the strong centrifugal forces created in the swirling flowfield sling the fuel out to the outer wall, and if so, how are the sprayrings to be designed to compensate for this?

The current program was designed to obtain data on the dispersion and trajectory of JP-5-type kerosene injected into a swirling flowfield. Using the data thus obtained, a set of sprayrings were designed and their performance demonstrated during hot tests of the augmentor rig. The fuel dispersion tests and the sprayring demonstration tests were conducted at a nominal inlet temperature of 649°C (1200°F). The fuel dispersion tests were run at a 1-atmosphere pressure and the sprayring demonstration tests at a 2-atmosphere pressure.

TEST FACILITY

The augmentor was tested at the FRDC B-2 component test complex. The complex consists of several test pads, a control room, an air supply, and associated systems normally required for testing primary burners, augmentors, and ramburners.

Air Flow System

Test air was bled from the compressor of a J75 turbojet engine and delivered to the rig, as shown in figure 1. The system can deliver 12.7 Kg/sec (28 lb_m/sec) airflow at pressures up to 5.516 x 10^5 N/m^2 (80 psia). Air temperatures of approximately 288°C (550°F) can be obtained at the augmentor inlet without preburning.

Preheater

The facility was equipped with an in-line preheater to raise the augmentor inlet air temperature from the J75 compressor bleed value of about 260°C (500°F) to the 649°C (1200°F) test condition of the contract. To obtain the required temperature rise the preheater was normally operated at a fuel-air ratio of 0.0114. The preheater was a single can from a can-annular turbojet combustion system. The can was 30.5 cm (12.0 in.) in diameter and was equipped with a 10.2 cm (4 in.) centerbody so that the primary zone was actually an annulus. Fuel (JP-5) was supplied to the preheater through six dual orifice fuel nozzles which were equipped with an air swirler to provide flame stabilization. The can was modified to provide good combustion efficiency at the low temperature rises required by the test program by altering the flow area and hole pattern. The temperature rise across the combustor was only 371°C (700°F) since the preheater inlet temperature was approximately 260°C (500°F). To maintain a primary zone equivalence ratio of at least 0.8 for good flame stabilization, the hole pattern was altered to bypass most of the airflow to the dilution holes. Also, the combustor open area was increased from 290 cm^2 (45 $in.^2$) to 613 cm^2 (95 $in.^2$) to keep the pressure losses from becoming excessive. These changes, however, resulted in a very center-peaked temperature profile. This was corrected by installing a multi-hole mixer in the ducting downstream of the combustor. The preheater was ignited by injecting a pyrophoric fluid, triethylborane.

Fuel Flow System

The facility was equipped with three high-pressure fuel zones. Each zone was capable of supplying 1225 Kg/hr (2700 lb_m/hr) of JP-5 type fuel at pressures up to 6.895x10^6 N/m^2 gage (1000 psig). The augmentor fuel zones - preheater, pilot, and the sprayrings - were connected to the facility fuel system as shown in figure 2. The preheater and pilot fuel zones were on one of the facility fuel zones exclusively. The augmentor sprayrings were then connected to the remaining two facility fuel zones. The crossover line connecting the two facility fuel pumps supplying the augmentor sprayrings was provided so that fuel flows in excess of the capability of either pump could be tested.

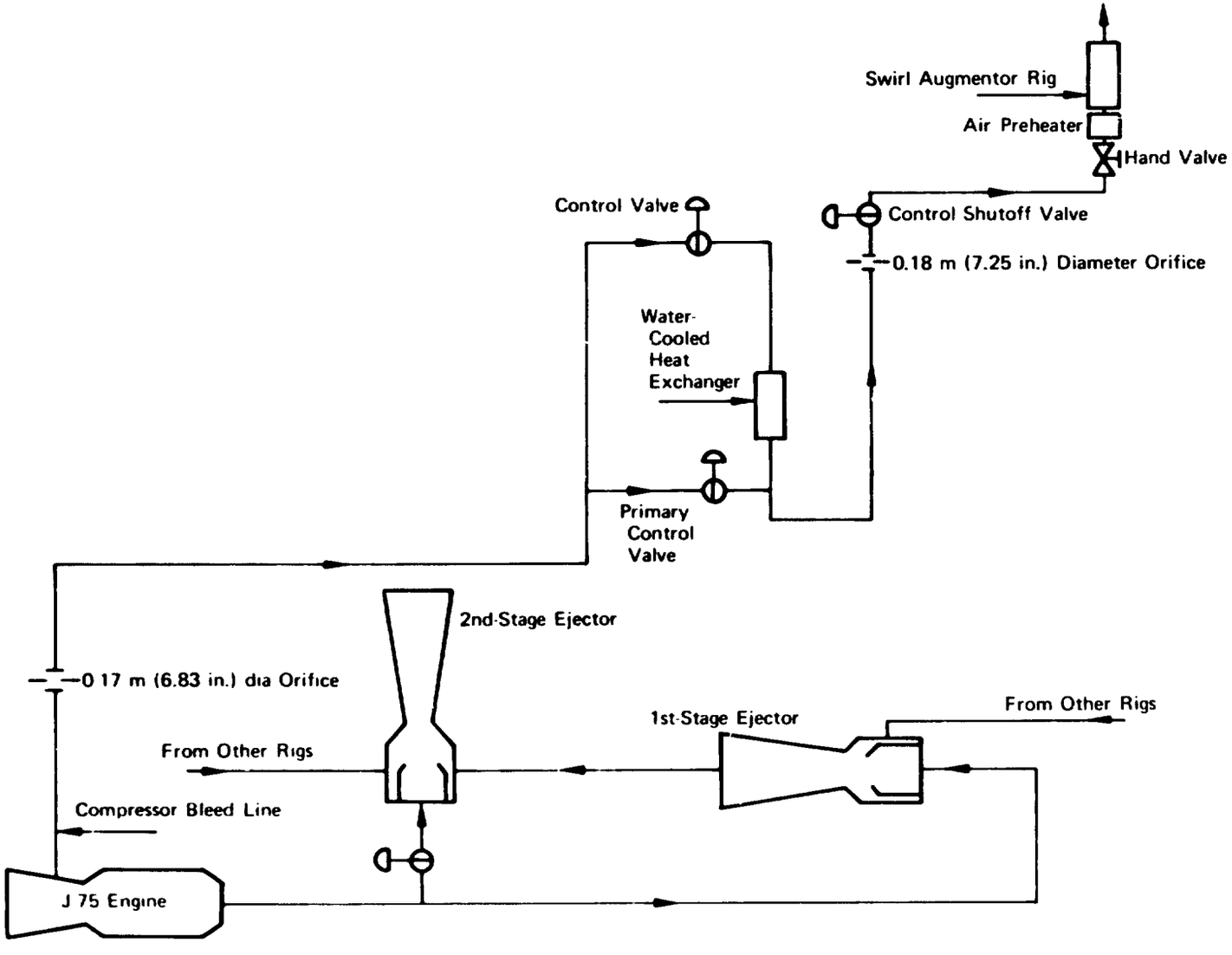

Figure 1. Test Facility Air Supply Schematic

CD 95577

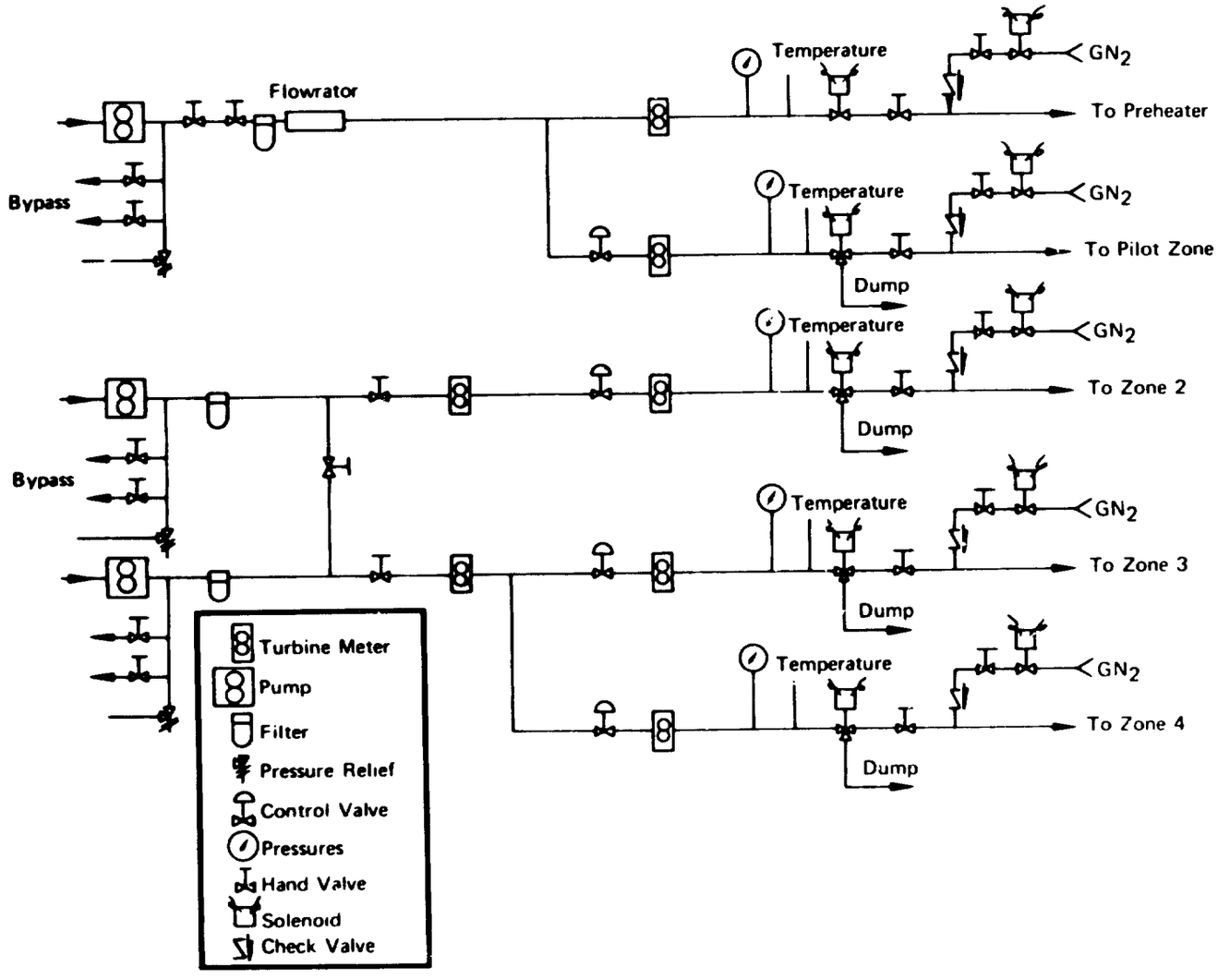

Figure 2. Schematic of Test Facility Fuel System

FD 97542

Facility Instrumentation

Serving the test stand was a 100-channel digital recorder capable of recording at a maximum sampling rate of 6666 samples per second. Data were recorded on magnetic tape that is directly compatible with a high-speed digital computer. Also provided were 10 channels of strip chart recorders for real-time test monitoring and a 36-channel oscillograph for higher frequency data recording.

AUGMENTOR DESIGN FEATURES

The experimental augmentor used in this program is shown in figure 3. The rig was configured to simulate the conditions typical of augmented turbojets. Consequently, all of the tests, both the fuel dispersion and performance demonstration tests, were conducted at or near 649°C (1200°F) inlet total temperature. The rig was nominally 0.381 meters (15 inches) in diameter. This size was selected to be compatible with the test facility airflow and pressure capabilities.

To simulate the close proximity of the turbine and its resistance to slight downstream pressure perturbations, the turbine simulator vane assembly shown in figures 3 and 4 was used. This rig section was equipped with 21 accelerating and diffusing vanes designed to simulate the pressure drop characteristics of a turbine. The vanes were sized to accelerate the flow to a Mach number of approximately 0.8. The flow was then gradually diffused over the rear portion of the vanes to minimize distortion and total pressure loss.

To create the strongly swirling flowfield essential to the concept, the swirl vane assembly shown in figure 5 was used. The vanes had a nominal turning angle of 0.61 radians (35 degrees). The swirl intensity created by these vanes was approximately 67^0 times the standard acceleration due to gravity at the pilot when operating at a vane inlet Mach number of 0.250. The turning vanes were a simple curved sheet metal design to minimize cost.

An annular pilot burner (figure 3) functioned as the ignition source for the mainstream flow as well as the flame stabilization device. Since the flame spreads radially in toward the augmentor centerline, the pilot passage was designed to surround the swirling flow combustion chamber. The pilot burner was constructed along the lines of a primary combustor. Fuel was injected through 20 air-blast-type fuel nozzles equally spaced around the circumference. To stabilize the flame, air swirlers at each fuel nozzle were employed. The pilot fuel nozzles and swirlers were designed to flow approximately 4.5% of the total augmentor flow.

The rig was provided with two water-cooled combustor cases of differing length. This allowed the effect of length-to-diameter ratio (L/D) on performance to be evaluated. The two cases provided L/D's of 0.87 and 1.37.

To minimize the cost of the rig, a fixed-area convergent nozzle was utilized. The exit diameter was 27.2 cm (10.69 inches). As with the combustor cases, the nozzle was water cooled.

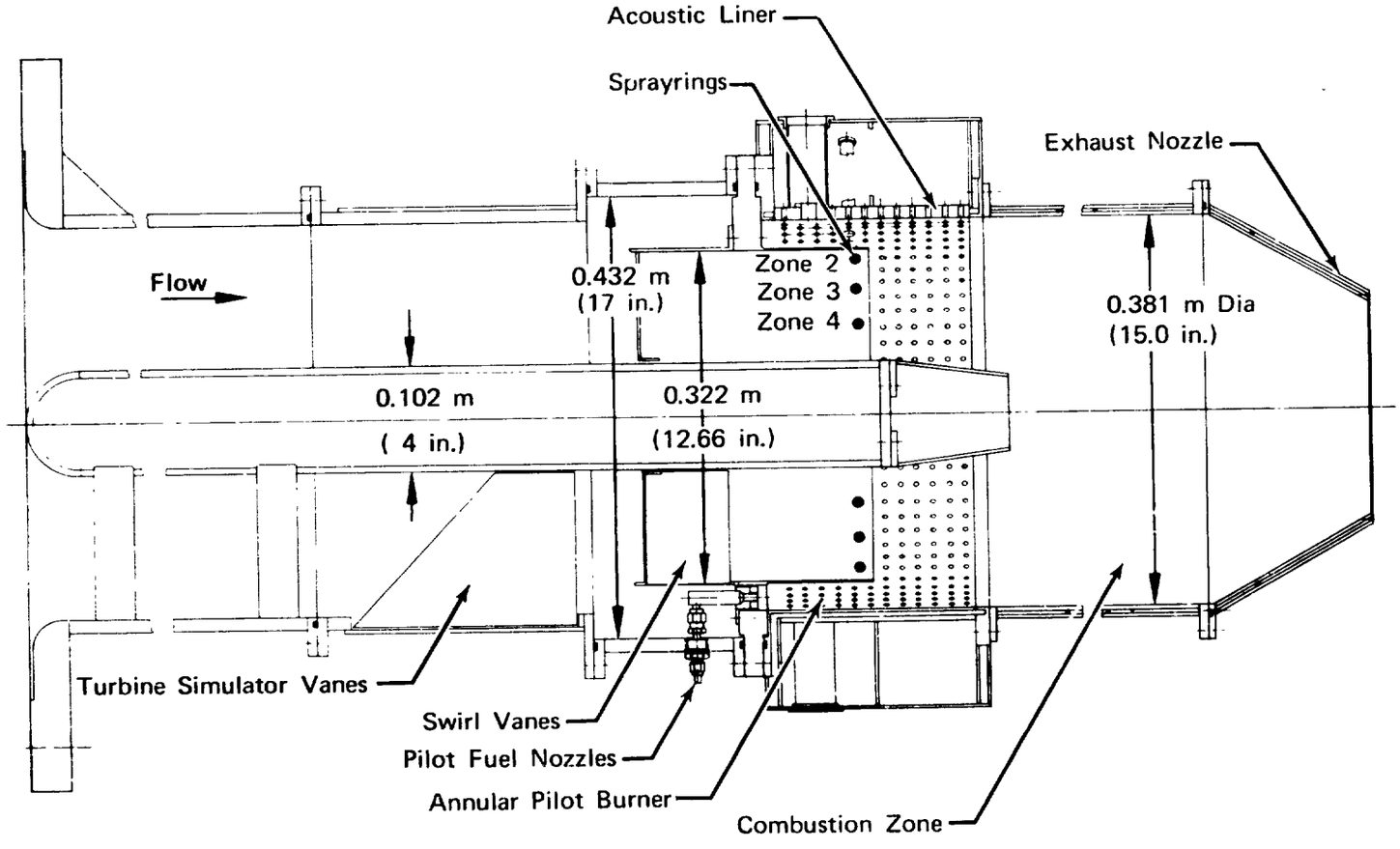

Figure 3. Swirl Augmentor Rig

FD 95566

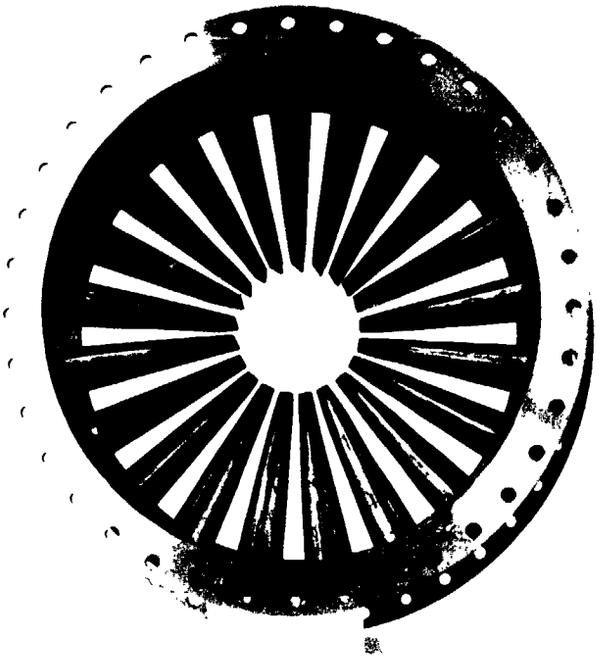

Figure 4. Turbine Simulator Case Assembly FE 124160

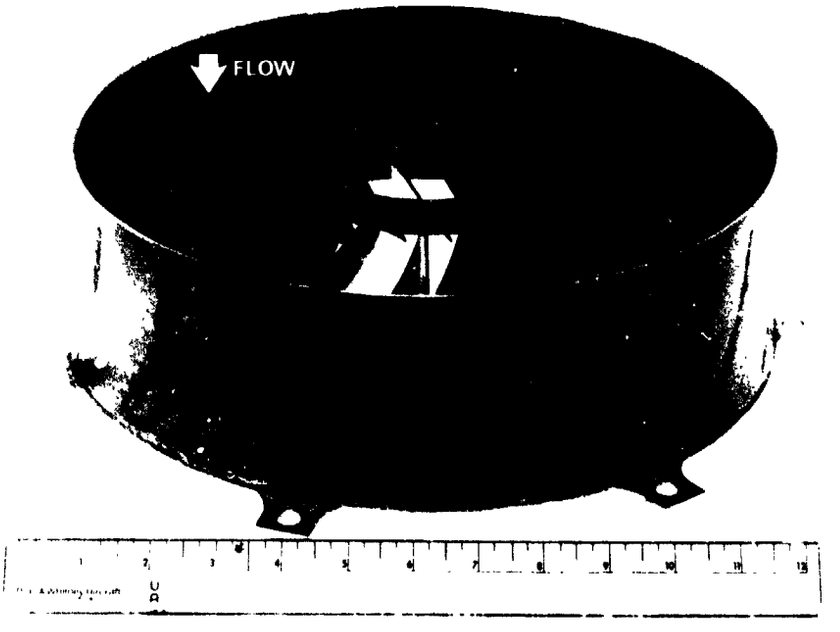

Figure 5. 35-deg Swirl Vane Assembly FE 124159

The augmentor was equipped with an acoustic liner, as shown in figure 3. During preliminary testing prior to the award of this contract, combustion instability in the frequency range of 500 to 1000 Hz was obtained when operating on the pilot burner only. Consequently, the acoustic liner was designed to primarily cover the pilot zone. The liner was not designed as a "flight-type" liner as this was outside the scope of the experimental work for which the rig was designed. The liner was tuned for maximum absorption at a frequency of 500 Hz. The absorption coefficient, which is the measure by which an incident pressure pulse in the frequency range of interest is attenuated, was approximately 0.6. The liner open area and backing distance were 142 cm^2 (22 $in.^2$) and 8.57 cm (3.83 in.), respectively.

The augmentor was equipped with three concentric sprayrings for admitting fuel to the combustion zone. In designing these rings the effect of a swirling flowfield on the dispersion and trajectory of fuel sprays had to be determined. For this reason, the fuel dispersion tests were conducted.

FUEL DISPERSION TEST HARDWARE DESIGN

A set of four single-point, drilled-orifice fuel injectors was designed for use during the fuel dispersion tests. Single-point injectors were used to isolate the effects of the swirling flowfield on the spray. These injectors were located at various radii from the augmentor centerline because the centrifugal loads imposed on the spray vary with radial distance from the centerline. The radial locations were 8.3, 10.7, 13.1, and 15.2 centimeters (3.25, 4.20, 5.15, and 5.96 inches). A typical sprayring element design is shown in figure 6. The deflector tab located just downstream of the orifice acts to break up the spray, thus aiding fuel atomization. Due to the high inlet air temperature (649°C) and the relatively low fuel flows (3.6 to 18.1 Kg/hr), the element design was directed toward preventing the thermal decomposition of the fuel inside the sprayring. To do this, a large amount of fuel in excess of that injected into the augmentor was passed through the element. The high fuel flowrate prevented the fuel from reaching the temperature where decomposition could occur. Fuel was supplied through one leg of the element, with the excess fuel passing out the other leg to a catch tank.

The amount of fuel injected into the augmentor was controlled by setting the fuel pressure at the injection orifice. Thus, by using calibration curves of fuel flow vs fuel pressure for each sprayring element, the fuel flowrate could be determined.

The sprayring elements were installed in the rig as shown in figure 7. Two of the four test elements were installed for each test. They were located 3.14 radians (180 degrees) apart to ensure no overlapping of the sprays.

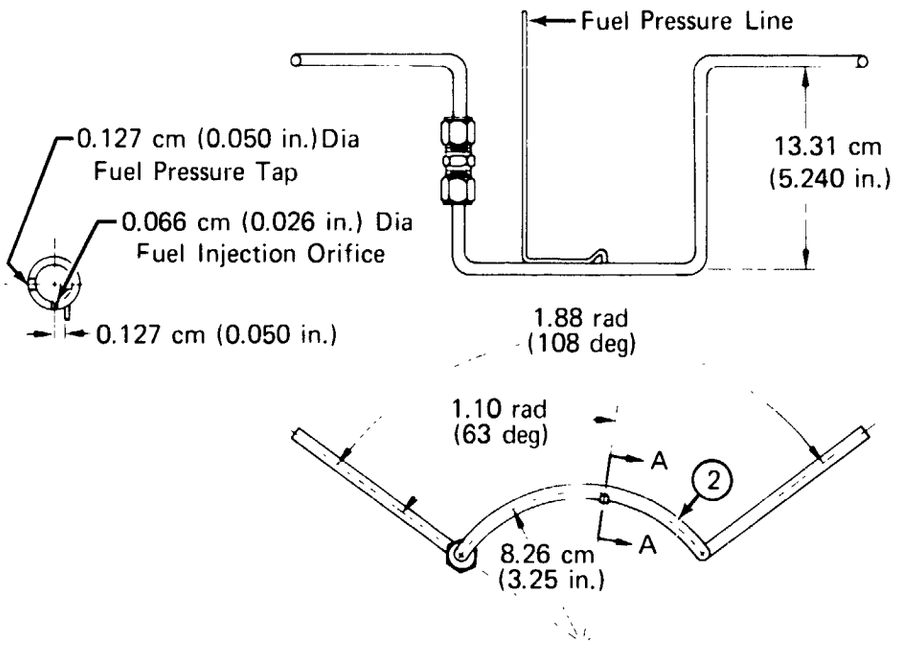

Figure 6. Typical Design of Single-Point FD 95567

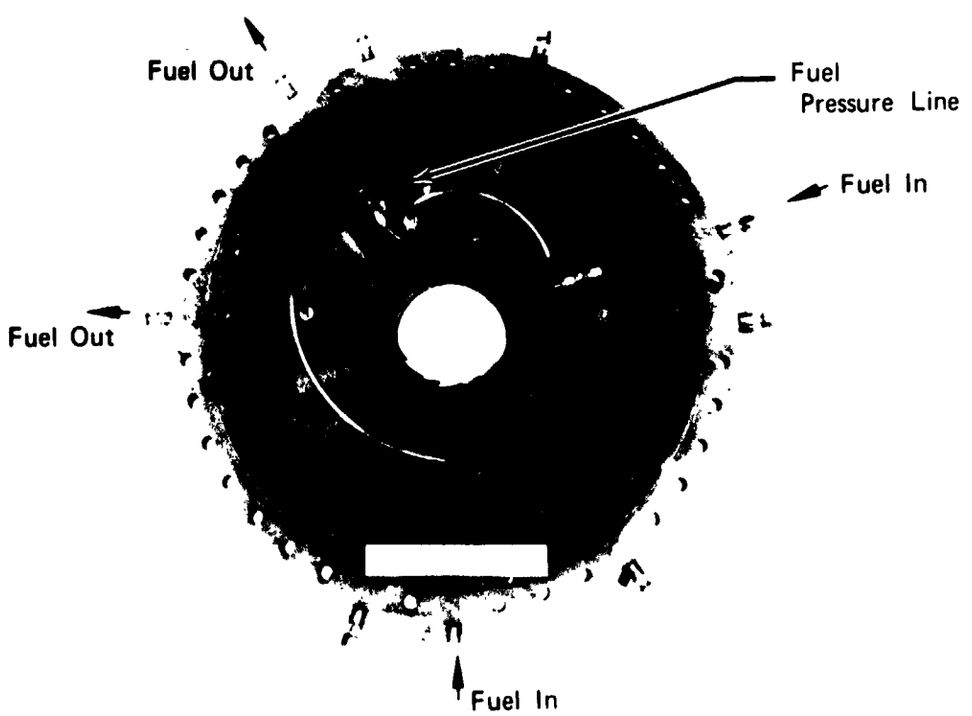

Figure 7. Typical Installation of Sprayring Element FAE 144900A

AUGMENTOR SPRAYRING DESIGN

The sprayrings used in the performance demonstration tests were designed using the results of the fuel dispersion data obtained with the sprayring elements described above. In designing the sprayrings it was desired to locate them radially and axially to provide a reasonably uniform fuel-air mixture at the flamefront. In order to do this, the flamefront location had to be determined. By analyzing the flame propagation as the buoyant motion of hot gas bubbles in a strong centrifugal flowfield (as described in Reference 3) the flamefront position was calculated to be that shown in figure 8.

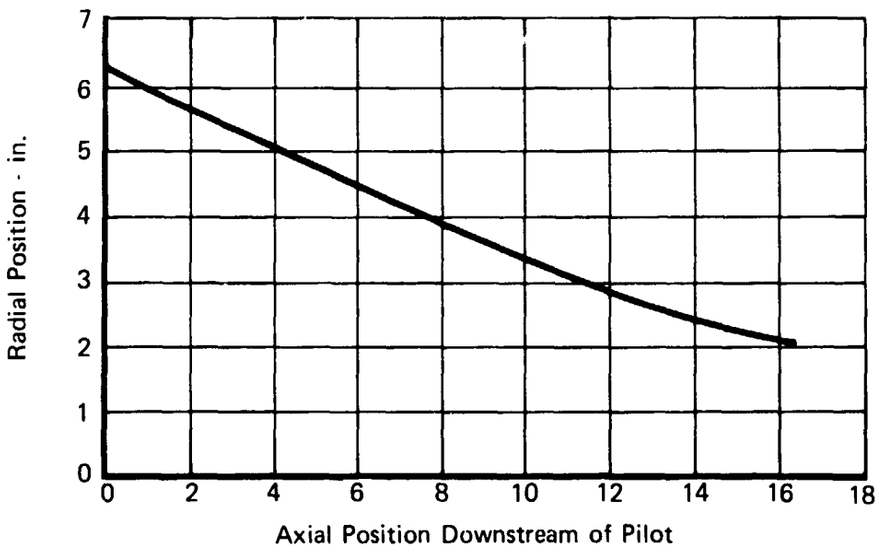

Figure 8. Flamefront Location Based on Bubble Mechanics FD 95568

Note that the flamefront is assumed to start at the inner wall of the pilot passage. Therefore, in order to provide for some mixing of the outer sprayring (zone 2) prior to ignition by the pilot, the sprayrings were located upstream of the pilot discharge. The location was somewhat arbitrary in that it was not considered prudent to locate the sprayrings too close to the swirl generating vanes. Vane wakes could entrap the fuel, resulting in flameholding off of the vanes. Consequently, the sprayrings were located 3.8 cm (1.5 inches) upstream of the pilot.

In designing the sprayrings, consideration was given to several factors. First, the effect of the centrifugal flowfield on the radial movement of the spray had to be determined. Any radial movement of the fuel spray due to the centrifugal flowfield would have to be allowed for in the design of the sprayrings. Second, the degree of spreading in the spray pattern by the time it reaches the flamefront had to be determined. The degree of spray pattern spreading fixes the flow area to be fed by each zone as well as the number and flowrate of the orifices in each zone. Third, the penetration of the fuel spray into the airstream due to fuel jet momentum had to be determined. This factor also affects

the radial location of the sprayrings. The analysis of the fuel dispersion data, to be discussed later, showed that the centrifugal flowfield had no effect on the radial position of the spray. Therefore, the sprayring design was reduced to the consideration of the second and third factors discussed above, fuel spray spreading and fuel spray momentum.

The design of the zone 2 sprayring, which is the outermost sprayring, is discussed in detail; the remaining sprayrings (zones 3 and 4) were designed in a similar manner. The fuel dispersion data show that, at an axial position of 3.8 cm (1.5 inches) downstream of the fuel injection plane, the pattern expanded to approximately 2.54 cm (1.0 inch) in diameter. As mentioned above, the sprayrings were located at that same distance upstream of the pilot discharge, which is the starting location of the flamefront. Therefore, the zone 2 sprayring was considered to supply the annular area between 16.1 and 13.3 cm (6.33 and 5.25 inches) radii.

The fuel dispersion data also showed that the spray pattern spread to approximately the same diameter at any given axial position, regardless of the fuel flowrate. This result requires that for the zone 2 sprayring, the individual orifice fuel flows must be kept low to prevent excessively peaked radial fuel-air ratio distributions. For the two inner fuel zones, zones 3 and 4, the individual orifice flows can be increased without seriously affecting the radial fuel-air distribution, since the flamefront is located further downstream. Consequently, the zone 2 sprayring individual orifice fuel flow was set at 4.35 Kg/hr (9.6 pph). This was done because by the time the spray, at that flow, reached the flamefront it had decayed to a fairly uniform fuel-air ratio distribution of 0.02. The number of orifices in the sprayring was calculated by requiring that an overall equivalence ratio of 1.0 exist in the area fed by the zone 2 sprayring. This resulted in 150 orifices in the zone 2 sprayring. By overlapping the appropriate fuel-air distributions obtained during the fuel dispersion tests for each orifice, the total sprayring distribution was determined. This procedure is shown in figure 9.

The zone 3 and zone 4 sprayrings were designed in a similar manner. The individual orifice fuel flows selected were 15.1 and 20.00 Kg/hr (33.9 and 44.1 pph) for the zone 3 and zone 4 sprayrings, respectively. For those sprayrings, the number of fuel injection orifices required to obtain an equivalence ratio of 1.0 was 50 and 25, respectively. As with the zone 2 sprayring, the combined fuel-air distributions for the zone 3 and 4 sprayrings were determined by overlapping the appropriate distribution obtained from the fuel dispersion tests. These results are shown in figures 10 and 11.

By averaging these distributions circumferentially, the radial fuel-air ratio profile was calculated. This is shown in figure 12.

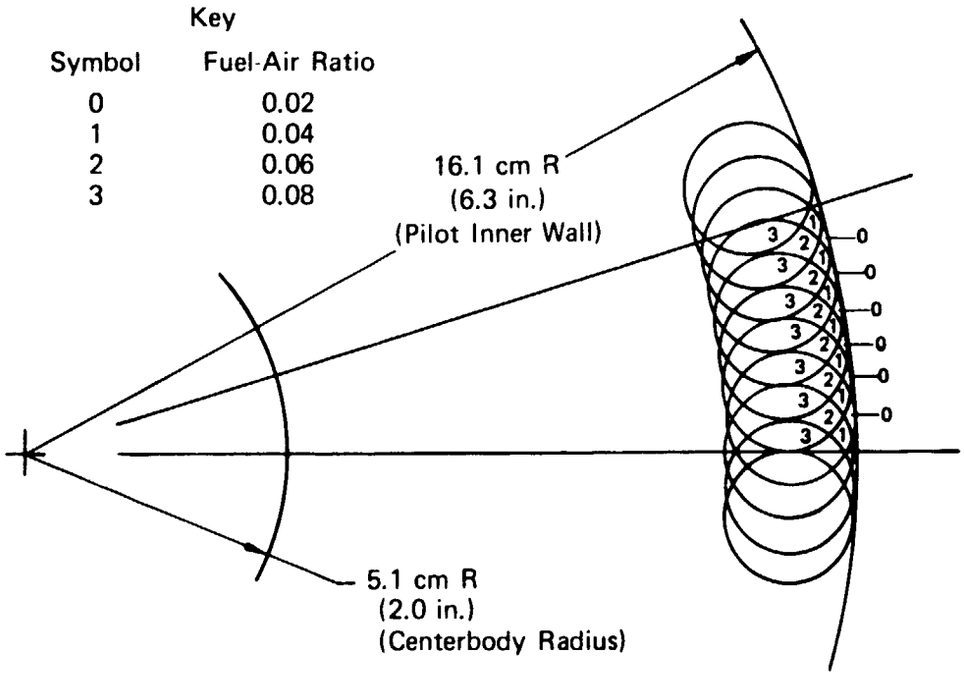

Figure 9. Fuel Distribution at the Pilot Due to Zone 2 FD 95569

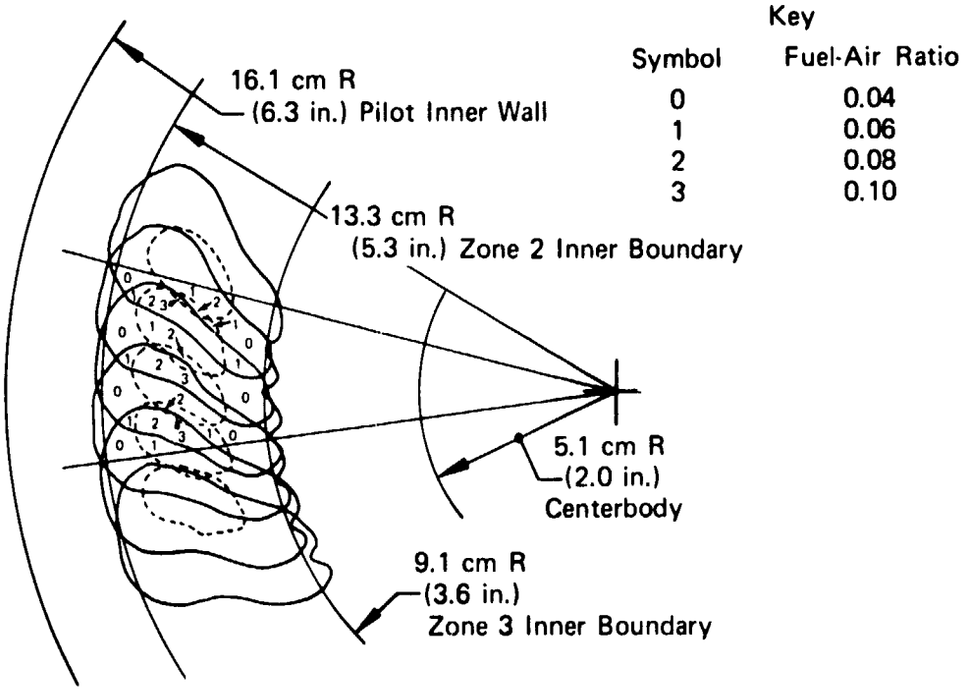

Figure 10. Fuel Distribution at Flamefront Due to Zone 3 FD 95570

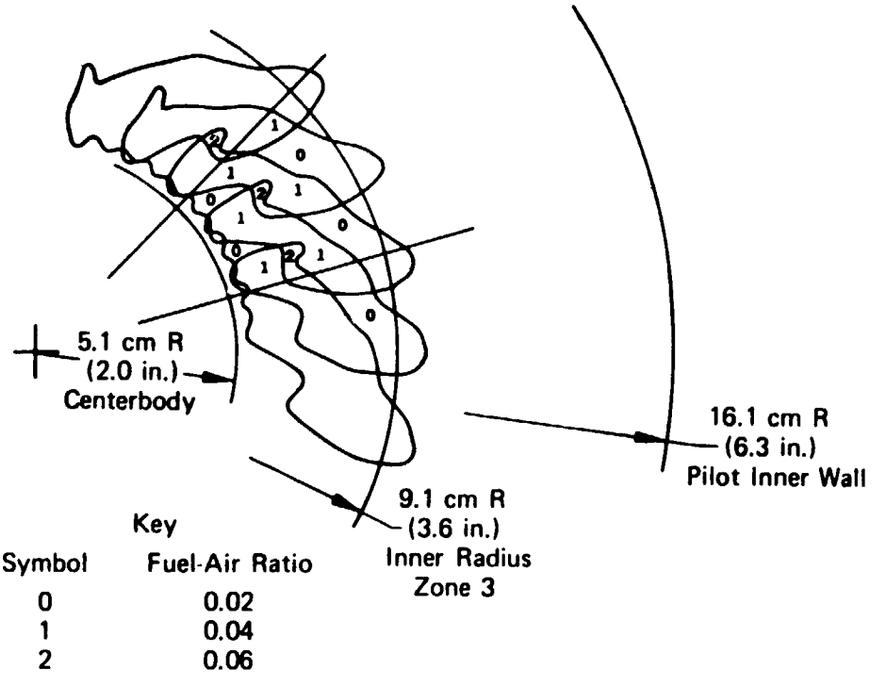

Figure 11. Fuel Distribution at Flamefront Due to Zone 4 FD 95571

The final requirement in the design was fixing the exact radial position of the sprayring by considering the momentum of the fuel spray. Fuel jet momentum causes the fuel spray to penetrate into the high velocity airstream to some distance that can be determined by considering the momentums of the air and the fuel. The fuel dispersion data indicate that, for the orifice size selected, the fuel did not penetrate into the gas stream for any of the fuel flows and pressures tested. However, alignment problems with the temperature traverse probe made it difficult to fully verify this observation. Therefore, use was made of a P&WA internal report presenting data on the penetration of fuel sprays into a moving airstream. That data, shown in figure 13, correlates the fuel jet penetration with the parameter:

$$D_H \sqrt{\frac{\text{FUEL } \Delta P}{q_{air}}}$$

where:

D_H = Hole diameter, cm

Fuel ΔP = Fuel injector orifice pressure drop, N/m^2

q_{air} = Dynamic head of the mainstream airflow, N/m^2

The data show that for values of this parameter below 0.43 the fuel jet does not penetrate.

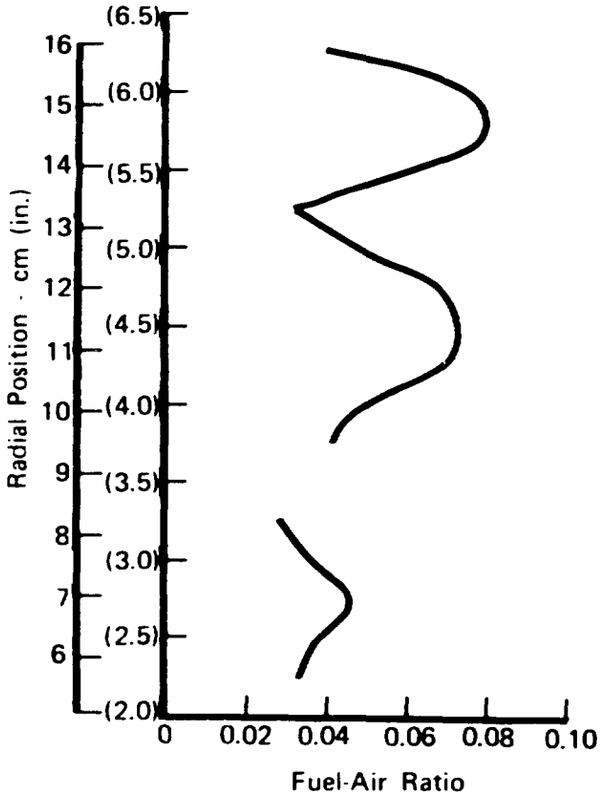

Figure 12. Predicted Radial Distribution of Fuel-Air Ratio FD 95572

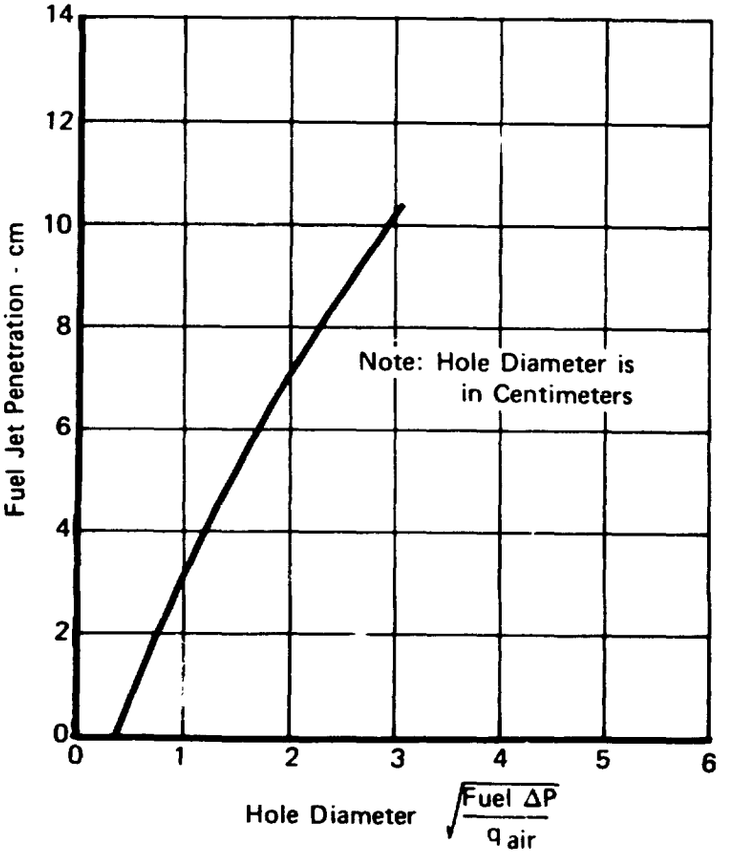

Figure 13. Penetration of a Fuel Jet Into a Cross-Flowing Airstream FD 97543

The hole diameter for all of the above sprayrings was 0.066 cm (0.026 inch). This diameter was used to ensure that fuel contaminants, as well as deposits that may be formed by fuel decomposition at the high test temperatures, would not clog the injection orifices. With this value of hole diameter in the correlating parameter, it was determined that the fuel sprays from any of the sprayrings would not penetrate. Consequently, all of the sprayrings were located at the geometric center of their respective flow areas.

Figure 14 shows the location of the sprayrings, while figure 15 shows the design details. The small deflector tabs on the zone 3 and 4 sprayrings and the deflector ring on the zone 2 sprayring aid in breaking up the fuel jets, thus, enhancing fuel atomization.

A modified zone 4 sprayring was also tested. The details of this sprayring are shown in figure 16. The diameter of this sprayring was larger than that of the baseline zone 4 sprayring described above. The fuel injection orifices were larger, 0.081 cm (0.032 inch), compared with 0.066 cm (0.026 inch) for the baseline zone 4. Also, there were 48 orifices instead of 25, and they injected fuel both radially inward and outward.

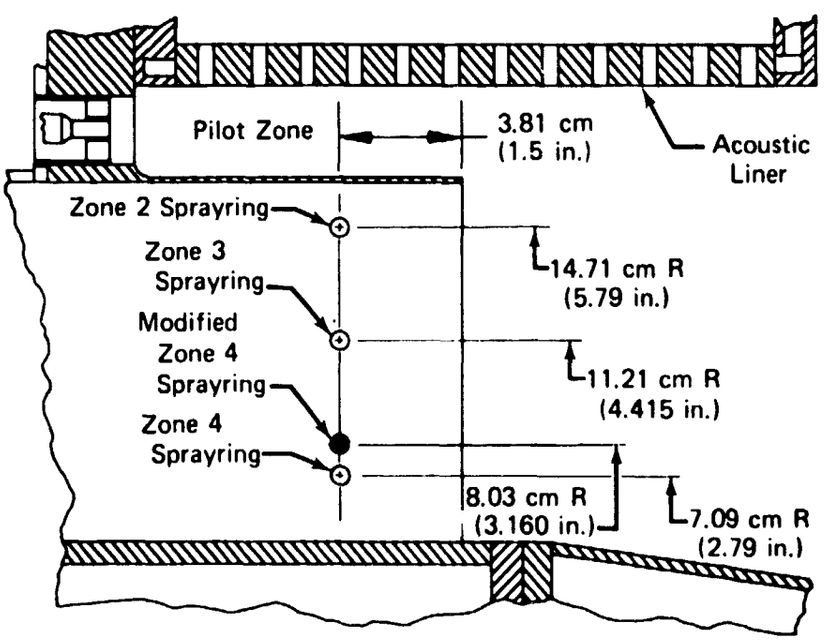

Figure 14. Location of Fuel Injection Sprayrings FD 95575

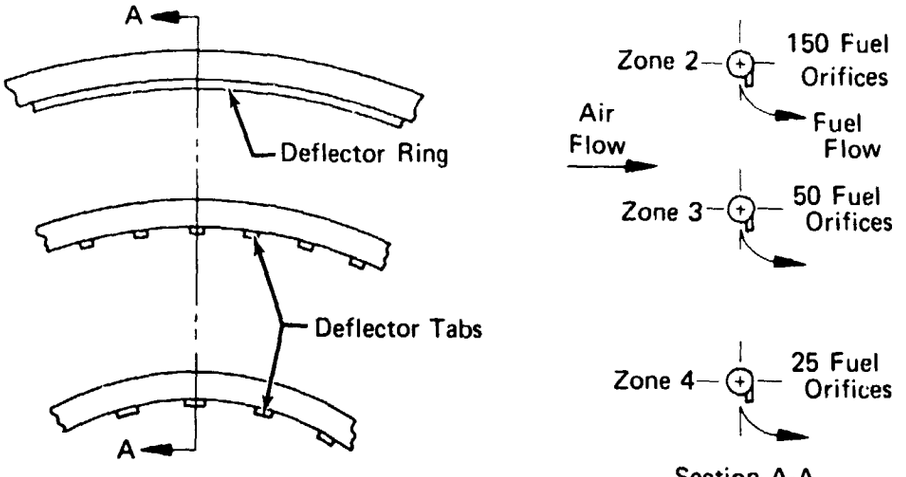

Note: Orifice Diameter = 0.066 cm (0.026 in.)
All Sprayrings

Figure 15. Fuel Sprayring Details FD 95573

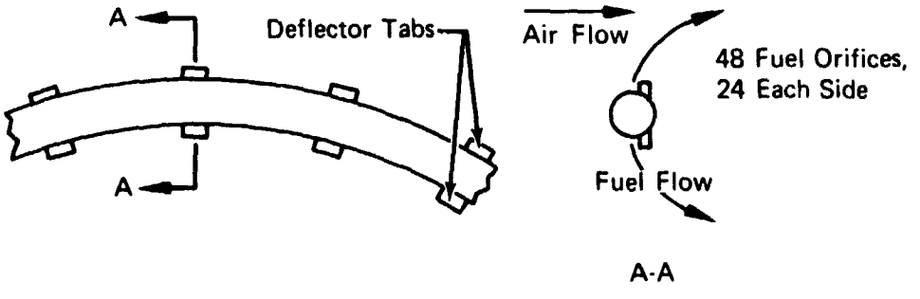

Note: Orifice Diameter = 0.081 cm (0.032 in.)

Figure 16. Details of Modified Zone 4 FD 95574

INSTRUMENTATION

The test rig was instrumented as shown in figure 17 to provide data on rig airflow, fuel flow, augmentor inlet total pressure, combustion zone static pressure, and the exhaust nozzle wall temperature. The rig cooling water flowrate and inlet and outlet temperature were measured as well. These data were used to correct the combustion efficiency for the heat rejected to the cooling water. Specialized instrumentation was used to measure the mainstream air angle, the location of the flamefront, and the emission levels of unburned hydrocarbon, carbon monoxide, and the oxides of nitrogen. The instrumentation used is briefly discussed in the following paragraphs.

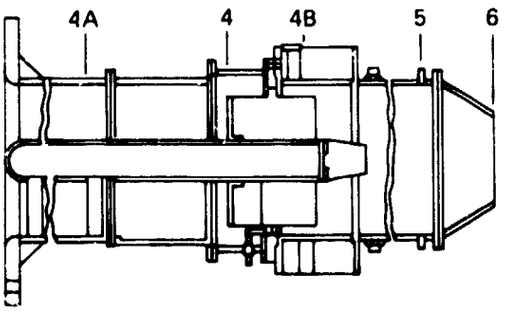

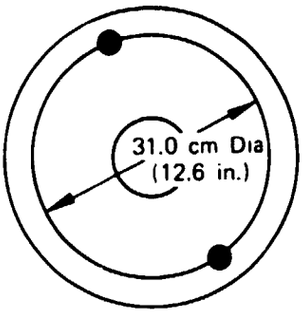

Plane 4
Swirl Vane Inlet

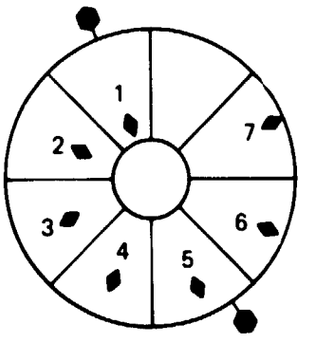

Plane 4A
Turbine Simulator
Vane Inlet

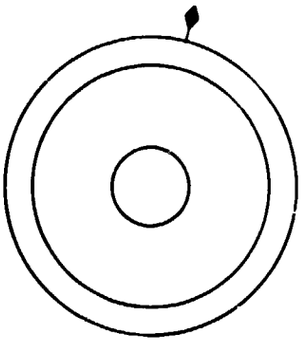

Plane 4B
Swirl Vane Discharge

Temperature Probe	Radial Position
1	7.06 cm (2.78 in.)
2	9.91 cm (3.90 in.)
3	12.09 cm (4.76 in.)
4	13.94 cm (5.49 in.)
5	15.57 cm (6.13 in.)
6	17.04 cm (6.71 in.)
7	13.42 cm (7.25 in.)

Symbol Key

- Static Pressure, Wall Tap
- Total Pressure, Kiel Head Probe
- Total Temperature, C/A T/C
- Wall Temperature, C/A T/C
- Dynamic Pressure, Kistler Probe

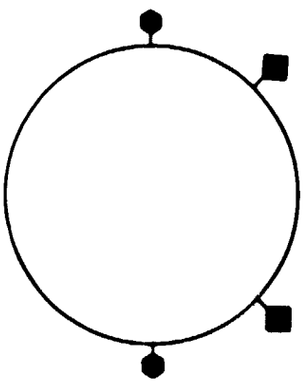

Plane 5
Nozzle Inlet

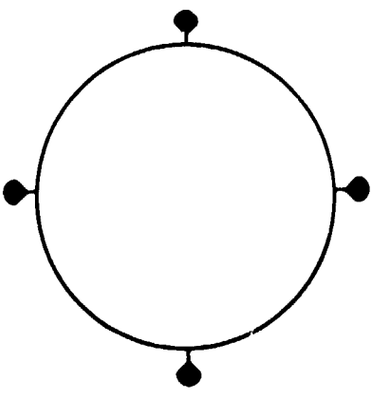

Plane 6

Figure 17. Basic Rig Instrumentation FD 95576

1. Augmentor Airflow - The airflow to the rig was measured with a 0.184 m (7.25 inch) diameter sharp-edged orifice. The orifice upstream and downstream pressures were measured with flange static pressure taps. The air temperature was measured with two chromel-alumel thermocouples located downstream of the orifice. In case the instrumentation on this orifice should fail, a backup 0.173 cm (6.83 inch) diameter orifice was available to measure rig airflow. The instrumentation on that orifice was similar to that of the primary orifice.

2. Augmentor Fuel Flow - The fuel flows to the preheater, pilot, and zones 2, 3, and 4 were measured with turbine-type flowmeters.

3. Preheater Inlet Air Temperature - This temperature was measured with two shielded chromel-alumel thermocouples.

4. Augmentor Inlet Temperature (Preheater Exit Temperature) - The augmentor inlet temperature was measured with seven chromel-alumel thermocouples for purposes of setting test conditions. However, for all performance calculations the augmentor inlet temperature was equated to the preheater inlet temperature plus the preheater ideal temperature rise calculated from airflow and fuel flow measurements.

5. Augmentor Inlet Total Pressure - The augmentor inlet total pressure was measured with two Kiel-type total pressure probes.

6. Combustion Zone Static Pressure - The static pressure in the combustion zone was measured with two wall taps located immediately upstream of the exhaust nozzle.

7. Exhaust Nozzle Total Pressure - The total pressure at the exhaust nozzle was calculated by an iterative procedure using the nozzle inlet and throat geometric areas, the augmentor mass flow, and the combustion zone static pressure at the nozzle inlet.

8. Exhaust Nozzle Wall Temperature - The wall temperature of the exhaust nozzle was measured with four chromel-alumel thermocouples located at the nozzle throat and equally spaced around the circumference. These data were used to correct the nozzle throat diameter for thermal expansion.

9. Cooling Water Flowrate - The cooling water flowrate to the rig was measured with a 0.031 m (1.225 inch) diameter sharp edged orifice located in the discharge manifold. The orifice was equipped with flange static pressure taps.

10. Cooling Water Temperature - The inlet and outlet cooling water temperatures were measured with chromel-alumel thermocouples. The inlet thermocouple was located in the supply manifold. The outlet thermocouple was located in the discharge manifold just upstream of the waterflow orifice.

11. Twenty-Point, Linear-Rotary Temperature Probe - This probe, shown in figure 18, was used to track the trajectory and dispersion of the fuel following its injection into the swirling flowfield. The probe had 20 bare wire, chromel-alumel thermocouples, with 10 thermocouples on each of two arms. The probe arms were located 3.141 radians (180-degrees) apart. The thermocouples were spaced at 1.27 cm (0.5 inch) intervals between an inner radius of 6.35 cm (2.5 inches) and an outer radius of 17.8 cm (7.5 inches).

    The probe was driven by a linear-rotary actuator that was capable of 3.246 radians (186-degrees) angular rotation and 30.5 cm (12 inches) linear travel.

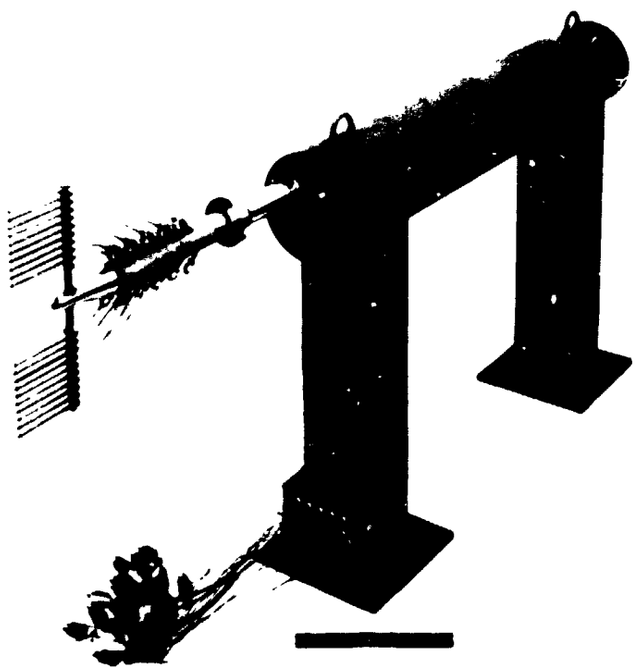

Figure 18. 20-Point, Linear-Rotary Traverse Assembly FE 144899

12. Air Angle - During the fuel dispersion tests the mainstream air angle was measured at three axial positions downstream of the sprayring elements, as shown in figure 19. The probes used to obtain these data are shown in figure 20. The probes

were 0.349-radian (20-degree) wedge-type probes. The probes had static pressure taps located on either side of the wedge. The air angle was determined by rotating the probe until the static pressures balanced. The rotation of the probes and the determination of pressure balance was controlled continuously by null balance circuitry in the traversing mechanism. Consequently, the probes could be radially traversed continuously without having to stop to ensure that pressure balance was obtained.

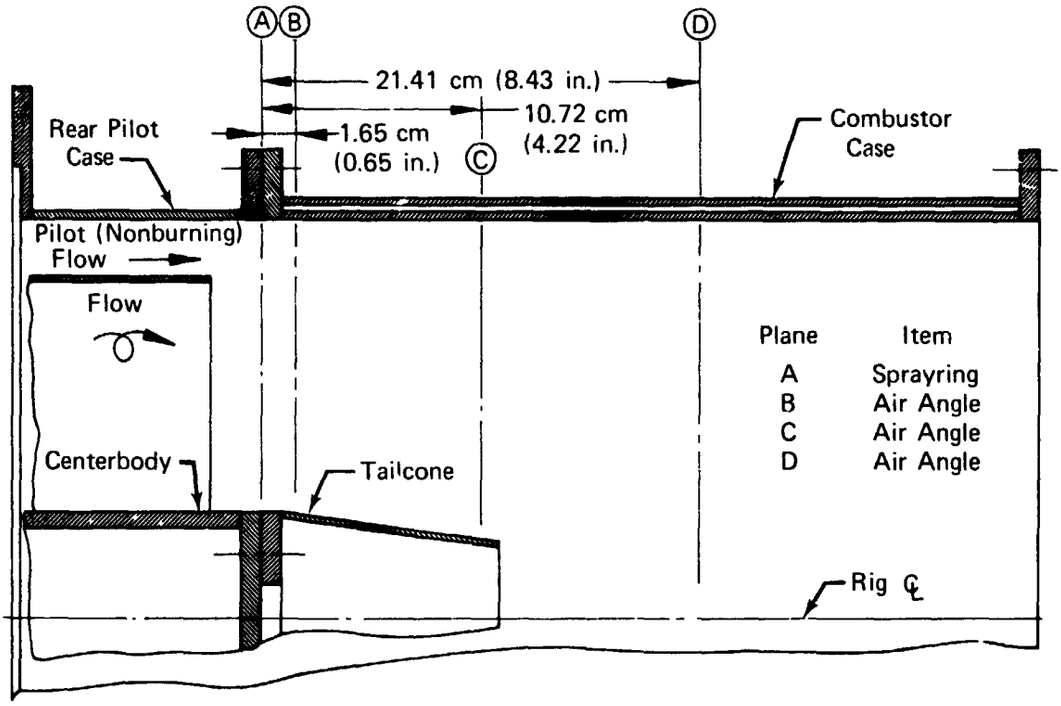

Figure 19. Location of Air Angle Probes During Fuel Dispersion Testing FD 95579

13. Flamefront Location - The location of the flamefront was to be determined by measuring the increase in ionization that occurs in the flamefront. To do this, the ionization probe shown in figure 21 was used. The probe was simply a length of 0.318 cm (0.125 inch) diameter chromel-alumel thermocouple wire surrounded by a water jacket. The lead wires of the probe were approximately 0.127 cm (0.050 inch) apart at the tip. The probe was hooked to a 10-volt power supply in series with a micro-ampere meter to measure the ionization current. The voltage drop across the micro-ampere meter was recorded on the automatic data recording system. There were two probes located on the augmentor, as shown in figure 22. Each probe was mounted on a linear actuator so that they could be traversed to the centerline of the augmentor.

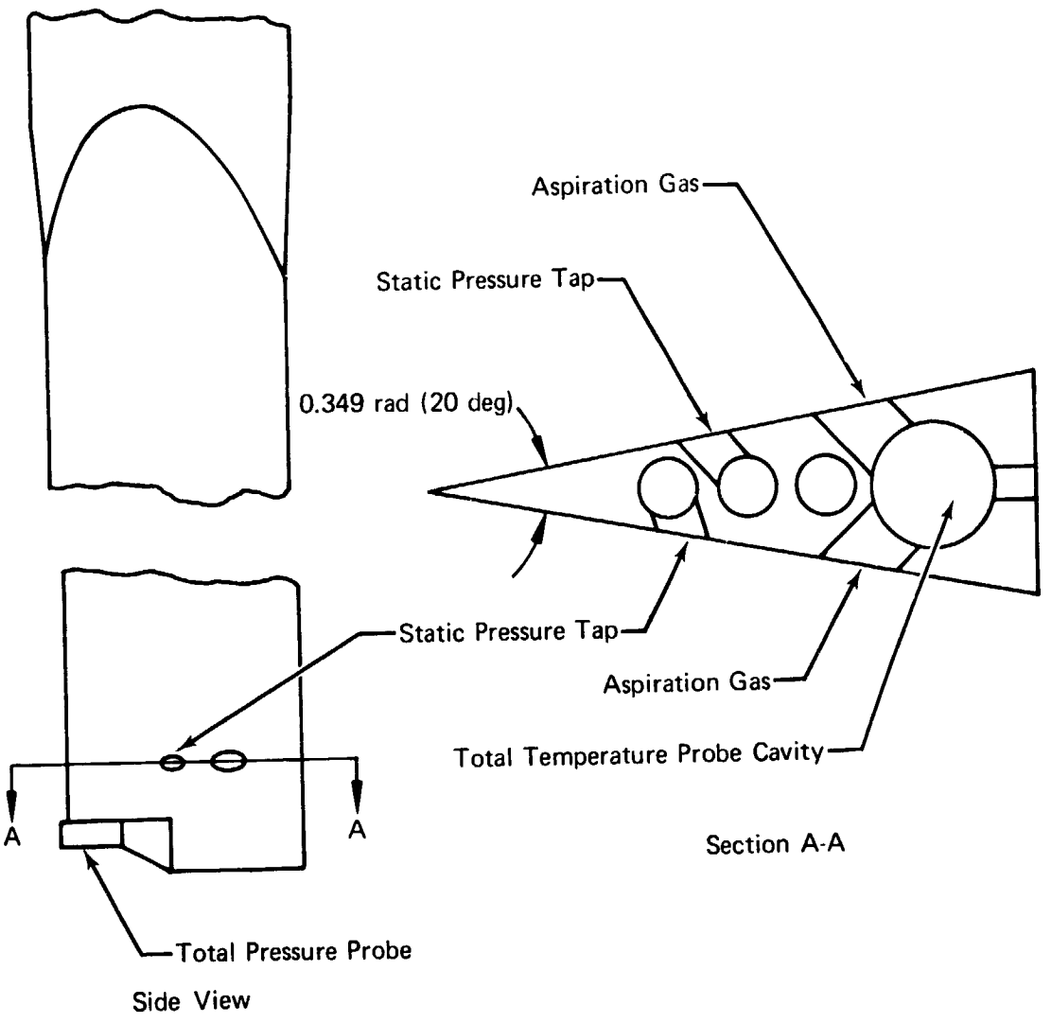

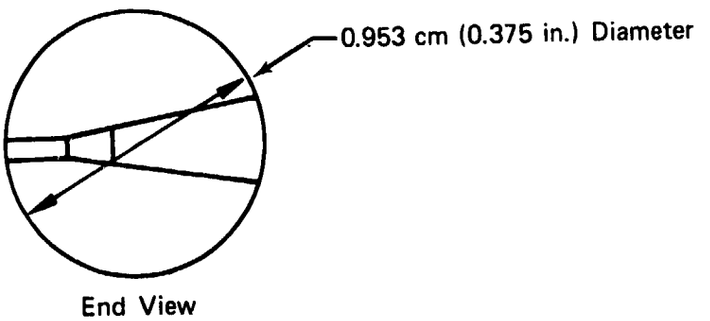

Figure 20. Air Angle Probe Used at the Swirl Vane Discharge

FD 95578

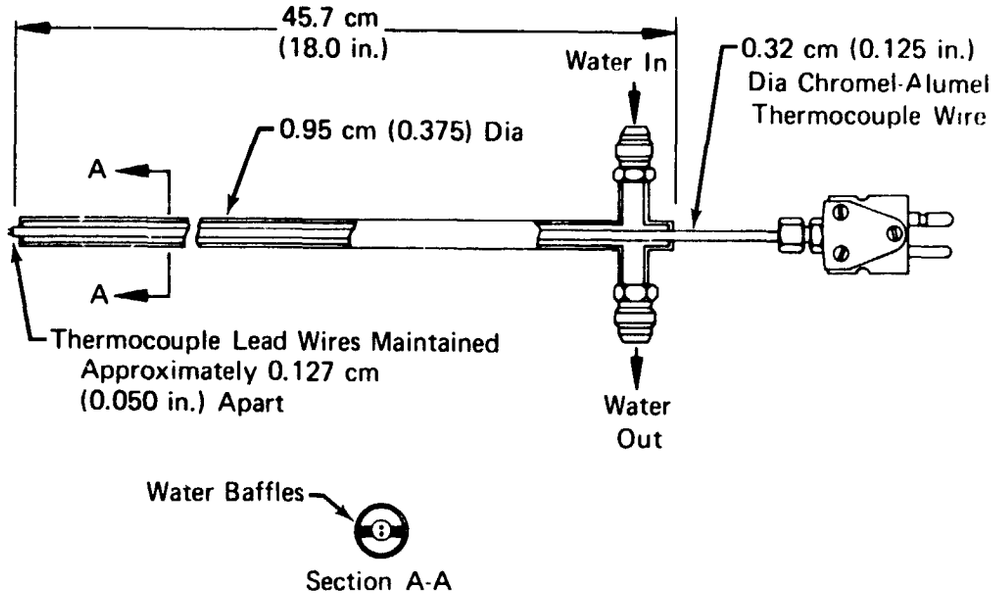

Figure 21. Ionization Probe FD 95580

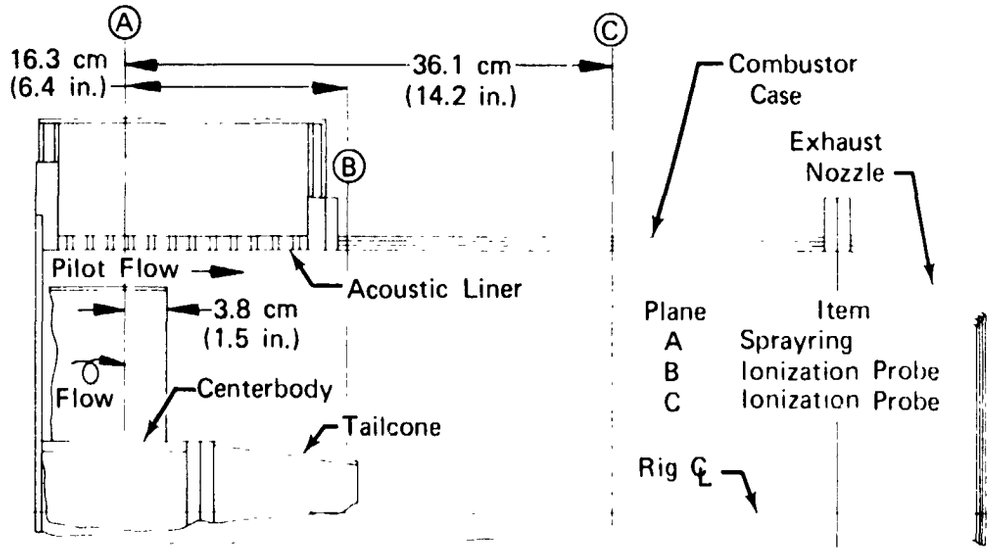

Figure 22. Location of Ionization Probes FD 95581

During the course of the test program one of the probes was converted to a thermocouple by simply welding the lead wires together. It was hoped that the flamefront could be determined by direct temperature measurements. It should be noted that the temperature recorded by the probe would not be accurate due to severe heat losses to the probe cooling water.

14. Exhaust Emissions - The exhaust gas was sampled for the emission levels of unburned hydrocarbon, carbon monoxide, carbon dioxide, and the oxides of nitrogen.

The sampling probe used is shown in figure 23. There were four probes spaced 1.571 radians (90-degrees) apart and located just downstream of the nozzle exit plane, as shown in figure 24. Each probe had five sampling ports spaced on the basis of equal areas. Each port was 0.102 cm (0.040 inch) in diameter. This diameter results in a transfer manifold flow area to sampling area ratio of 3/1. As a result, the principle pressure drop occurred across the sampling orifices.

The probes were water cooled to protect them from the hot exhaust gases of the augmentor. After passing through the probes, the cooling water was injected into the augmentor exhaust.

The sample gases from the probes were collected in a 0.953 cm (0.375 inch) diameter stainless steel manifold and then transferred to the analysis equipment via the same diameter Teflon lines. The transfer line was electrically heated. It was also aspirated to maintain a high sample gas velocity to reduce the transit time between the probes and the analysis system.

The sample gas was analyzed for the concentration of unburned hydrocarbon with a flame ionization detector. The concentrations of carbon monoxide and carbon dioxide were determined using nondispersive infrared analyzers. The concentration of nitrogen oxides was measured using a chemiluminescent analyzer. Figure 25 is a schematic of the gas analysis system.

15. Dynamic Pressure Oscillation - The augmentor was equipped with two Kistler high-response pressure transducers, as shown in figure 17. These instruments were used to record the occurrence, if any, of combustion instabilities such as rumble or screech.

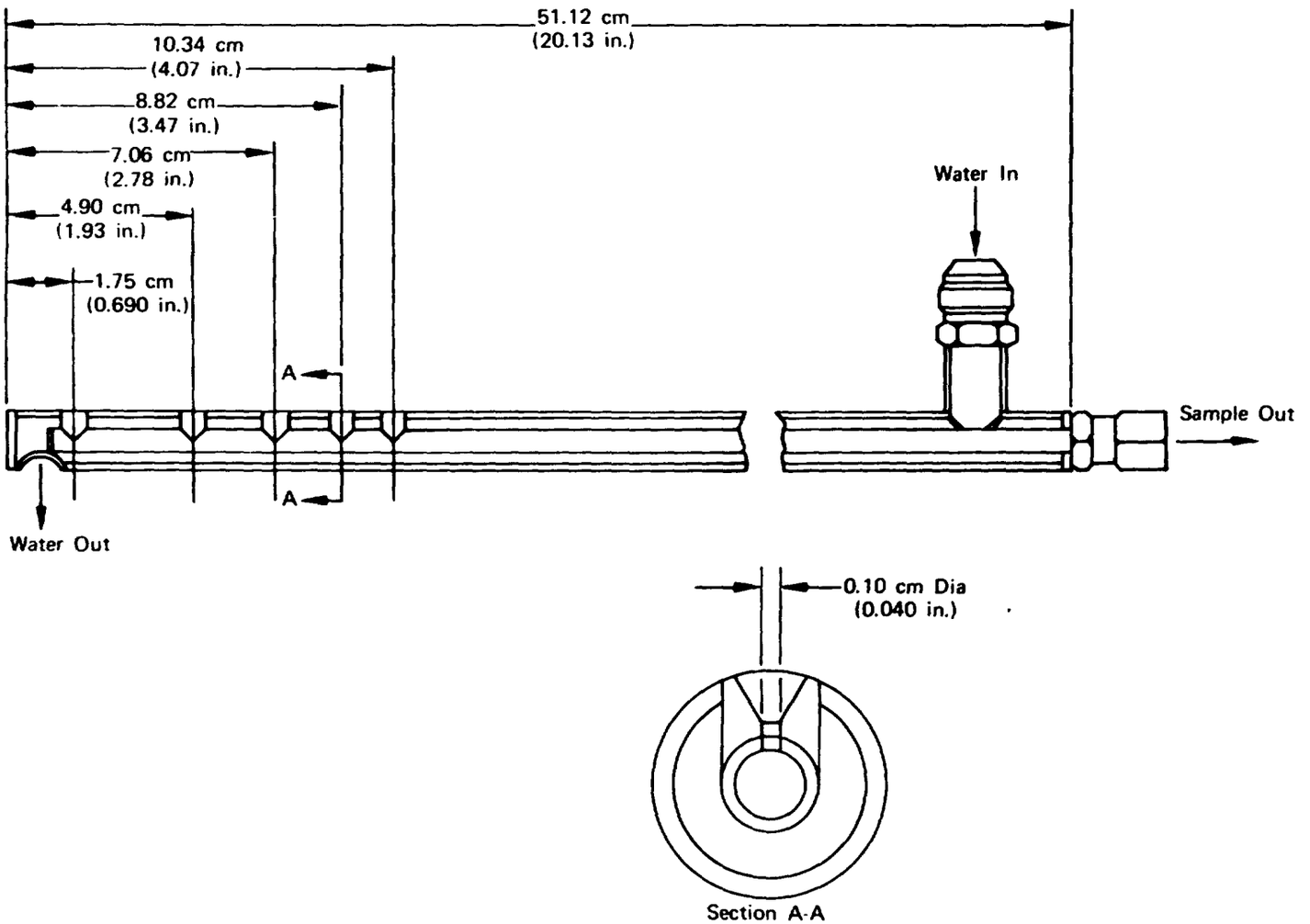

Figure 23. Gas Sampling Probe

FD 95582

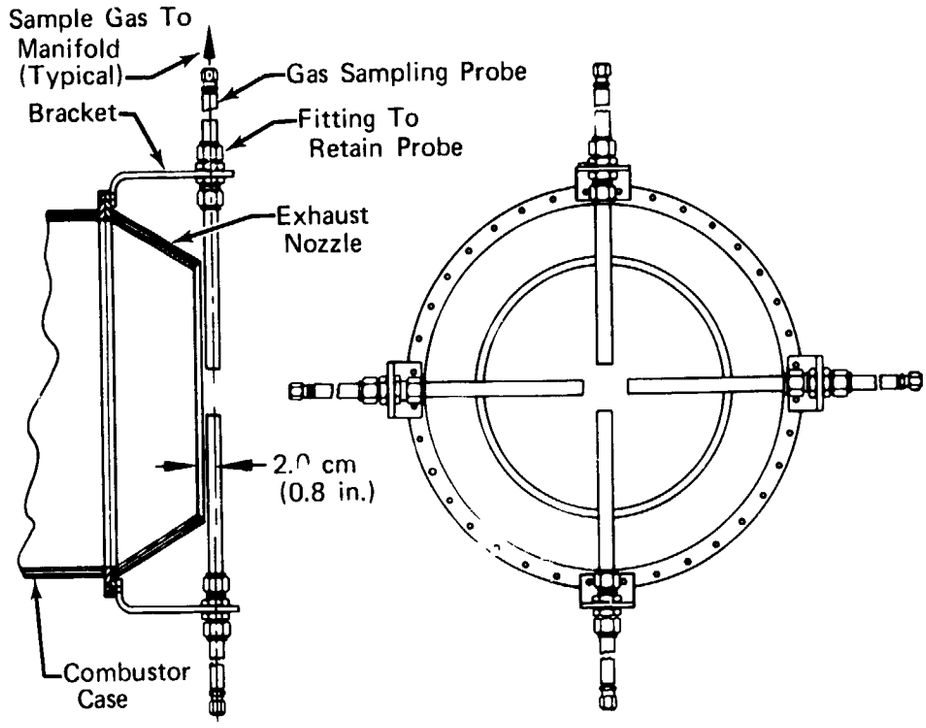

Figure 24. Location of Gas Sampling Probes FD 95583

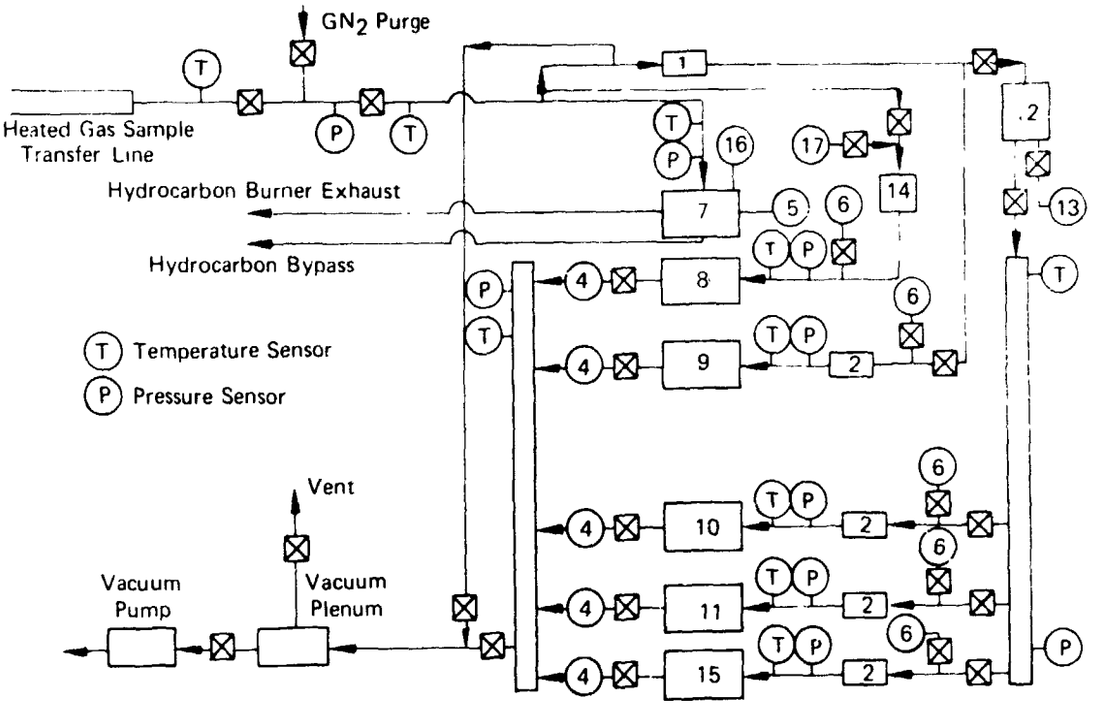

1. 10-Micron Filter
2. Drierite Cylinder
3. Particulate Trap
4. Calibrated Orifices
5. Oven Temperature
6. Calibration Gas
7. Hydrocarbon Analyzer
8. Water Vapor Analyzer
9. Chemiluminescence NO_x
10. Carbon Monoxide Analyzer
11. Carbon Dioxide Analyzer
12. Cooling Coil and Ice Bath
13. Water Sample Tap
14. 50-Micron Filter
15. Oxygen Analyzer
16. Burner Temperature
17. Rig Air Sample Inlet

Figure 25. Schematic Diagram of Gas Sampling Equipment FD 97544

EXPERIMENTAL PROCEDURE

Fuel Dispersion Test Procedures

The trajectory and dispersion of the fuel sprays from the single point injectors were tracked by measuring the temperature depression in the airstream caused by fuel evaporation. The tests were conducted at approximately 1-atmosphere pressure and at air temperatures close to 649°C (1200°F). The airflow was set to give a swirl vane inlet Mach number of 0.250. The temperature depressions caused by the fuel evaporation were measured by traversing the augmentor flow with the 20 point traverse probe described earlier. These traverses were made at four axial positions (3.8, 7.6, 15.2, and 24.9 cm) downstream of the fuel injection plane. At each axial position traverses were made at four injector fuel flows. These flows were approximately 3.9, 8.4, 15.4 and 19.2 Kg/hr (8.6, 18.6, 33.9, and 42.3 pph).

Prior to conducting the test, the sprayring elements were calibrated. As mentioned earlier, the elements were designed to flow more fuel than was injected into the augmentor. Therefore, there was no direct method of measuring

the injected fuel flow. The sprayring elements were calibrated by setting some arbitrary input fuel flow, then measuring the injection orifice fuel flow and the fuel pressure at the orifice. The flow out of the injection orifice was determined by measuring the time required to fill a volume-calibrated container. The injector flowrate could be altered by adjusting a valve on the element discharge line. The input flow was held constant. This procedure was repeated using a different input fuel flow to obtain any effects of varying input flow on injector flow. Over the range of element input fuel flows investigated, there was no effect on the injection orifice fuel flows, as long as the fuel injection pressure was held constant.

The result of the sprayring element calibrations was a set of curves of injection orifice fuel flow as a function of pressure. During the fuel dispersion tests, the orifice fuel flows were set by setting the fuel pressure in accordance with the calibration curve.

At the start of testing, an isothermal temperature traverse was made at each axial position. These traverses were used as the baseline for determining the temperature depression caused by the evaporating fuel. The probe was then returned to the axial position closest to the fuel injectors. The fuel was set to the lowest desired flow and a traverse made. The angular sweep rate of the traverse probe was adjusted to approximately 0.035 rad/sec (2 deg/sec). The data were recorded on the automatic data recording system at the rate of one complete scan of all data channels per second. Maintaining the same fuel flow, the traverse probe was moved to the next axial position and another traverse was made. This was continued until traverses were made at all four of the axial positions desired. The fuel flow was then increased to the next higher value and the traverses repeated. This process was continued until data were obtained at all of the four desired fuel flows.

Performance Demonstration (Hot Testing) Procedures

The performance tests were conducted at a near constant pressure of 2-atmospheres. With the 27.2 cm (10.69 inch) exhaust nozzle installed, the airflow required to choke the nozzle was greater than the test facility capability when operating at equivalence ratios below 0.2. Therefore, during startup an initial airflow of approximately 9.0 Kg/sec (20 lb_m/sec) was set. The pilot was then ignited at a local equivalence ratio of 1.0, using an automotive-type spark plug. The augmentor zone 2 fuel flow was set to give an overall equivalence ratio of 0.2. The increase in the nozzle outlet temperature then made it possible to choke the nozzle within the airflow capacity of the facility. Whenever the augmentor fuel flow was varied, the airflow and preheater fuel flow had to be adjusted to maintain the desired test point of 2-atmospheres pressure and 649°C (1200°F) inlet temperature. This was due to the use of a fixed area exhaust nozzle.

All of the data, with the exception of the gas sampling data, were recorded using the high-speed digital recording system. Between desired test points the recording system was operated at a recording speed of 1 scan/second, which means that all of the data channels were recorded one time each second. When a test point was set, however, the recording speed was increased to 10 scans/second, and data were recorded over a 5-second interval. These 50 readings were subsequently averaged to provide a good value for each data channel. Following these readings and with the test condition held constant, the exhaust emission data were manually recorded. A second high-speed, 5-second data scan was taken

on all the rig parameters following the exhaust emissions readings. Thus, two complete readings of all the rig pressures, temperatures and fuel flows were obtained at each test point.

Gas Sampling and Calibration Procedures

The gas sampling instrumentation was calibrated by passing a zero and several span gases through each instrument at some constant pressure or flow. The response of the nondispersive infrared analyzers, CO and CO_2, varies with the pressure in the detector cell. Therefore, it was considered desirable to set the sample pressure into these instruments equal to the calibration pressure to avoid having to make excessive corrections to the data. The unburned hydrocarbon flame ionization detector and the chemiluminescence NO_x analyzer are flow sensitive; however, they have built-in flow control systems. During calibration, the zero and span gases were admitted to the analyzers at a constant pressure of 1.29×10^5 N/m^2 (18.7 psia). The pressure, calibration gas concentration, and analyzer response were recorded. All data were recorded as millivolts. Calibration curves were then generated and these curves were used to reduce the test data. The calibration curves for all of the analyzers are shown in figures 26 through 29. As can be seen, the response of the CO and CO_2 analyzers was nonlinear, which points out the importance of calibrating over the full range of emissions. Two response curves are shown for the CO analyzer because the gain setting on the amplifier was arbitrarily changed during calibration prior to the last test conducted (test number 42.01).

Prior to taking sample data at each test point, the flows and pressures into each of the analyzers were set equal to the calibration values. The system was then allowed to come to equilibrium by monitoring the sample temperatures. The sample data, including sample pressure and temperatures, were then manually recorded.

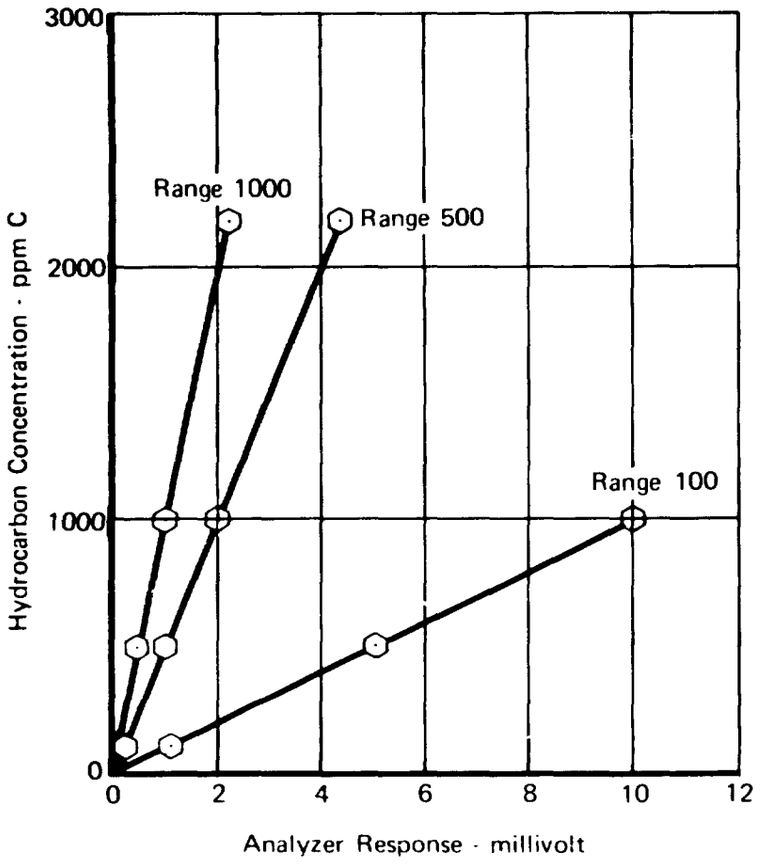

Figure 26. Calibration Curve of Unburned Hydrocarbon Analyzer FD 97545

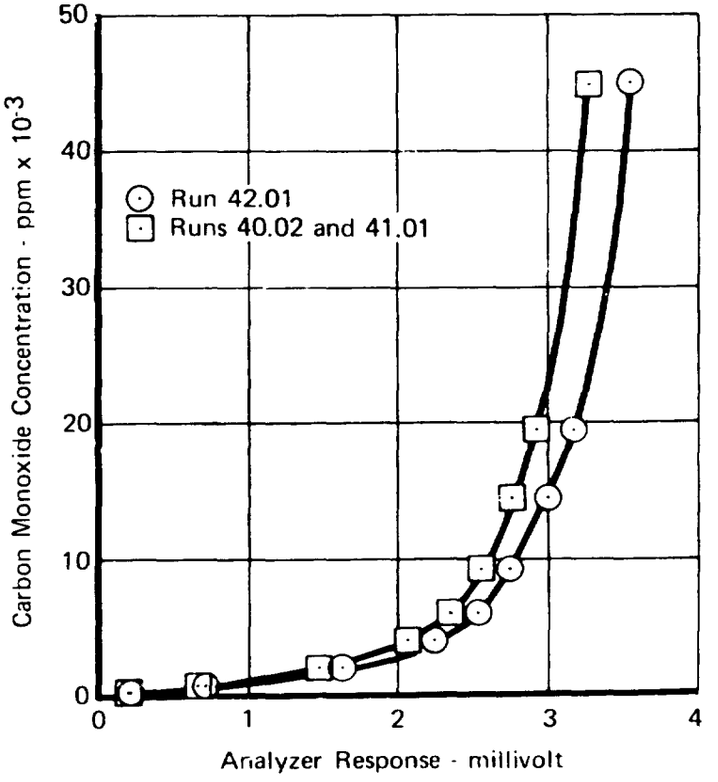

Figure 27. Calibration Curve of CO Analyzer FD 97546

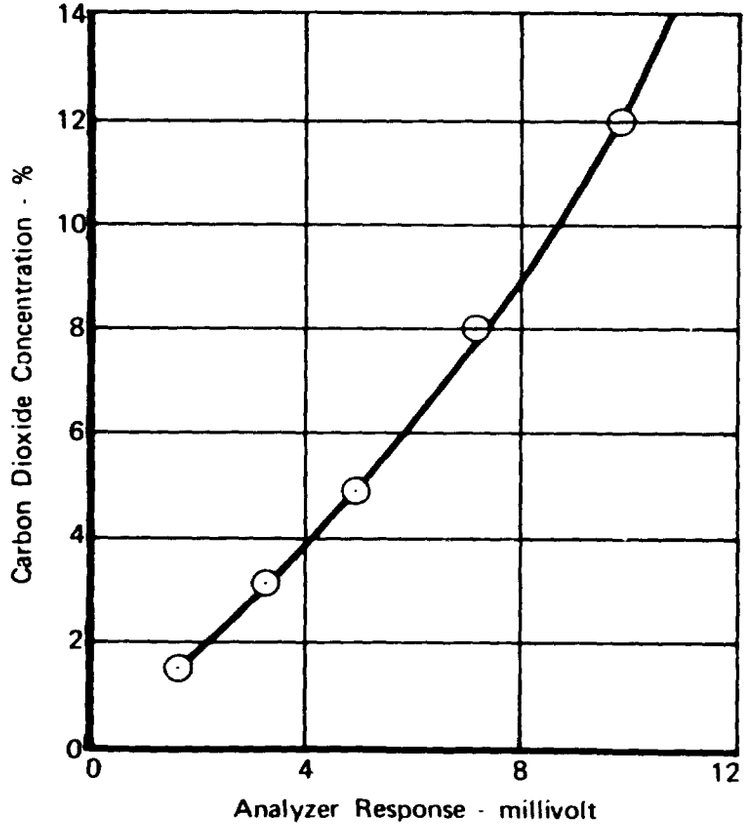

Figure 28. Calibration Curve of CO_2 Analyzer FD 97547

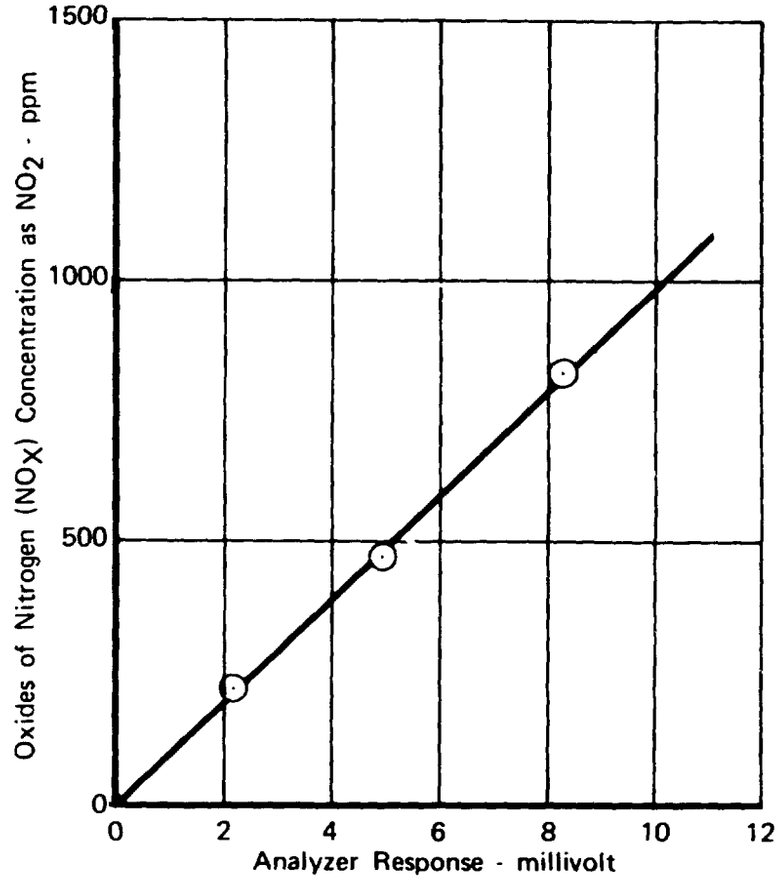

Figure 29. Calibration Curve of NO_X Analyzer FD 97548

CALCULATIONS

The basic equations used to calculate the combustion efficiency, total pressure losses, inlet Mach number, swirl intensity, and fuel-air ratio from measured temperature depression are presented in this section.

Combustion Efficiency

The augmentor combustion efficiency is normally given by:

$$EFFMB = 100 \left[\frac{T_{T6} - T_{T4A}}{T_{T6IDEAL} - T_{T4A}} + \frac{3600\ Q_{loss}}{4.273 \times 10^{7}\ WFT} \right]$$

where:

EFFMB = augmentor combustion efficiency, %

T_{T6} = actual outlet total temperature, °C (°F)

$T_{T6IDEAL}$ = ideal outlet total temperature, °C (°F)

T_{T4A} = inlet total temperature, °C (°F)

Q_{loss} = heat rejected to combustion chamber jacket cooling water, Joules/sec (Btu/sec)

WFT = augmentor fuel flow, Kg/hr (pph)

The heating value of the JP-5 kerosene fuel was taken as 4.273×10^7 Joules/Kg (18,370 Btu/lb_m).

This method of determining combustion efficiency was supplemented by a second method based on analysis of the exhaust products. By determining the amount of unburned hydrocarbons and carbon monoxide still present in the gases passing through the nozzle, the combustion efficiency can be determined from:

$$EFFMB = 100 - 100 \left[\frac{HV_{co}\ (CO - CO_{equil}) + HV_f\ (UHC)}{HV_f \times 10^{3}} \right]$$

where:

EFFMB = augmentor combustion efficiency, %

CO = emission index of carbon monoxide

CO_{equil} = equilibrium carbon monoxide emission index

UHC = emission index of unburned hydrocarbons

HV_{co} = heating value of carbon monoxide = 1.010×10^7 Joules/Kg (4343 Btu/lb_m)

HV_f = heating value of the fuel = 4.273×10^7 Joules/Kg (18,370 Btu/lb_m)

Total Pressure Losses

The overall augmentor total pressure loss is given by:

$$DPAUG = 100 \left[\frac{P_{T4A} - P_{T6A}}{P_{T4A}} \right]$$

where:

DPAUG = augmentor total pressure loss, %

P_{T4A} = inlet total pressure, N/m^2 (psia)

P_{T6A} = outlet total pressure, N/m^2 (psia)

The total pressure loss due to combustion (momentum loss) is calculated from:

$$DPMOM = \left[\frac{P_{T4A} - P_{T5IDEAL}}{P_{T4A}} \right] 100$$

where:

DPMOM = momentum pressure loss, %

$P_{T5IDEAL}$ = ideal total pressure at the exhaust nozzle, N/m^2 (psia)

$P_{T5IDEAL}$ is calculated using the relations for simple heating of a perfect gas (Rayleigh line calculation) in a constant area duct.

The swirl vane total pressure loss was calculated by subtracting the momentum pressure loss from the overall pressure loss, or

DPSV = DPAUG - DPMOM

where:

DPSV = Swirl vane pressure loss, %

Swirl Vane Mach Number

The swirl vane Mach number is the Mach number of the flow as it enters the swirl vanes. It is given by:

$$M_4 = \left[\frac{\left(W_a\right)\ (1 + HUM + FAPH)\ SVFR}{P_{T4A}\ \left(A_4\right)}\right] * \frac{}{\sqrt{\frac{R_4\ T_{T4A}}{G(GAM4)}\ \left(1 + \frac{GAM4-1}{2}\ M_4^{\,2}\right)^{\frac{GAM4+1}{GAM4-1}}}}$$

where:

M_4	=	swirl vane inlet Mach number
W_a	=	augmentor dry airflow, Kg/sec (lb_m/sec)
SVFR	=	fraction of total mass flow passing through the swirl vanes
HUM	=	specific humidity
FAPH	=	preheater fuel-air ratio
P_{T4A}	=	inlet total pressure, N/m^2 (psia)
A_4	=	swirl vane inlet area = 0.0729 m^2 (113 $in.^2$)
GAM4	=	gas specific heat ratio
R_4	=	gas constant at swirl vane inlet
G	=	standard acceleration due to gravity

Swirl Intensity

The nominal swirl intensity at the pilot zone inner wall expressed in terms of the standard gravitational constant or "g's" is:

$$g_s = (V_4 \text{ Tan } \theta)^2/(RG)$$

where:

g_s	=	swirl intensity in "g's"
V_4	=	swirl vane inlet velocity, m/sec (ft/sec)

θ = swirl vane turning angle, radians (degrees)

R = pilot zone inner wall radius, meters (feet)

Augmentor Equivalence Ratio

The augmentor equivalence ratio was calculated by subtracting the preheater fuel-air ratio from the stoichiometric fuel-air ratio as follows:

$$\phi_{aug} = \frac{(F/A)_{aug}}{0.0681 - (F/A)_{preheater}}$$

where:

ϕ_{aug} = augmentor equivalence ratio

$(F/A)_{aug}$ = augmentor fuel-air ratio

$(F/A)_{preheater}$ = preheater fuel-air ratio

Gas Sample Calculated Fuel-Air Ratio

The total rig fuel-air ratio, including preheater, was calculated from the measured values of CO_2, CO, and UHC, using the following equation; and assuming the fuel to be represented by the formula $CH_{1.9185}$:

$$F/A = \frac{M_c + aM_h}{M_{air}} \left[\frac{\left(\frac{CO}{10^4} + CO_2\right)\left(1 + \frac{a}{2}\frac{UHC}{10^6}\right) + \frac{UHC}{10^4}}{100 + \frac{CO}{10^4}\left(\frac{a}{4} - \frac{1}{2}\right) + \frac{a}{4} CO_2} \right]$$

where:

F/A = fuel-air ratio

CO = carbon monoxide, ppm

CO_2 = carbon dioxide, %

UHC = unburned hydrocarbon, ppmc

M_c = atomic weight of carbon

M_h = atomic weight of hydrogen

M_{air} = molecular weight of air

a = atomic hydrogen-carbon ratio of fuel (the value of a was assumed to be 1.9185 for the fuel used in this program)

Fuel Dispersion Study Data Reduction Procedures

As stated previously, the fuel spray was tracked following injection into the augmentor by measuring the temperature depression brought about by the evaporation of the fuel. The measured decreases in temperature were converted into fuel-air ratios by performing an enthalpy balance between the heat lost by the air and the heat gained by the fuel.

Therefore: $$M_{air}\left(h_{air\ in} - h_{air\ mix}\right) - M_{fuel}\left(h_{fuel\ mix} - h_{fuel\ in}\right) = 0$$

where:

M_{air} = local mass flowrate of air, Kg/sec (lb_m/sec)

M_{fuel} = local mass flowrate of fuel, Kg/sec (lb_m/sec)

$h_{air\ in}$ = enthalpy of air at the rig inlet temperature, Joules/Kg (Btu/lb_m)

$h_{air\ mix}$ = enthalpy of air at mixture temperature, Joules/Kg (Btu/lb_m)

$h_{fuel\ in}$ = enthalpy of fuel at fuel inlet temperature, Joules/Kg (Btu/lb_m)

$h_{fuel\ mix}$ = enthalpy of fuel at mixture temperature, Joules/Kg (Btu/lb_m)

Rearranging the equation gives

$$\frac{M_{fuel}}{M_{air}} = (F/A)_{local} = \frac{h_{air\ in} - h_{air\ mix}}{h_{fuel\ mix} - h_{fuel\ in}}$$

The air and fuel enthalpies were obtained from published properties for each. The fuel inlet temperature was calculated by linearly interpolating between the sprayring element inlet and outlet temperatures. The interpolation is given by

$$T_{fuel\ in} = T_{s_{in}} + \left(T_{s_{out}} - T_{s_{in}}\right) \times \left(\frac{L_o}{L_T}\right)$$

where:

$T_{fuel\ in}$ = fuel temperature at the injection orifice

$T_{s_{in}}$ = fuel temperature at sprayring element inlet

$T_{s_{out}}$ = fuel temperature at sprayring element outlet

L_o = sprayring length from fuel inlet temperature station to the injection orifice

L_T = sprayring length from fuel inlet temperature station to fuel outlet temperature station

The point-by-point fuel-air ratios thus obtained were converted to lines of constant fuel-air ratio by performing linear interpolations in both the radial and circumferential directions. Due to the large amount of data, these calculations were performed on a digital computer. The results were plotted using an X-Y plotter slaved to the computer.

RESULTS AND DISCUSSIONS

A test program was conducted with an augmentor that employed swirling flow as a means of promoting rapid flame propagation. The program had two primary objectives: (1) measure the dispersion and trajectory of JP-5 kerosene sprayed into a strongly swirling flowfield, and (2) design a set of sprayrings based on the fuel dispersion data and evaluate them by hot testing in the swirl augmentor rig. Both the fuel dispersion tests and the performance evaluation tests were conducted at a nominal inlet temperature of 649°C (1200°F). The fuel dispersion tests were conducted at near ambient pressure and the performance tests at a 2-atmosphere pressure. The performance test data are summarized in table 1. In addition to these primary objectives, measurements were made to determine the mainstream air angle and the location of the flamefront and exhaust emissions. The exhaust emission data are summarized in table 2.

Fuel Dispersion Test Results

The dispersion and trajectory of JP-5-type kerosene was measured by recording the temperature depression caused by the evaporation of the fuel. The measurements were made using a multipoint temperature traverse probe at four axial positions downstream of the fuel injection plane. The point-to-point temperatures were converted to fuel-air ratios by performing an enthalpy balance in which heat lost by the air equaled the heat gained by the fuel. Contour plots of constant fuel-air ratio were made by linearly interpolating between the point-to-point fuel-air ratios.

The data obtained are presented in figures 30 through 37. On each figure are plotted lines of constant fuel-air ratio for each of the axial positions investigated. The location of each injector is also shown for comparison. The axial location of each fuel spray pattern is denoted, as well as the injector fuel flow at which the traverses were made. The data of figures 30 through 33 were obtained with injectors located at 8.26 and 13.08 cm (3.25 and 5.15 inches) radius. The remaining data were obtained with injectors located at 10.7 and 15.1 cm (4.20 and 5.96 inches) radius.

TABLE 1. TEST SU

Run No.	Point No.	Vane Angle, rad	Vane Angle, deg	L/D	Airflow Kg/sec	Airflow lb_m/sec	Inlet Pressure $N/m^2 10^{-3}$	Inlet Pressure psia	Inlet Temp., °C	Inlet Temp., °F	M_{in}	M_{ref}	Ref Velocity, m/sec	Ref Velocity, ft/sec	Swirl, g's	DPS %
40.02	580	0.61	35	1.37	10.7	23.6	236.5	34.3	684	1263	0.285	0.202	119	390	3352	8.
40.02	1500	0.61	35	1.37	10.65	23.5	235.1	34.1	682	1259	0.285	0.202	118	387	8266	8.
40.02	1601	0.61	35	1.37	10.57	23.3	239.9	34.8	681	1258	0.275	0.195	114	375	7741	7.
40.02	1770	0.61	35	1.37	10.65	23.5	239.9	34.8	682	1259	0.277	0.196	115	376	7801	7.
40.02	1900	0.61	35	1.37	10.61	23.4	244.8	35.5	681	1258	0.271	0.192	112	369	7511	7.
40.02	2305	0.61	35	1.37	10.61	23.4	244.8	35.5	679	1254	0.271	0.192	113	370	7523	6.
40.02	2495	0.61	35	1.37	9.89	21.8	235.1	34.1	668	1235	0.260	0.185	108	354	6891	5.
40.02	2620	0.61	35	1.37	9.93	21.9	235.8	34.2	669	1236	0.260	0.185	108	355	6922	6.
40.02	2710	0.61	35	1.37	9.84	21.7	238.6	34.6	669	1236	0.256	0.182	106	349	6688	5.
40.02	2890	0.61	35	1.37	9.89	21.8	237.9	34.5	672	1241	0.258	0.183	107	351	6788	5.
40.02	3040	0.61	35	1.37	9.80	21.6	239.9	34.8	673	1243	0.252	0.180	105	345	6548	5.
40.02	3170	0.61	35	1.37	9.89	21.8	240.6	34.9	671	1240	0.253	0.180	105	345	6564	5.
40.02	3650	0.61	35	1.37	9.84	21.7	251.0	36.4	669	1237	0.240	0.171	100	328	5913	4.
40.02	3760	0.61	35	1.37	9.80	21.6	250.3	36.3	667	1233	0.239	0.171	100	327	5877	4.
40.02	3985	0.61	35	1.37	8.94	19.7	233.7	33.9	675	1247	0.235	0.167	98	323	5722	3.
40.02	4131	0.61	35	1.37	8.94	19.7	233.0	33.8	676	1248	0.237	0.169	99	325	5813	4.
40.02	4305	0.61	35	1.37	8.66	19.1	230.3	33.4	665	1229	0.229	0.163	95	313	5392	3.
40.02	4440	0.61	35	1.37	8.62	19.0	229.6	33.3	668	1234	0.229	0.163	96	314	5423	3.
40.02	4945	0.61	35	1.37	8.57	18.9	231.0	33.5	677	1251	0.227	0.162	95	313	5390	3.
40.02	5045	0.61	35	1.37	8.53	18.8	231.0	33.5	680	1256	0.227	0.162	96	313	5388	3.
40.02	5255	0.61	35	1.37	8.57	18.9	233.0	33.8	681	1258	0.224	0.160	94	307	5169	3.
40.02	5355	0.61	35	1.37	8.53	18.8	232.4	33.7	680	1256	0.224	0.160	94	309	5252	3.
40.02	5910	0.61	35	1.37	8.39	18.5	230.3	33.4	683	1261	0.223	0.160	94	309	5248	3.
40.02	6085	0.61	35	1.37	8.34	18.4	230.3	33.4	677	1251	0.222	0.159	94	307	5162	3.
40.02	6216	0.61	35	1.37	8.26	18.2	229.6	33.3	680	1256	0.221	0.158	93	305	5108	3.
40.02	6390	0.61	35	1.37	8.26	18.2	229.6	33.3	682	1259	0.221	0.158	93	306	5124	3.
40.02	6574	0.61	35	1.37	8.21	18.1	229.6	33.3	680	1256	0.220	0.157	93	304	5070	3.
40.02	6665	0.61	35	1.37	8.30	18.3	231.7	33.6	676	1248	0.220	0.157	92	303	5031	2.
41.01	368	0.61	35	0.87	11.20	24.7	245.5	35.6	686	1266	0.289	0.205	121	398	8650	10.
41.01	557	0.61	35	0.87	11.07	24.4	244.8	35.5	686	1266	0.288	0.204	121	396	8574	10.
41.01	655	0.61	35	0.87	10.61	23.4	241.3	35.0	682	1259	0.277	0.197	116	381	7952	8.
41.01	812	0.61	35	0.87	10.57	23.3	240.6	34.9	681	1258	0.276	0.196	116	381	7929	8.
41.01	951	0.61	35	0.87	10.12	22.3	237.9	34.5	681	1258	0.267	0.190	112	369	7455	7.
41.01	1114	0.61	35	0.87	10.02	22.1	235.8	34.2	683	1261	0.267	0.190	112	369	7445	7.
41.01	1211	0.61	35	0.87	9.98	22.0	239.2	34.7	683	1261	0.262	0.187	111	363	7211	7.
41.01	1340	0.61	35	0.87	10.07	22.2	239.9	34.8	682	1260	0.263	0.187	111	364	7255	7.
41.01	2540	0.61	35	0.87	9.89	21.8	238.6	34.6	676	1248	0.260	0.185	109	358	7034	6.
41.01	2740	0.61	35	0.87	9.80	21.6	237.9	34.5	684	1263	0.259	0.184	109	359	7050	6.
41.01	2820	0.61	35	0.87	9.66	21.3	237.2	34.4	670	1238	0.254	0.181	107	350	6716	6.
41.01	2975	0.61	35	0.87	9.66	21.3	236.5	34.3	668	1234	0.254	0.181	107	350	6707	6.
41.01	3242	0.61	35	0.87	9.48	20.9	235.8	34.2	669	1237	0.250	0.179	105	346	6542	5.
41.01	3360	0.61	35	0.87	9.57	21.1	237.2	34.4	669	1236	0.251	0.179	105	346	65	6.0
41.01	4212	0.61	35	0.87	8.80	19.4	228.9	33.2	674	1245	0.238	0.170	101	330	59	4.7
41.01	4397	0.61	35	0.87	8.80	19.4	228.9	33.2	674	1246	0.238	0.170	101	331	5990	4.7
41.01	4487	0.61	35	0.87	8.80	19.4	229.6	33.3	673	1244	0.239	0.171	101	331	5999	4.7
41.01	4605	0.61	35	0.87	8.85	19.5	229.6	33.3	673	1244	0.238	0.170	101	330	5972	4.
41.01	4720	0.61	35	0.87	8.85	19.5	230.3	33.4	672	1241	0.238	0.170	101	330	5957	4.7
41.01	4835	0.61	35	0.87	8.85	19.5	231.0	33.5	672	1241	0.238	0.170	101	330	5957	4.
41.01	4938	0.61	35	0.87	8.66	19.1	230.3	33.4	670	1238	0.233	0.166	98	323	5710	4.
41.01	5480	0.61	35	0.87	8.62	19.0	229.6	33.3	673	1243	0.233	0.166	98	323	5729	4.
41.01	5686	0.61	35	0.87	8.62	19.0	231.7	33.6	672	1242	0.231	0.165	98	320	5627	3.
41.01	5822	0.61	35	0.87	8.62	19.0	231.7	33.6	672	1241	0.231	0.165	98	320	5618	3.7
41.01	5916	0.61	35	0.87	8.57	18.9	232.4	33.7	671	1239	0.229	0.163	97	317	5509	3.6
41.01	6053	0.61	35	0.87	8.44	18.6	228.9	33.2	673	1244	0.228	0.163	97	317	5506	3.5
41.01	6430	0.61	35	0.87	8.35	18.4	228.2	33.1	677	1250	0.227	0.162	96	316	5487	3.
41.01	6570	0.61	35	0.87	8.39	18.5	228.9	33.2	673	1243	0.227	0.162	96	315	5453	3.
41.01	6665	0.61	35	0.87	8.39	18.5	229.6	33.3	671	1240	0.227	0.162	96	314	5423	3.2
41.01	6917	0.61	35	0.87	8.39	18.5	229.6	33.3	644	1191	0.226	0.161	95	312	5361	3.1
42.01	1281	0.61	35	1.37	11.16	24.6	241.3	35.0	677	1250	0.294	0.208	123	402	8866	11.1
42.01	1585	0.61	35	1.37	11.07	24.4	240.6	34.9	680	1256	0.293	0.208	123	402	8845	11.1
42.01	1785	0.61	35	1.37	11.07	24.4	244.1	35.4	674	1245	0.288	0.204	120	395	8551	10.
42.01	1991	0.61	35	1.37	11.16	24.6	245.5	35.6	671	1240	0.288	0.204	120	395	8521	10.3
42.01	2215	0.61	35	1.37	10.80	23.8	243.4	35.3	667	1233	0.280	0.199	117	384	8076	9.3
42.01	2375	0.61	35	1.37	10.57	23.3	238.6	34.6	669	1237	0.279	0.198	117	383	8012	9.
42.01	2536	0.61	35	1.37	10.52	23.2	242.7	35.2	668	1234	0.272	0.194	114	375	7699	8.8
42.01	2665	0.61	35	1.37	10.39	22.9	240.6	34.9	673	1243	0.272	0.193	114	375	7695	8.8
42.01	2980	0.61	35	1.37	10.34	22.8	242.7	35.2	671	1239	0.267	0.190	112	368	7418	8.
42.01	3090	0.61	35	1.37	10.39	22.9	244.1	35.4	667	1233	0.267	0.190	112	367	7363	8.
42.01	3290	0.61	35	1.37	10.02	22.1	241.3	35.0	666	1230	0.260	0.185	109	358	7009	7.
42.01	3395	0.61	35	1.37	9.98	22.0	239.9	34.8	669	1237	0.260	0.185	109	359	7057	7.
42.01	3550	0.61	35	1.37	9.75	21.5	239.2	34.7	666	1230	0.255	0.182	108	353	6811	7.
42.01	3701	0.61	35	1.37	9.84	21.7	239.9	34.8	669	1236	0.256	0.183	108	354	6840	7.
42.01	4225	0.61	35	1.37	9.62	21.2	237.9	34.5	661	1222	0.252	0.180	106	348	6631	6.4
42.01	4430	0.61	35	1.37	9.62	21.2	237.2	34.4	667	1232	0.253	0.181	107	350	6706	6.4
42.01	4920	0.61	35	1.37	9.30	20.5	235.8	34.2	663	1226	0.246	0.176	104	341	6363	5.
42.01	5045	0.61	35	1.37	9.43	20.8	237.9	34.5	660	1220	0.247	0.176	104	341	6376	5.8
42.01	5530	0.61	35	1.37	9.12	20.1	233.0	33.8	665	1229	0.244	0.175	103	339	6274	5.7
42.01	5870	0.61	35	1.37	9.21	20.3	237.9	34.5	659	1219	0.239	0.171	101	332	6004	5.4
42.01	6005	0.61	35	1.37	9.21	20.3	237.9	34.5	660	1221	0.239	0.171	101	332	6014	5.4
42.01	6200	0.61	35	1.37	9.12	20.1	239.2	34.7	663	1225	0.236	0.169	100	327	5856	5.
42.01	6355	0.61	35	1.37	9.12	20.1	239.2	34.7	662	1224	0.236	0.169	100	328	5862	5.3
42.01	6610	0.61	35	1.37	8.75	19.3	235.1	34.1	660	1220	0.230	0.165	98	320	5577	4.8
42.01	6745	0.61	35	1.37	8.80	19.4	235.8	34.2	660	1221	0.231	0.165	98	320	5605	4.8
42.01	7010	0.61	35	1.37	8.44	18.6	231.0	33.5	663	1225	0.226	0.162	96	314	5485	4.4
42.01	7130	0.61	35	1.37	8.48	18.7	231.7	33.6	661	1222	0.226	0.162	96	315	5496	4.5
42.01	7375	0.61	35	1.37	8.48	18.7	233.7	33.9	662	1223	0.223	0.160	95	311	5275	4.
42.01	7525	0.61	35	1.37	8.44	18.6	233.7	33.9	666	1230	0.224	0.161	95	312	5317	4.3
42.01	7725	0.61	35	1.37	8.35	18.4	233.0	33.8	671	1239	0.222	0.159	94	310	5253	4.2
42.01	7880	0.61	35	1.37	8.39	18.5	233.7	33.9	667	1233	0.222	0.159	94	310	5243	4.2
42.01	8545	0.61	35	1.37	8.39	18.5	236.5	34.3	667	1232	0.219	0.157	93	308	5114	4.1
42.01	8895	0.61	35	1.37	8.21	18.1	233.7	33.9	676	1249	0.219	0.157	94	308	5152	4.1
42.01	9416	0.61	35	1.37	8.12	17.9	233.0	33.8	659	1219	0.215	0.154	91	300	4909	3.
42.01	9530	0.61	35	1.37	8.16	18.0	233.0	33.8	662	1223	0.215	0.155	92	301	4926	3.
42.01	11310	0.61	35	1.37	7.94	17.5	229.6	33.3	672	1242	0.215	0.155	92	303	4982	4.0
42.01	11525	0.61	35	1.37	7.98	17.6	229.6	33.3	670	1238	0.215	0.155	92	302	4962	4.0
42.01	11995	0.61	35	1.37	8.30	18.3	229.6	33.3	666	1230	0.223	0.160	95	312	5297	4.
42.01	12300	0.61	35	1.37	8.26	18.2	234.4	34.0	668	1235	0.218	0.157	93	306	5100	4.1
42.01	12500	0.61	35	1.37	8.26	18.2	235.1	34.1	668	1235	0.218	0.156	93	305	5040	4.1

FOLDOUT FRAME

ORIGINAL PAGE IS
OF POOR QUALITY

TABLE 1. TEST SUMMARY

	M_{ref}	Ref Velocity, m/sec	ft/sec	Swirl, g's	DPSV, %	DPMON, %	DPAUG, %	CDAUG	F/A	ϕ_{aug}	ϕ_2	ϕ_3	ϕ_4	Outlet Temp., °C	°F	EFFMB Sample	EFFMB Choke Nozzle
5	0.202	119	390	3352	8.6	1.7	10.3	2.00	0.017	0.306	0.252	-	-	1191	2175	95	103
.	0.202	118	387	8266	8.3	1.7	10.0	1.95	0.017	0.303	0.252	-	-	1183	2162		103
5	0.195	114	375	7741	7.4	2.0	9.4	1.96	0.020	0.359	0.308	-	-	1316	2401	97	110
7	0.196	115	376	7801	7.4	1.9	9.3	1.92	0.020	0.356	0.305	-	-	1294	2361		108
71	0.192	112	369	7511	7.0	2.1	9.1	1.95	0.023	0.405	0.354	-	-	1372	2502	97	107
71	0.192	113	370	7523	6.9	2.1	9.0	1.93	0.023	0.405	0.353	-	-	1372	2501		107
0	0.185	108	354	6891	5.9	2.4	8.3	1.93	0.027	0.483	0.427	-	-	1497	2727	9	107
0	0.185	108	355	6922	6.1	2.3	8.4	1.95	0.027	0.482	0.426	-	-	1490	2714		107
	0.182	106	349	6688	5.6	2.5	8.1	1.94	0.030	0.534	0.479	-	-	1561	2841	9	105
	0.183	107	351	6788	5.6	2.4	8.0	1.91	0.030	0.531	0.475	-	-	1536	2797		103
2	0.180	105	345	6548	5.4	2.5	7.9	1.95	0.033	0.583	0.527	-	-	1606	2923	9	102
	0.180	105	345	6564	5.3	2.5	7.8	1.92	0.033	0.577	0.522	-	-	1593	2899		102
	0.171	100	328	5913	4.1	2.9	7.0	1.89	0.039	0.677	0.399	0.246	-	1894	3441	97	109
	0.171	100	327	5877	4.2	2.9	7.1	1.91	0.039	0.680	0.396	0.245	-	1864	3387		107
	0.167	98	323	5722	3.9	2.9	6.8	1.91	0.042	0.738	0.429	0.306	-	1961	3561	9	109
7	0.169	99	325	5813	4.0	2.9	6.9	1.90	0.042	0.731	0.423	0.308	-	1949	3540		107
	0.163	95	313	5392	3.6	3.0	6.6	1.94	0.045	0.796	0.428	0.364	-	2012	3653	9	107
	0.163	96	314	5423	3.6	3.0	6.6	1.93	0.046	0.802	0.431	0.369	-	2022	3672		108
7	0.162	95	313	5390	3.3	3.0	6.3	1.89	0.049	0.858	0.427	0.421	-	2032	3689	9	106
7	0.162	95	313	5388	3.4	3.0	6.4	1.93	0.049	0.868	0.431	0.422	-	2041	3706		106
	0.160	94	307	5169	3.4	3.0	6.4	2.00	0.052	0.909	0.421	0.484	-	2059	3738	91	105
4	0.160	94	309	5252	3.4	3.0	6.4	1.97	0.052	0.913	0.424	0.482	-	2073	3763		106
3	0.160	94	309	5248	3.3	3.0	6.3	1.94	0.055	0.973	0.421	0.539	-	2081	3777	92	104
	0.159	94	307	5162	3.3	3.0	6.3	1.98	0.055	0.969	0.420	0.542	-	2077	3770		104
1	0.158	93	305	5108	3.2	3.0	6.2	1.98	0.058	1.028	0.421	0.593	-	2094	3802	9	105
1	0.158	93	306	5124	3.2	3.0	6.2	1.96	0.058	1.032	0.421	0.586	-	2095	3803		105
0	0.157	93	304	5070	3.1	3.0	6.1	1.95	0.061	1.077	0.415	0.226	-	1826	3318		110
0	0.157	92	303	5031	2.9	3.0	5.9	1.91	0.060	1.063	0.409	0.5[illegible]	-	1823	3314		111
	0.205	121	398	8650	10.7	1.4	12.1	2.31	0.016	0.287	0.236	-	-	1098	2008	91	87
	0.204	121	396	8574	10.4	1.5	11.9	2.28	0.017	0.292	0.241	-	-	1125	2057		90
77	0.197	116	381	7952	8.9	1.8	10.7	2.21	0.020	0.356	0.305	-	-	1257	2294	9	97
6	0.196	116	381	7929	8.9	1.8	10.7	2.22	0.020	0.358	0.306	-	-	1270	2318		99
7	0.190	112	369	7455	7.9	2.1	10.0	2.19	0.024	0.424	0.370	-	-	1392	2538	9	102
67	0.190	112	369	7445	7.9	2.1	10.0	2.21	0.024	0.430	0.375	-	-	1392	2537		100
62	0.187	111	363	7211	7.3	2.2	9.5	2.18	0.027	0.477	0.422	-	-	1467	2673	9	101
63	0.187	111	364	7255	7.4	2.2	9.6	2.18	0.027	0.473	0.418	-	-	1447	2637		99
60	0.185	109	358	7034	6.9	2.3	9.2	2.13	0.030	0.534	0.478	-	-	1490	2714	9	95
	0.184	109	359	7050	6.8	2.3	9.1	2.14	0.030	0.538	0.483	-	-	1517	2762		97
	0.181	107	350	6718	6.4	2.4	8.8	2.13	0.033	0.587	0.531	-	-	1551	2824	92	94
54	0.181	107	350	6707	6.3	2.4	8.7	2.11	0.034	0.591	0.533	-	-	1555	2832		94
0	0.179	105	346	6542	5.9	2.5	8.4	2.10	0.037	0.650	0.589	-	-	1604	2919	9	92
1	0.179	105	346	6545	6.0	2.5	8.5	2.11	0.037	0.643	0.582	-	-	1589	2892		91
38	0.170	101	330	5969	4.7	2.7	7.4	2.05	0.043	0.756	0.455	0.238	-	1803	3277	9	98
	0.170	101	331	5990	4.7	2.7	7.4	2.04	0.043	0.759	0.456	0.240	-	1807	3284		98
39	0.171	101	331	5990	4.7	2.7	7.4	2.03	0.043	0.748	0.444	0.241	-	1799	3270	9	98
	0.170	101	330	5972	4.8	2.7	7.5	2.07	0.043	0.747	0.444	0.241	-	1801	3273		99
38	0.170	101	330	5957	4.7	2.7	7.4	2.06	0.042	0.736	0.429	0.245	-	1813	3296	9	101
38	0.170	101	330	5957	4.8	2.7	7.5	2.07	0.042	0.735	0.428	0.245	-	1807	3284		101
33	0.166	98	323	5710	4.2	2.8	7.0	2.02	0.046	0.802	0.430	0.309	-	1901	3454	9	102
33	0.166	98	323	5729	4.2	2.8	7.0	2.01	0.046	0.804	0.431	0.310	-	1910	3470		103
1	0.165	98	320	5627	3.8	2.9	6.7	1.95	0.048	0.844	0.421	0.361	-	1942	3528	90	102
31	0.165	98	320	5618	3.7	2.9	6.6	1.94	0.051	0.846	0.416	0.362	-	1954	3549		103
	0.163	97	317	5509	3.6	2.9	6.5	1.94	0.051	0.895	0.416	0.416	-	1989	3613	90	102
8	0.163	97	317	5506	3.5	2.9	6.4	1.91	0.052	0.914	0.426	0.424	-	2000	3632		102
7	0.162	96	316	5487	3.4	2.9	6.3	1.90	0.055	0.963	0.418	0.480	-	2009	3649	9	100
27	0.162	96	315	5453	3.2	2.9	6.1	1.86	0.055	0.961	0.413	0.481	-	2007	3645		100
7	0.162	96	314	5423	3.2	2.9	6.1	1.85	0.057	1.005	0.410	0.529	-	1997	3626	9	98
26	0.161	95	312	5361	3.1	2.9	6.0	1.85	0.057	1.006	0.410	0.526	-	2003	3637		98
94	0.208	123	402	8866	11.1	1.3	12.4	2.28	0.013	0.227	0.177	-	-	1043	1910	9	98
3	0.208	123	402	8845	11.1	1.3	12.4	2.30	0.013	0.221	0.171	-	-	1057	1934		103
	0.204	120	395	8551	10.3	1.5	11.8	2.25	0.015	0.262	0.211	-	-	1129	2064	9	103
8	0.204	120	395	8521	10.3	1.5	11.8	2.26	0.015	0.258	0.208	-	-	1119	2046		103
0	0.199	117	384	8076	9.3	1.7	11.0	2.22	0.018	0.310	0.259	-	-	1221	2230	9	106
	0.198	117	383	8012	9.3	1.7	11.0	2.24	0.018	0.317	0.265	-	-	1229	2244		106
72	0.194	114	375	7699	8.5	1.9	10.4	2.22	0.021	0.362	0.310	-	-	1316	2401	9	108
72	0.193	114	375	7695	8.5	1.9	10.4	2.22	0.021	0.366	0.314	-	-	1329	2422		108
67	0.190	112	368	7418	8.0	2.1	10.1	2.21	0.023	0.405	0.354	-	-	1381	2517	9	107
7	0.190	112	367	7363	8.0	2.1	10.1	2.24	0.023	0.404	0.353	-	-	1385	2525		108
0	0.185	109	358	7009	7.4	2.2	9.6	2.25	0.026	0.457	0.405	-	-	1477	2691	9	109
0	0.185	109	359	7057	7.4	2.2	9.6	2.24	0.026	0.461	0.408	-	-	1477	2691		108
5	0.182	108	353	6811	7.0	2.3	9.3	2.26	0.029	0.513	0.457	-	-	1542	2807	9	106
6	0.183	108	354	6840	7.0	2.3	9.3	2.23	0.029	0.510	0.452	-	-	1524	2776		105
2	0.180	106	348	6631	6.4	2.4	8.8	2.18	0.031	0.540	0.377	0.105	-	1587	2888	9	107
3	0.181	107	350	6706	6.4	2.4	8.8	2.15	0.030	0.531	0.368	0.104	-	1589	2893		109
46	0.176	104	341	6363	5.8	2.6	8.4	2.17	0.033	0.583	0.371	0.162	-	1696	3084	9	112
7	0.176	104	341	6376	5.8	2.6	8.4	2.15	0.033	0.576	0.366	0.161	-	1678	3052		111
4	0.175	103	339	6274	5.7	2.6	8.3	2.17	0.034	0.607	0.374	0.185	-	1714	3118		110
	0.171	101	332	6004	5.4	2.7	8.1	2.21	0.036	0.633	0.365	0.220	-	1791	3255	9	114
	0.171	101	332	6014	5.4	2.7	8.1	2.21	0.036	0.637	0.368	0.221	-	1794	3262		113
1	0.169	100	327	5856	5.2	2.8	8.0	2.22	0.038	0.670	0.360	0.261	-	1858	3376	9	115
1	0.169	100	328	5862	5.2	2.8	8.0	2.22	0.038	0.661	0.359	0.254	-	1850	3362		115
0	0.165	98	320	5577	4.8	2.9	7.7	2.24	0.042	0.733	0.366	0.316	-	1942	3527	9	114
1	0.165	98	320	5605	4.8	2.8	7.6	2.23	0.042	0.732	0.366	0.315	-	1937	3518		114
26	0.162	96	314	5385	4.4	2.9	7.3	2.23	0.045	0.800	0.374	0.374	-	2021	3670	9	114
26	0.162	96	315	5396	4.5	2.9	7.4	2.25	0.045	0.801	0.374	0.375	-	2020	3668		113
3	0.160	95	311	5275	4.3	3.0	7.3	2.26	0.048	0.842	0.368	0.422	-	2060	3740	9	113
4	0.161	95	312	5317	4.3	2.9	7.2	2.25	0.048	0.846	0.370	0.424	-	2061	3741		113
22	0.159	94	310	5253	4.2	3.0	7.2	2.25	0.051	0.902	0.371	0.478	-	2103	3818	9	112
2	0.159	94	310	5243	4.2	3.0	7.2	2.27	0.052	0.896	0.369	0.474	-	2099	3810		112
	0.157	93	306	5114	4.1	3.0	7.1	2.29	0.052	0.919	0.364	0.418	0.085	2154	3910	9	115
19	0.157	94	308	5152	4.1	3.0	7.1	2.30	0.053	0.943	0.374	0.428	0.087	2168	3934		114
	0.154	91	300	4909	3.9	3.0	6.9	2.31	0.057	1.001	0.370	0.418	0.158	2202	3996	9	114
15	0.155	92	301	4926	3.8	3.0	6.8	2.28	0.056	0.992	0.367	0.415	0.156	2186	3967		114
15	0.155	92	303	4982	4.0	3.0	7.0	2.34	0.058	1.035	0.383	0.434	0.160	2201	3993		114
15	0.155	92	302	4962	4.0	3.0	7.0	2.32	0.058	1.027	0.378	0.432	0.160	2193	3979		113
	0.160	95	312	5297	4.3	2.9	7.2	2.24	0.050	0.885	0.367	0.370	0.094	2058	3736		109
	0.157	93	306	5100	4.1	3.0	7.1	2.31	0.053	0.945	0.369	0.422	0.099	2164	3928	9	114
	0.156	93	305	5080	4.1	3.0	7.1	2.31	0.054	0.965	0.369	0.423	0.118	2169	3937		113

FOLDOUT FRAME 2

TABLE 2. GAS SAMPLE DATA

Run No.	Micro Time	UHC, ppmc	UHC, EI	CO, ppm	CO, EI	CO_2, %	CO_2, EI	NO_X, ppm	NO_X, EI	EFF, %	F A, sample	F A, measure	Yaug
10.02	580	1600	31.2	2066	71	5.08	2731	24	1.35	95	0.0257	0.0291	0.306
10.02	1600	1017	18.2	2183	68	5.99	2906	34	1.75	97	0.0292	0.0319	0.359
10.02	1900	529	8.78	2514	73	6.36	2905	46	2.20	97	0.0312	0.0314	0.405
10.02	2195	352	5.22	4557	118	7.13	2904	55	2.34	97	0.0355	0.0387	0.483
10.02	2710	240	...32	6731	163	7.03	2671	61	2.42	96	0.0360	0.0416	0.534
10.02	3040	180	2.34	12141	276	7.63	2721	62	2.31	93	0.0412	0.0414	0.583
10.02	3650	90	1.05	7355	150	9.70	3108	96	3. 2	97	0.0481	0.0497	0.677
10.02	3985	45	0.49	11167	214	9.93	2984	97	3.05	96	0.0508	0.0532	0.738
10.02	4305	24	0.25	13841	250	10.69	3037	112	3.33	95	0.0554	0.0565	0.796
10.02	1945	22	0.21	20273	346	11.08	2969	125	3.50	94	0.0600	0.0601	0.858
10.02	5255	10	0.09	32370	529	12.13	3113	132	3.54	91	0.0700	0.0629	0.909
10.02	5910	26	0.23	37150	575	12.11	2945	136	3.46	92	0.0721	0.0666	0.973
10.02	6210	113	0.96	55086	818	12.09	2818	140	3.41	88	0.0803	0.0697	1.028
11.01	368	3491	70.9	2192	78	1 85	2706	21	1.23	91	0.0256	0.0280	0.287
11.01	655	3016	54.6	2694	85	5.28	2628	23	1.20	93	0.0276	0.0315	0.356
11.01	952	2051	33.2	3617	102	6.43	2729	31	1.44	94	0.0314	0.0353	0.424
11.01	1212	1410	21.1	4658	122	6.43	2640	39	1.67	95	0.0330	0.0384	0.477
11.01	2543	1015	14.0	10531	254	7.41	2802	49	1.94	93	0.0399	0.0418	0.534
11.01	2820	730	9.44	13817	313	7.54	2682	50	1.86	92	0.0419	0.0446	0.587
11.01	3242	465	5.58	23756	499	7.92	2614	51	1.76	88	0.0481	0.0482	0.650
11.01	1213	1490	16.0	23808	448	9.33	2754	57	1.76	89	0.0548	0.0542	0.666
11.01	4488	1605	17.4	25322	480	9.45	2812	56	1.74	88	0.0561	0.0538	0.710
11.01	4720	1786	19.5	22209	426	9.25	2786	56	1.76	89	0.0539	0.0531	0.736
11.0	4938	1150	11.8	26648	479	10.10	2852	67	1.98	89	0.0593	0.0568	0.802
11.0	5686	990	9.78	28614	495	10.68	2899	70	1.99	90	0.0626	0.0593	0.844
11.01	5916	1300	12.28	30844	510	10.59	2750	76	2.06	90	0.0634	0.0621	0.895
11.01	6130	4201	37.50	47774	747	10.37	2544	64	1.64	84	0.0718	0.0660	0.962
11.01	6665	7447	64.3	56324	851	9.58	2273	52	1.29	80	0.0741	0.0681	1.005
11.01	9113	5024	50.0	33692	587	8.84	2420	30	0.86	83	0.0591	0.0588	0.836
12.01	1280	2171	50.8	1953	80	4.34	2792	28	1.87	93	0.0225	0.0212	0.227
12.01	1785	1876	40.6	1855	70	4.88	2906	27	1.70	94	0.0248	0.0262	0.262
12.01	2215	287	5.66	1886	65	5.34	2898	32	1.84	98	0.0261	0.0288	0.310
12.01	2535	204	3.65	2040	64	6.04	2969	41	2.13	98	0.0293	0.0319	0.362
12.01	2980	635	10.6	2157	63	6.61	3028	58	2.78	97	0.0322	0.0343	0.405
12.01	3290	350	5.39	2487	67	6.93	2932	81	3.58	98	0.0336	0.0372	0.457
12.01	3550	218	3.10	3582	89	7.50	2930	97	3.95	98	0.0367	0.0404	0.513
12.01	4225	770	10.5	4244	102	8.33	3133	87	3.42	97	0.0409	0.0421	0.540
12.01	4920	588	7.62	4262	97	8.73	3112	92	3.41	97	0.0427	0.0445	0.583
12.01	5870	291	3.56	4466	96	9.67	3253	109	3.84	98	0.0467	0.0473	0.633
12.01	6200	185	2.17	4531	93	10.11	3261	119	4.02	98	0.0486	0.0494	0.670
12.01	6610	80	0.88	6031	116	10.98	3316	142	4.47	98	0.0531	0.0530	0.733
12.01	7010	39	0.40	10114	182	11.70	3309	155	4.58	97	0.0580	0.0568	0.800
12.01	7375	27	0.27	14621	253	12.63	3435	164	4.68	96	0.0640	0.0591	0.842
12.01	7725	22	0.21	19338	317	12.75	3288	167	4.50	96	0.0667	0.0626	0.902
12.01	8545	9	0.08	20621	334	13.13	3339	179	4.75	96	0.0689	0.0635	0.919
12.01	9115	13	0.11	32969	500	13.88	3306	188	4.69	95	0.0776	0.0681	1.001
12.01	12300	8	0.07	22200	352	13.55	3372	185	4.81	96	0.0711	0.0650	0.945

As can be seen, the swirling flow field had no effect on the radial position of the fuel spray. Centrifugal forces created by the flowfield would be expected to force the fuel to the outer wall due to the larger density of the fuel. However, if the fuel evaporates and becomes partially mixed with the airflow the resulting mixture has a density essentially equal to that of air alone. As a result, the centrifugal flowfield would not be able to separate the fuel from the air. This is evidently what occurred in these tests. The high inlet temperature flash vaporized the fuel spray and the turbulence created by the sprayring elements aided in mixing the fuel and air. At the first measurement plane, which was 3.8 cm (1.5 inches) downstream of the injection plane, the fuel and air were sufficiently mixed to negate any effect of the swirling flowfield on the radial position of the fuel spray.

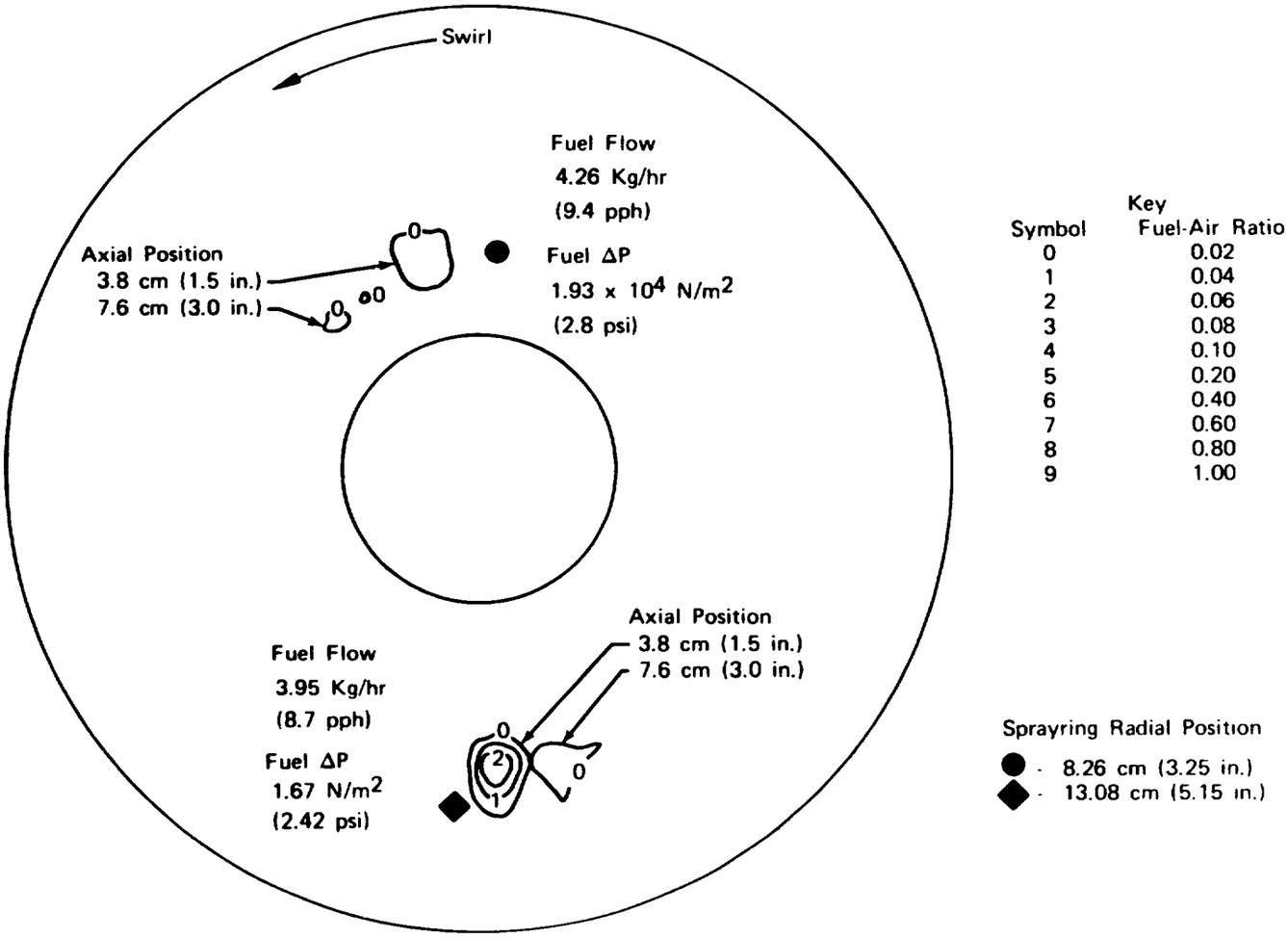

Figure 30. Fuel Dispersion Data: Airflow = 4.46 Kg/hr (9.84 lb_m/sec); Inlet Mach No. = 0.254; Inlet Temperature = 599°C (1110°F)

FD 95584

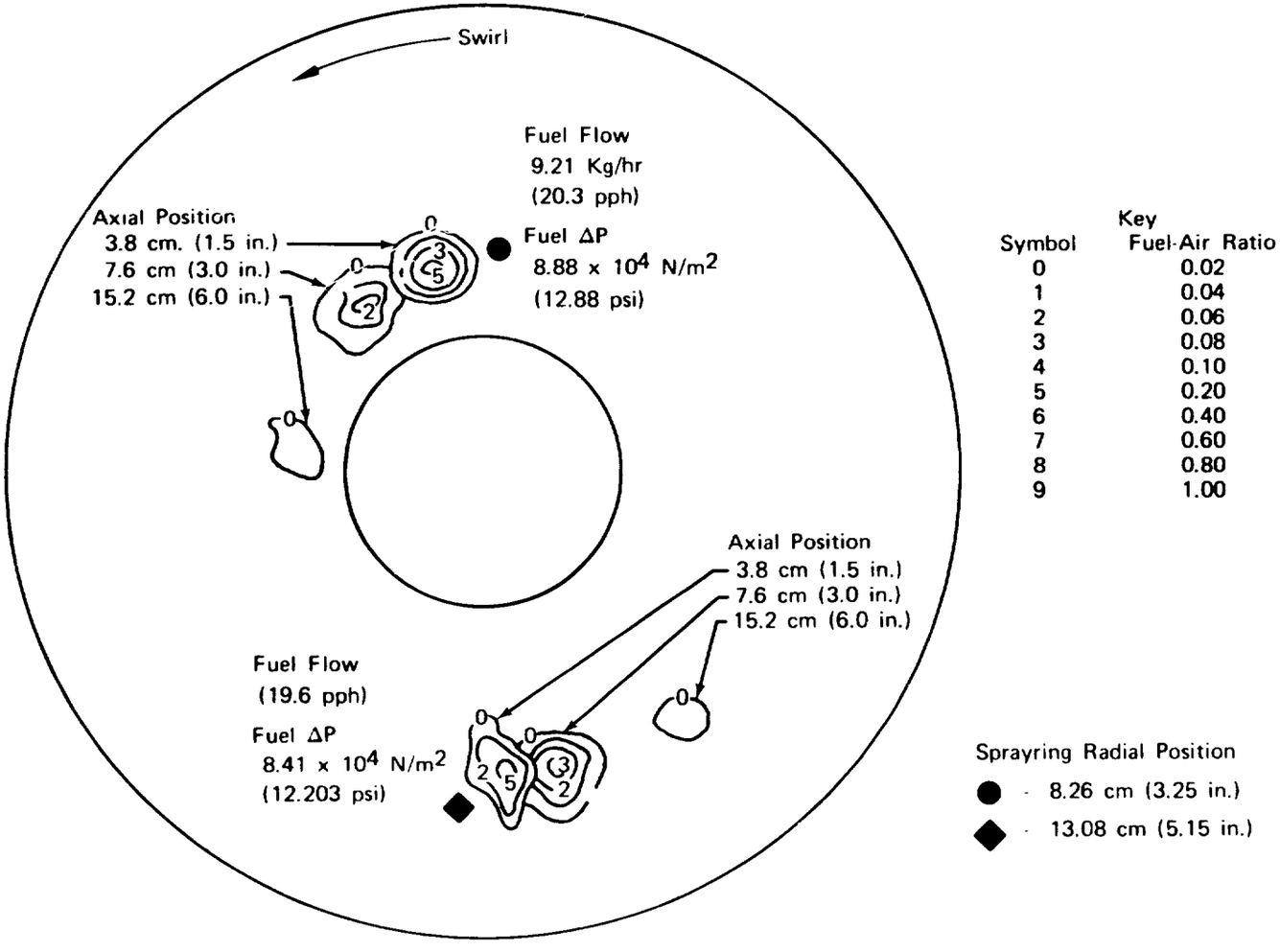

Figure 31. Fuel Dispersion Data: Airflow = 4.47 Kg/sec (9.86 lb_m/sec); Inlet Mach No. = 0.253; Inlet Temperature = 602°C (1116°F)

FD 95585

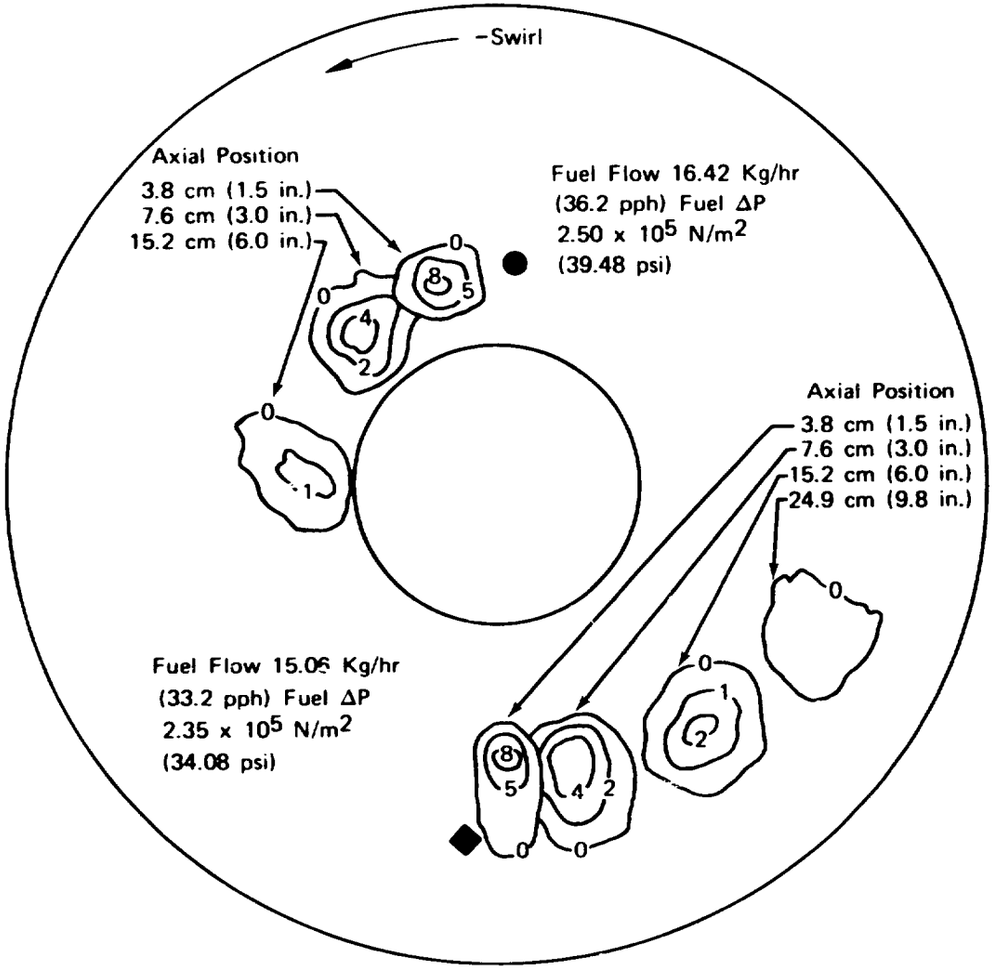

Key

Symbol	Fuel-Air Ratio
0	0.02
1	0.04
2	0.06
3	0.08
4	0.10
5	0.20
6	0.40
7	0.60
8	0.80
9	1.00

Sprayring Radial Position

● - 8.26 cm (3.25 in.)

◆ - 13.08 cm (5.15 in.)

Figure 32. Fuel Dispersion Data: Airflow = 4.51 Kg/sec (9.95 lb_m/sec); Inlet Mach No. = 0.255; Inlet Temperature - 599°C (1110°F)

FD 95586

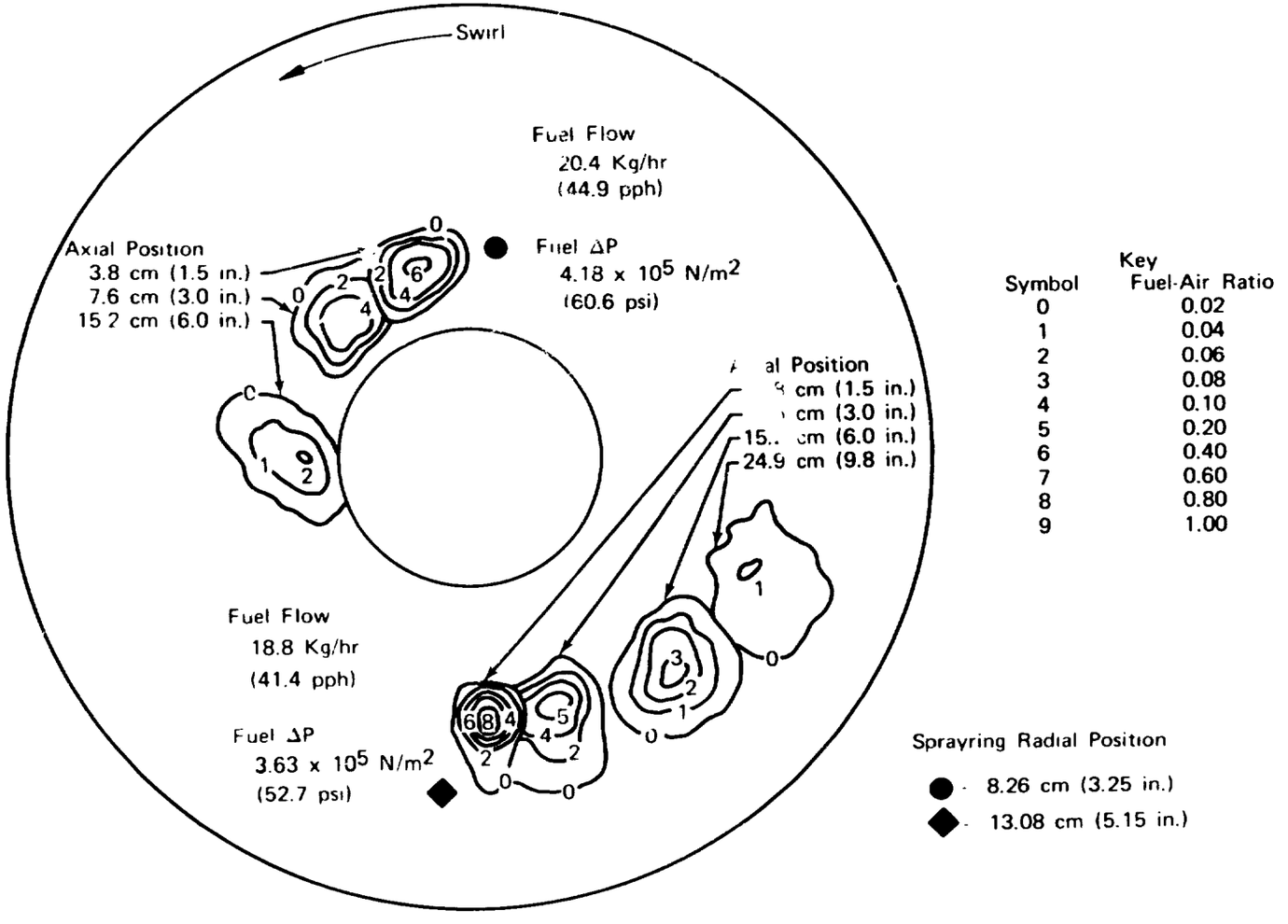

Figure 33. Fuel Dispersion Data: Airflow = 4.52 Kg/sec (9.95 lb_m/sec); Inlet Mach No. = 0.254; Inlet Temperature = 599°C (1110°F)

FD 95587

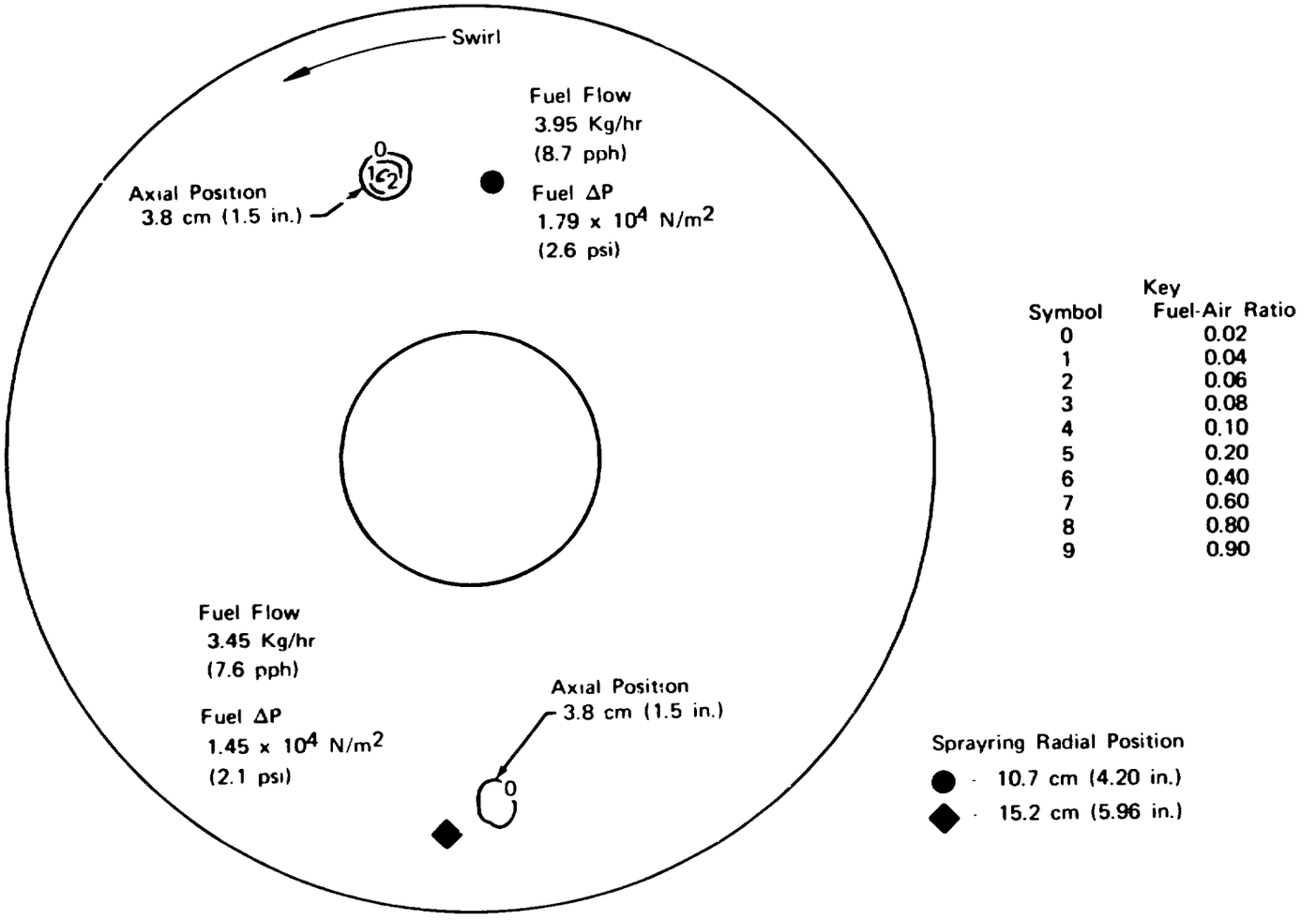

Figure 34. Fuel Dispersion Data: Airflow = 4.50 Kg/sec (9.92 lb_m/sec); Inlet Mach No. = 0.253 Inlet Temperature = 600°C (1112°F)

FD 95589

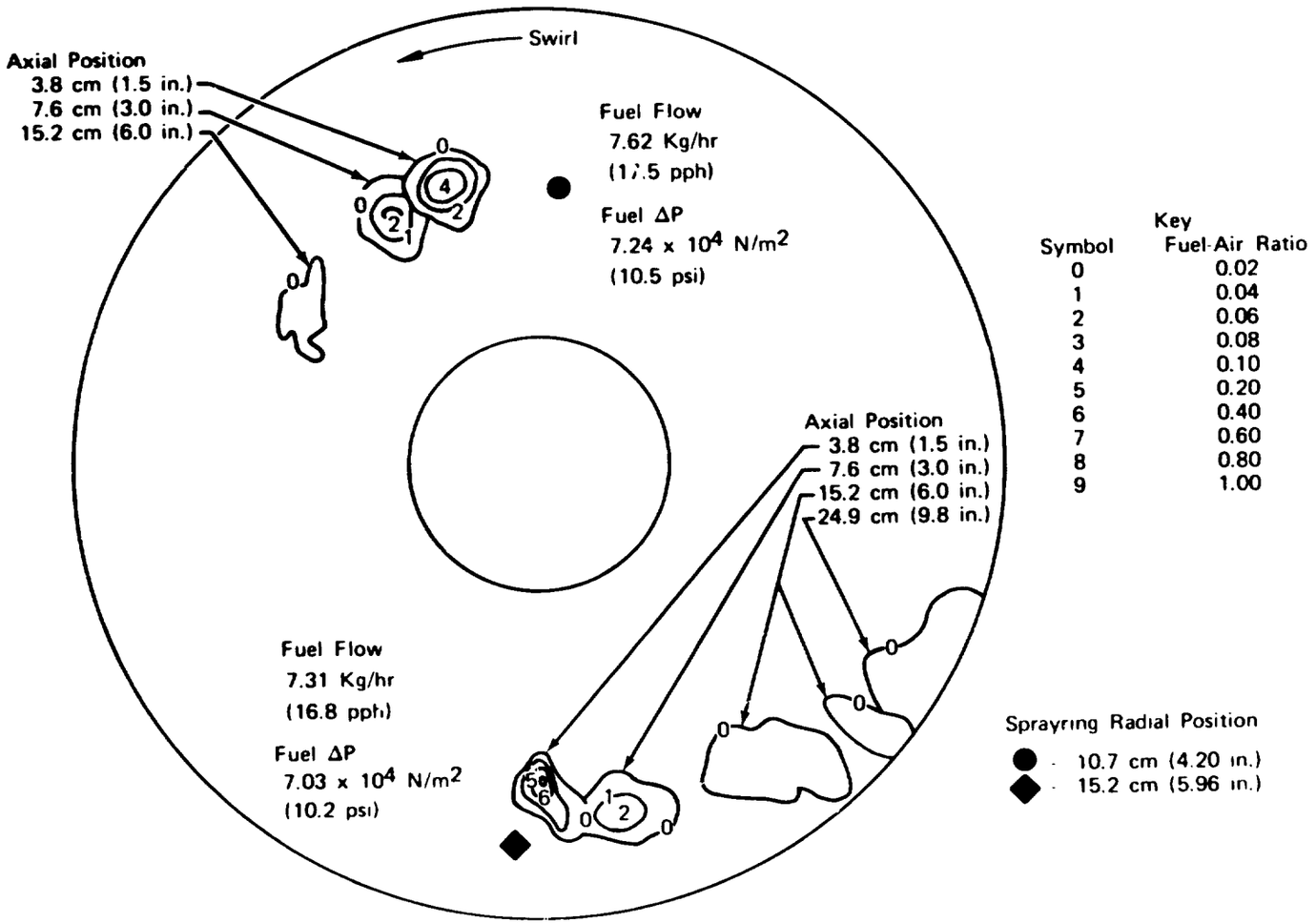

Figure 35. Fuel Dispersion Data: Airflow = 4.41 Kg/sec (10.13 lb_m/sec); Inlet Mach No. = 0.255; Inlet Temperature = 578°C (1073°F)

FD 95590

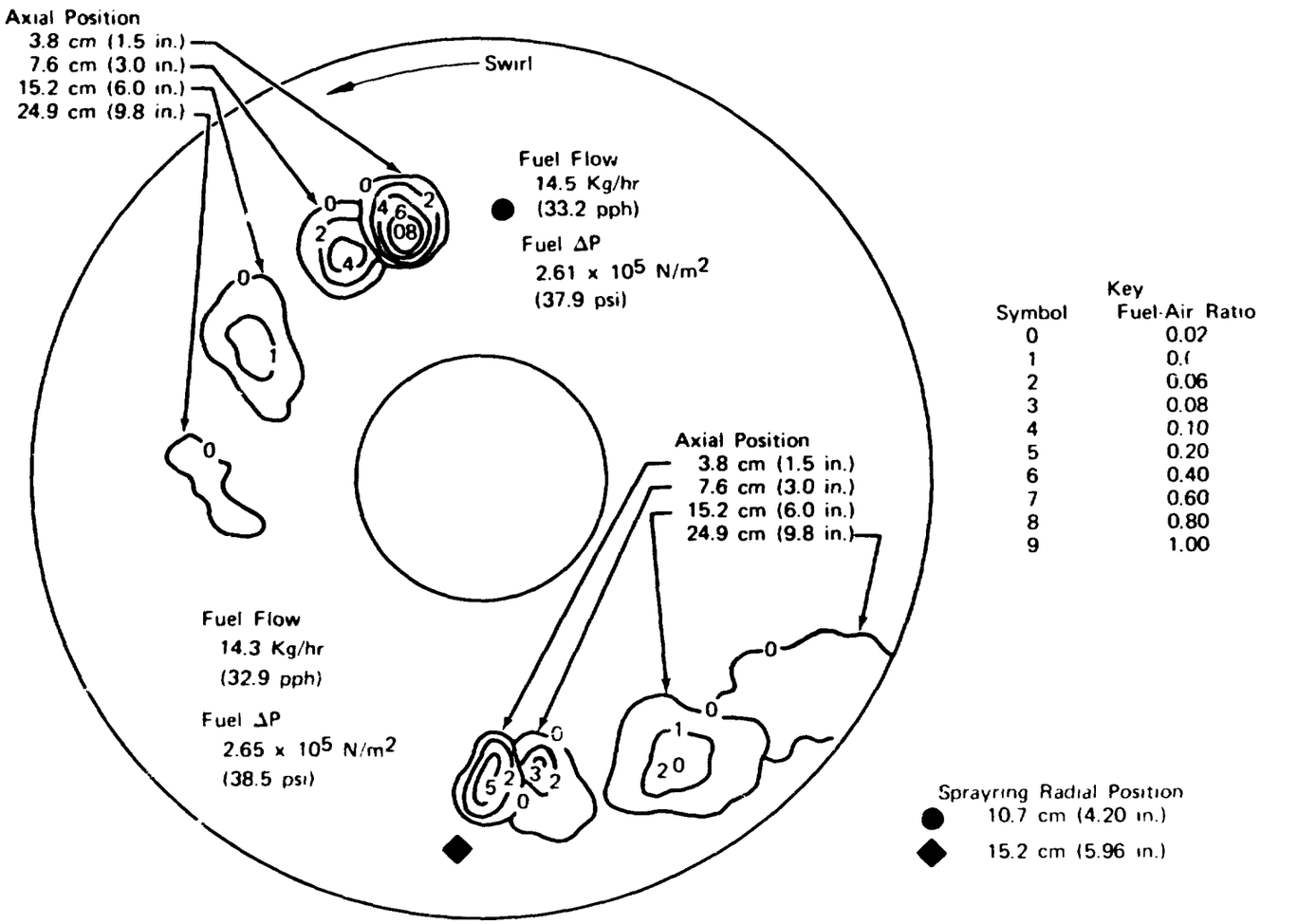

Figure 36. Fuel Dispersion Data: Airflow - 4.44 Kg/sec (10.2 lb_m/sec); Inlet Mach No. - 0.256; Inlet Temperature 578°C (1072°F) FD 95591

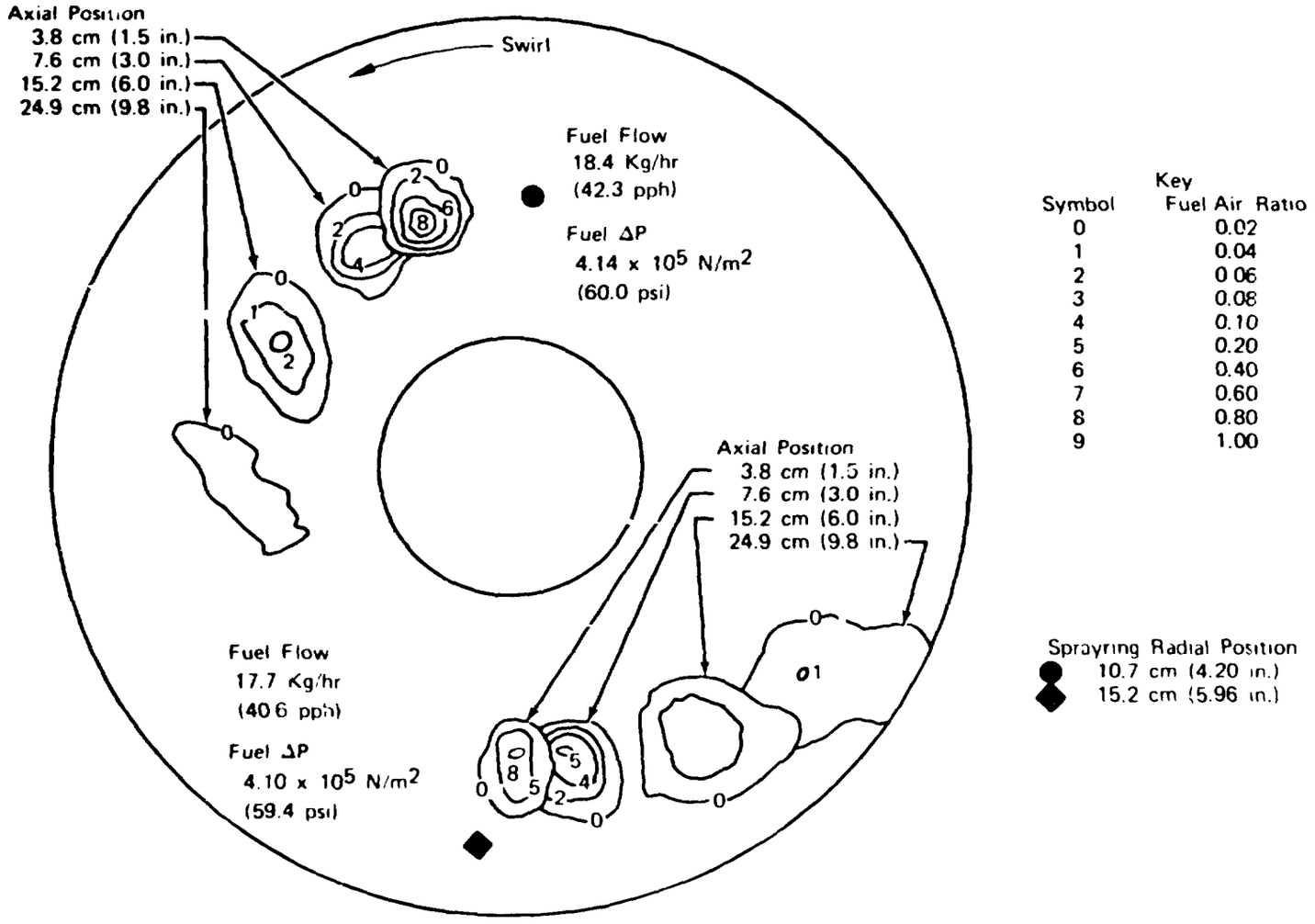

Figure 37. Fuel Dispersion Data: Airflow - 4.43 Kg/sec (10.18 lb_m/sec); Inlet Mach No. - 0.256; Inlet Temperature 578°C (1073°F) FD 95592

The data do show that the spray from the inner and outer sprayring elements - radial positions 8.26 and 15.2 cm (3.25 and 5.96 inches), respectively - were affected by the expansion of the flow downstream of the pilot and the tailcone. The spray at the inner sprayring element moved in toward the centerline as the flow expanded to fill the region downstream of the tailcone. Likewise, the spray from the outer sprayring element moved toward the outer wall as the flow expanded downstream of the pilot annular passage.

The circumferential motion of the spray can be simply described as a helix, with a helix angle equal to ($\pi/2$ - swirl vane angle).

The results of these measurements show that, for the augmented turbojet application, the sprayring design for a swirling flow augmentor can be based on conventional augmentor design techniques. The circumferential motion of the fuel spray should cause no problems since most augmentors are designed to be symmetrical and, therefore, circumferential displacement of the fuel would have no effect on the overall fuel distributions within the augmentor.

Air Angle Data

Concurrently with the fuel dispersion and trajectory measurements, the air angle between the mainstream flow direction and the axial flow direction was also determined. As indicated in figure 19, data were obtained by radially traversing the flow at axial positions 1.65, 10.72, and 21.41 cm (0.65, 4.22, and 8.43 inches) downstream of the fuel injection plane. The data are shown in figures 38, 39, and 40 for the respective axial positions.

The air angle was found to be constant and equal to the swirl vane angle over most of the radial span. Near the outer wall, the air angle increased due to the expansion of the flow downstream of the pilot resulting in a decrease in the axial component of the velocity near the outer wall. The tangential velocity was also decreasing due to the increasing radius. However, the radius change and, hence, tangential velocity change was small relative to the decrease in axial velocity. The result was an increase in local air angle.

Near the centerline the air angle also increased, as shown in figure 40. However, the increase was due both to a decrease in the axial velocity component resulting from expansion as well as an increase in the tangential component resulting from the decrease in radius. Inside a radius of approximately 2.54 cm (1.00 inch), the air angle increased to a measured value of 1.57 radians (90 degrees). This evidently represents a region of reverse flow. However, the measurement system was not able to measure air angles above this value, so definitive data are not available to verify this.

Augmentor Hot Test Results

Augmentor hot testing was also conducted to evaluate the performance of the concentric sprayring-type fuel injectors. The particular performance parameters determined were combustion efficiency, lean blowout limit, flame-front location, pressure loss, and combustion stability. In addition, in the process of determining combustion efficiency, exhaust emissions data on UHC, CO, and NO_x were obtained.

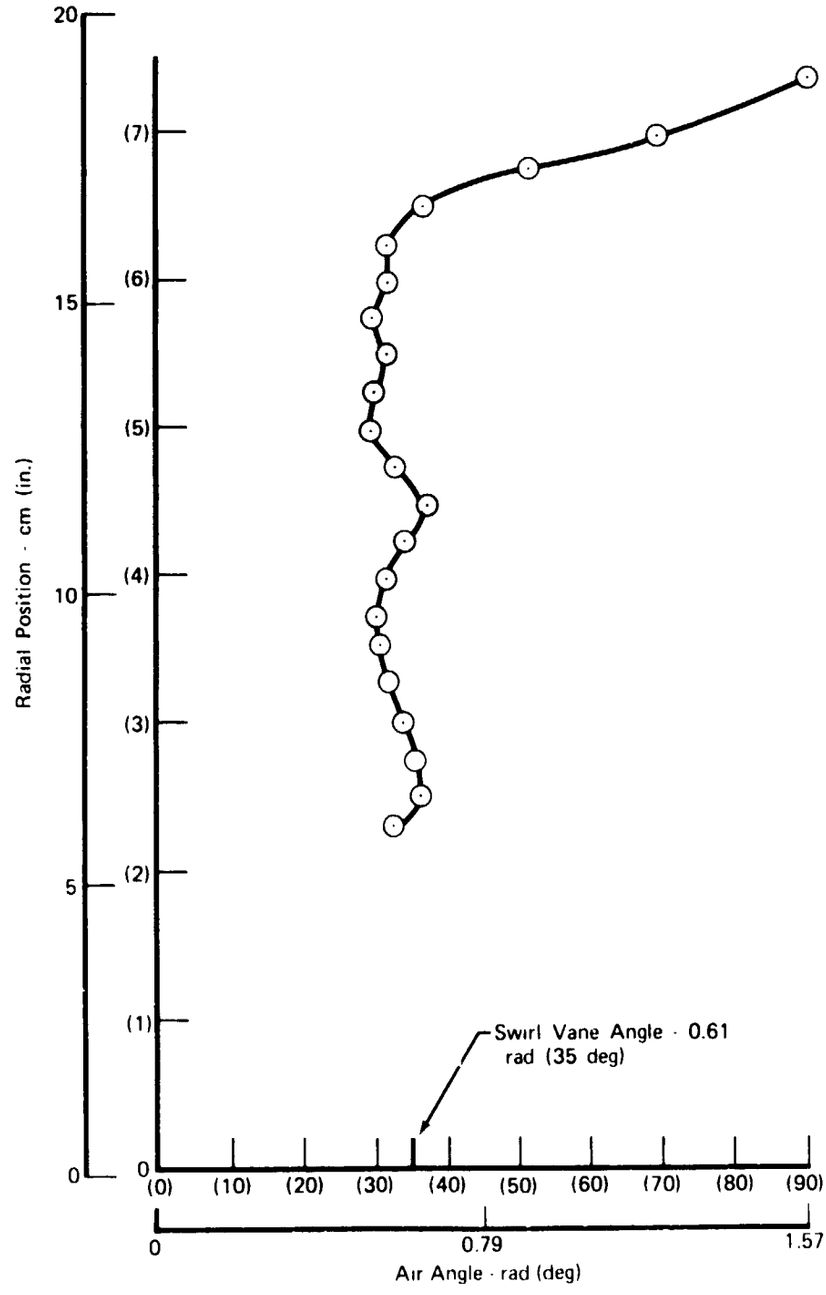

Figure 38. Air Angle Profile: Probe Location 1.65 cm FD 95593 (0.650 in.) Downstream of Sprayrings; Inlet Temperature = 591°C (1095°F); Inlet Pressure = 1.087×10^5 N/m^2 (15.77 psia); Inlet Mach No. = 0.254; Airflow = 4.38 Kg/sec (10.051 lb_m/sec)

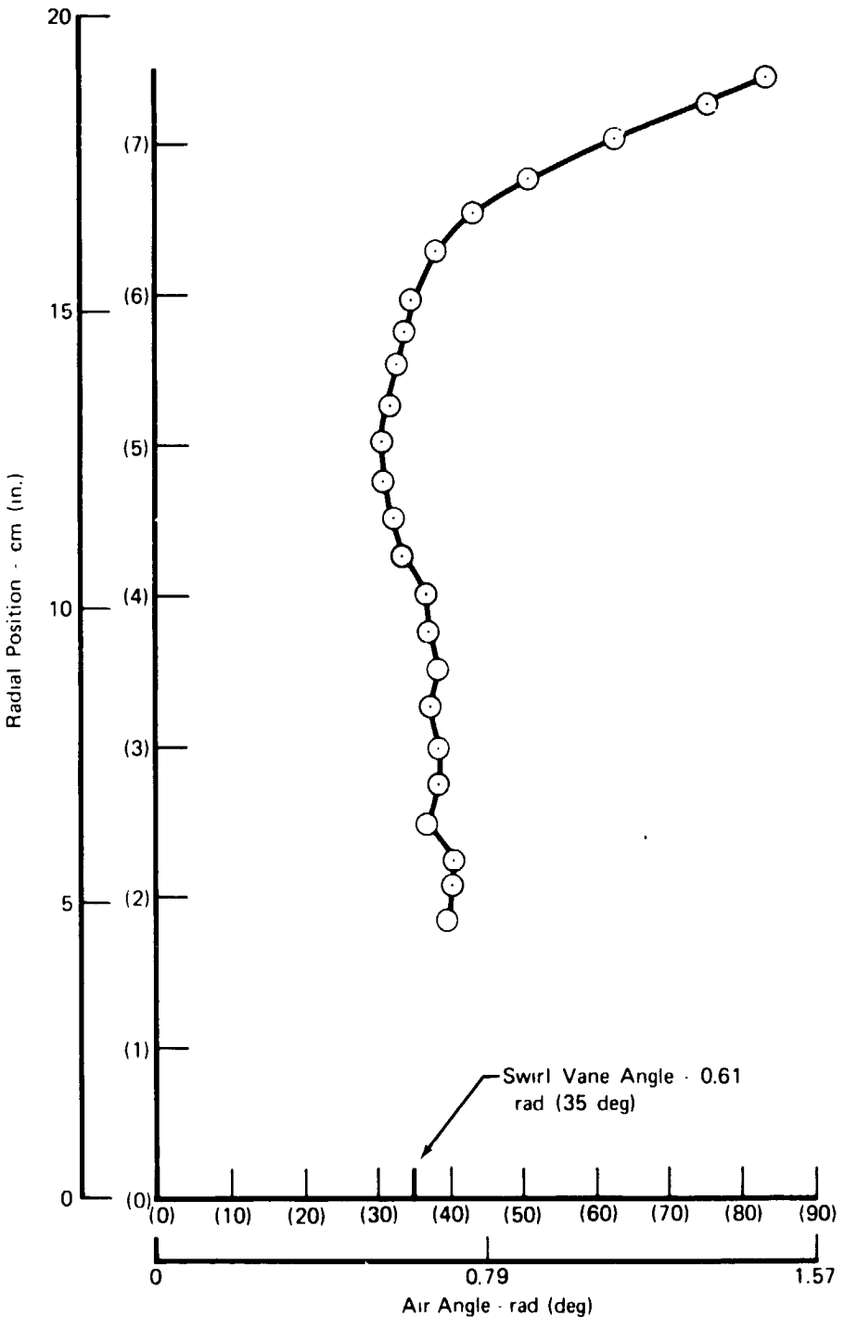

Figure 39. Air Angle Profile: Probe Location = 10.7 cm (4.220 in.) Downstream of Sprayrings; Inlet Temperature = 591°C (1095°F); Inlet Pressure = 1.087×10^5 N/m^2 (15.77 psia); Inlet Mach No. = 0.254; Airflow = 4.38 Kg/sec (10.051 lb_m/sec)

FD 95594

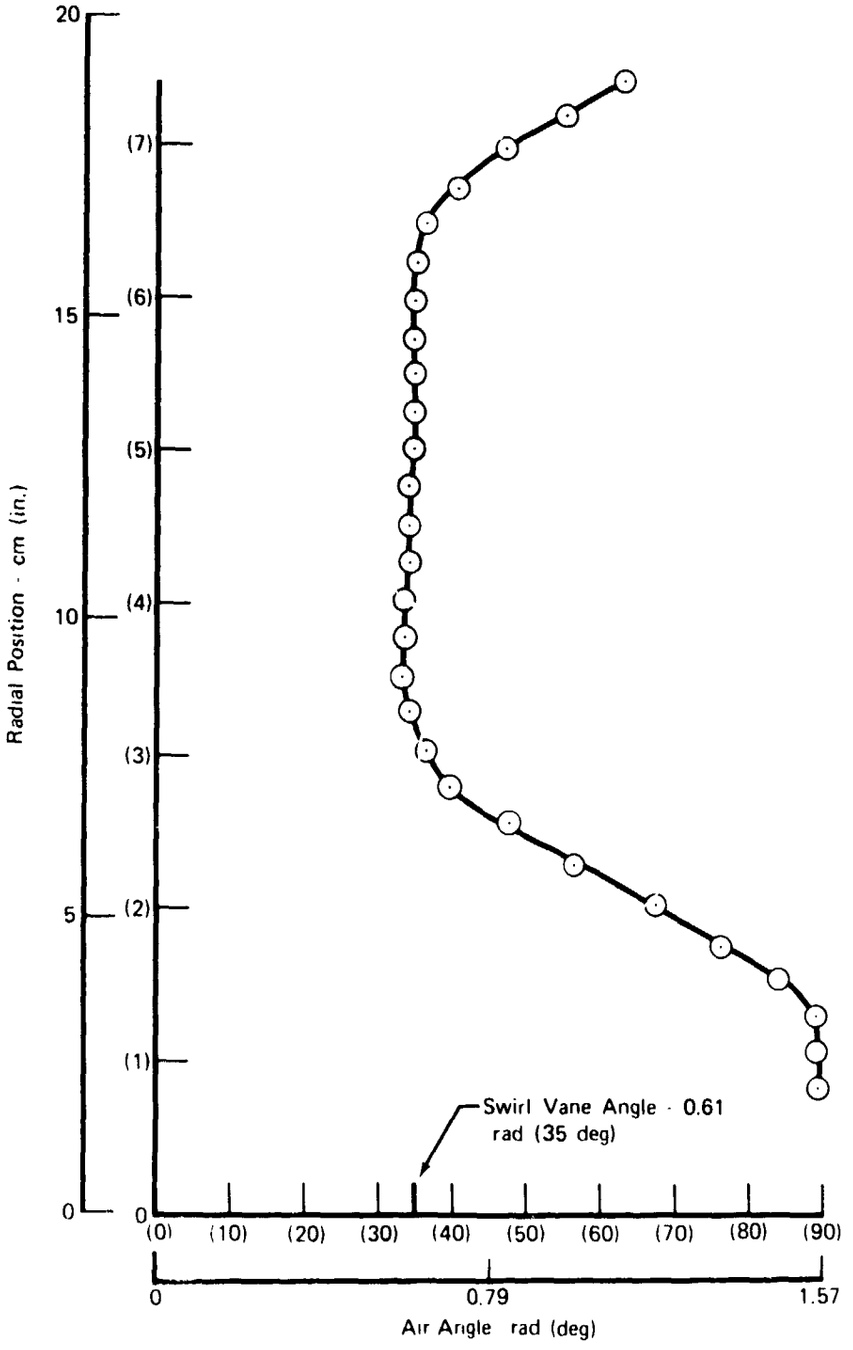

Figure 40. Air Angle Profile: Probe Location - 21.4 cm (8.430 in.) Downstream of Sprayrings; Inlet Temperature - 591°C (1095°F); Inlet Pressure - 1.087×10^5 N/m^2 (15.77 psia); Inlet Mach No. = 0.254; Airflow = 4.38 Kg/sec (10.051 lb_m/sec)

FD 95595

Combustion Efficiency

Two methods were used to calculate the combustion efficiency. In the first method, the outlet temperature was calculated from known values of mass flow, nozzle total pressure, geometric area, and discharge coefficient. The efficiency was then determined by comparing the calculated temperature rise with an ideal temperature rise based on fuel properties and known inlet conditions. In the second method, the combustion efficiency was calculated from the measured values of unburned hydrocarbon and carbon monoxide remaining in the exhaust.

The nozzle discharge coefficient used in the first method (the so called "choked-nozzle method") of calculating the combustion efficiency was determined during the test program described in Reference 2. The nozzle used in that program was also used in the present program. However, in reducing the data, all of the calculated combustion efficiencies were extremely high, greater than 118% at all test points. Following a thorough examination of the data, it was concluded that the presence of the gas sampling probes was interfering with the nozzle discharge flow. Consequently, a new nozzle discharge coefficient relationship was established using a single data point obtained during the current test programs with the gas sampling probes installed. This procedure is discussed in detail in Appendix A. However, the procedure failed to correct all of the efficiency data, as can be inferred from the greater than 100% efficiency values at a large number of test points. Only a full calibration of the exhaust nozzle could alleviate this problem. Therefore, only the combustion efficiencies calculated using the measured exhaust products will be discussed in the following paragraphs.

The gas sample calculated combustion efficiency data are considered to be accurate for the following reasons. First, the gas sample is representative of the total augmentor flow. This is evidenced by the good agreement between the gas sample calculated fuel-air ratio and the fuel-air ratio determined using measured values of fuel and airflow. Figure 41 shows the correlation between the two fuel-air ratios. As can be seen the gas sample calculated fuel-air ratio is within 10% of the measured fuel-air ratio for most of the test points investigated. Second, due to the fact that combustion inefficiency is measured by gas sampling, rather large errors in the sample can be tolerated before the error in efficiency becomes intolerable. In the following presentation the choked nozzle combustion efficiencies are also presented for the sake of completeness only.

The augmentor was tested with length-to-diameter (L/D) ratios of 0.87 and 1.37. Figure 42 shows the results obtained with the longer duct using the baseline sprayrings. The baseline sprayrings were those designed using the fuel dispersion and trajectory data. As can be seen, the efficiency was high, 95% over most of the operating range. At the higher equivalence ratios, the efficiency fell to approximately 92%. Note that the data shown were obtained with the zone 2 and 3 sprayrings only. The test point fuel flows were improperly set such that data in which the zone 4 sprayring was operating were obtained at equivalence ratios above 1.2. As this is too high for practical interest, these data are not shown.

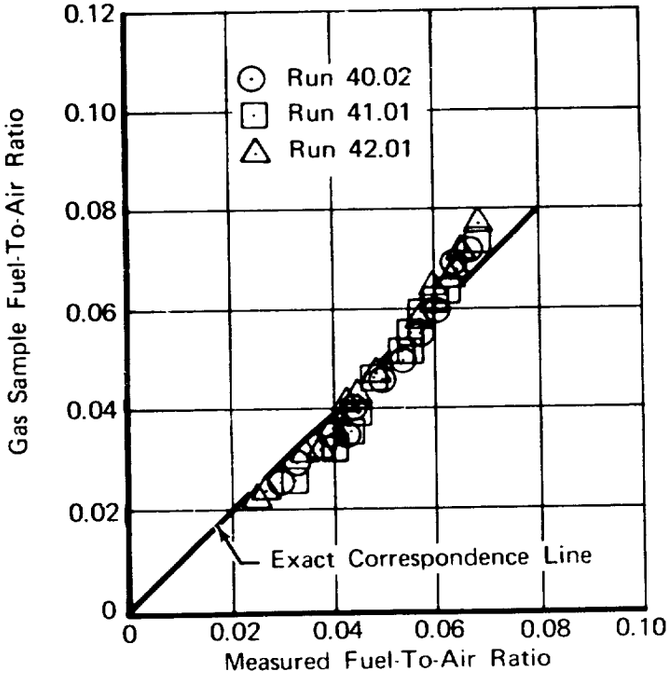

Figure 41. Comparison of Gas Sample Calculated Fuel-Air Ratio With Measured Fuel-Air Ratio

FD 95718

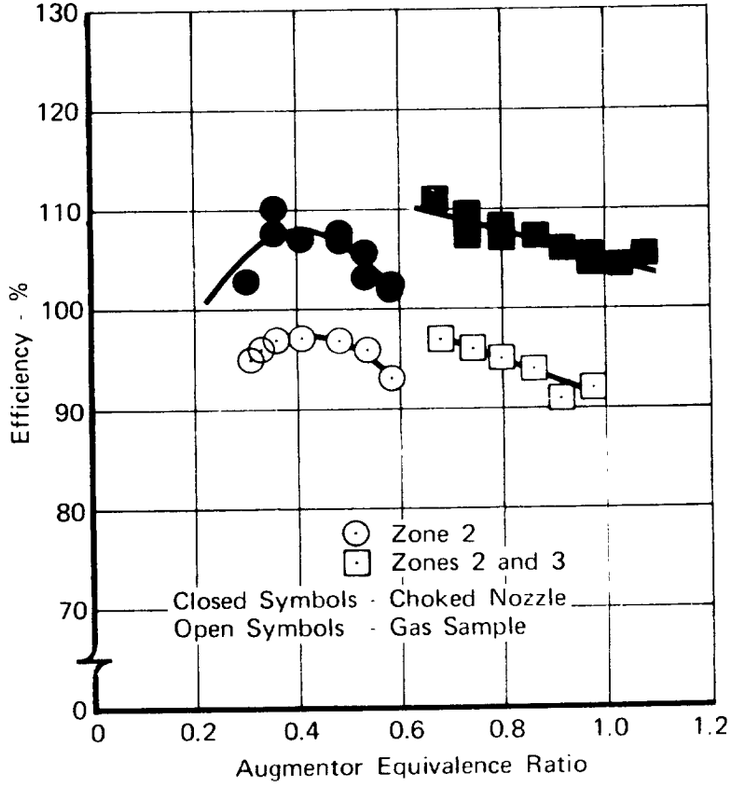

Figure 42. Augmentor Efficiency Test No. 40.02. Configuration Consisted of: 0.61-rad (35-deg) Swirl Vanes, L/D = 1.373

FD 95715

Following this test, it was found that the spray from the zone 4 sprayring was impinging on the rig centerbody. To correct this problem, the zone 4 sprayring designed using the fuel dispersion data was replaced with a modified zone 4 sprayring. This sprayring had more and larger injection orifices. Therefore, the fuel penetration was substantially less. Also, the mean diameter of the sprayring was larger than the baseline sprayring, thus, minimizing the possibility of fuel spray impingment on the centerbody.

The test results using the modified zone 4 sprayring are shown in figure 43. The data show that, by properly zoning the fuel flow between the three sprayrings, the combustion efficiency at full power (equivalence ratio = 1.0) was increased approximately 3 points. The combustion efficiency at ϕ_{aug} = 1.0 was 95% using all three sprayrings compared to 92% using only the zones 2 and 3 sprayrings.

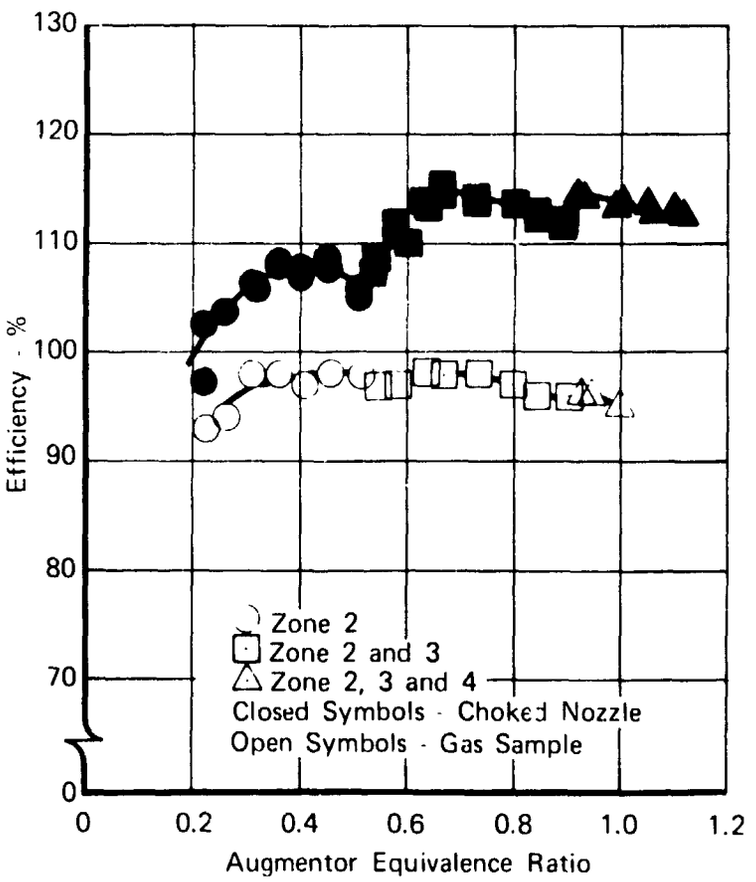

Figure 43. Augmentor Efficiency Test No. 42.01. Configuration Consisted of: 0.61-rad (35-deg) Swirl Vanes, L/D = 1.373, and Modified Zone 4 Sprayring FD 95716

In comparing the data of these two tests, a decrease of 3 efficiency points at the full-power condition using the zones 2 and 3 sprayrings only is not severe considering the poor fuel distribution. The tolerance of the augmentor to rather poor fuel distributions can be attributed to the duct length used. During the design of the augmentor sprayrings, the fuel dispersion data used were obtained over

a range of augmentor L/D's from 0.1 to 0.65 in accordance with the predicted flamefront location. The L/D of the augmentor using the longer duct was 1.37, or twice the maximum length used in the fuel dispersion studies. This increased length provides much more time for the fuel and air to mix and react, resulting in the high observed efficiencies using zones 2 and 3 only.

As shown in figure 44, when the augmentor was tested using the shorter duct (L/D = 0.87), the combustion efficiency using zones 2 and 3 only was not as good. As can be seen, the combustion efficiency, measured at an equivalence ratio of 1.0, and using zones 2 and 3 only, was 80%. The L/D of this configuration is roughly equal to that used to obtain the fuel dispersion data. Evidently this combustion length was not sufficient to wash out all of the effects of the off-design distribution of the fuel.

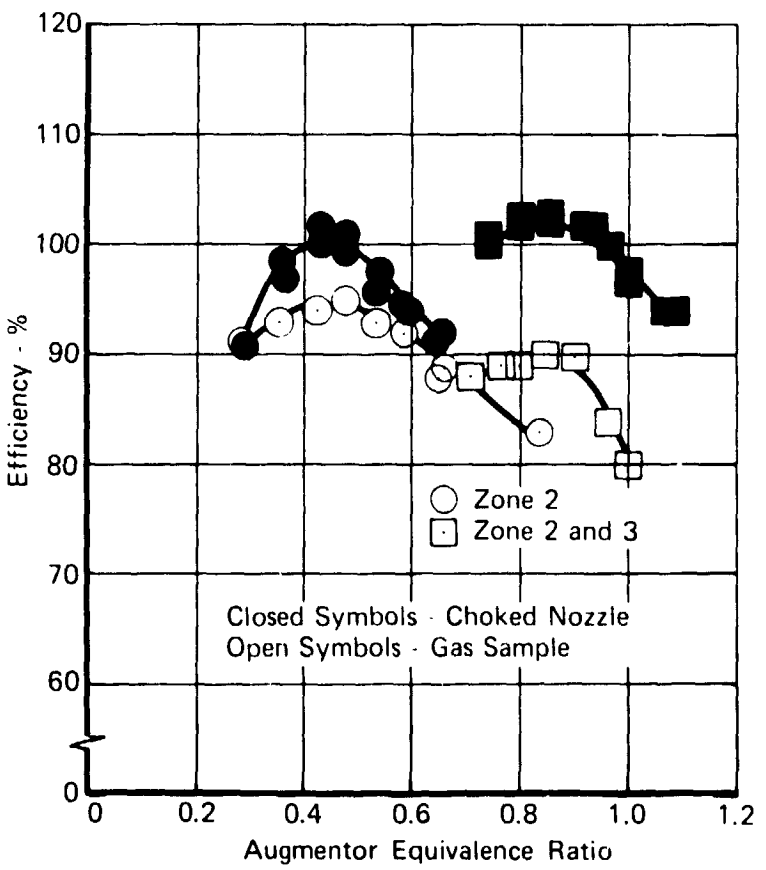

Figure 44. Augmentor Efficiency Test No. 41.01. Configuration consisted of 0.61-rad (35-deg) Swirl Vanes, L/D = 0.87, and Modified Zone 4 Sprayring

FD 95717

Augmentor Lean Blowout

In a swirling flow augmentor the only flameholding device is the pilot burner. As long as the pilot remains lit, the augmentor can be ignited. Consequently, the augmentor lean blowout is defined as the lean flamability limit of the pilot. This was determined to occur at an overall augmentor fuel-air ratio of 0.0618.

Flamefront Location

An attempt was made to locate the flamefront by measuring the increase in ionization that occurs in the reaction zone of a flame. As discussed in the Instrumentation Section, the ionization of the gases was determined by measuring the current passing between two electrodes immersed in the flame. Unfortunately, no definitive data were obtained using that system. Since the ionization probe was simply a length of chromel-alumel thermocouple wire, it was converted to a thermocouple by welding the lead wires together at the tip. A traverse was then made in which the temperature across the duct was measured. The resultant data are shown in figure 45 for the augmentor operating on all three fuel zones at an equivalence ratio of 1.12. The probe was located 36.1 cm (14.2 in.) downstream of the spray rings. The measured temperatures are much lower than gas stream temperatures due to heat conduction to the probe cooling water. It is not clear what the data means. The increase in temperature inside the 6.4-cm (2.5-inch) radius is probably due to flameholding off of the centerbody. Whether the increase in temperature above the 6.4-cm radius represents the location of the inward moving flamefront is not clear. Due to the high level of turbulence, there may not be a well-defined flamefront such as exists in laminar flame propagation.

Pressure Loss

The measured augmentor nonburning pressure loss data are shown in figure 46. These data were obtained by subtracting the Rayleigh heating losses from the overall augmentor total pressure loss. The data are presented in the form of a drag coefficient, which is given by

$$C_d = DPSV/Q_4$$

where

C_d = Drag Coefficient

Q_4 = Swirl Vane Inlet Dynamic Head, % of inlet total pressure

All tests conducted under this program were performed with the turbine simulator vanes installed. Independent tests conducted by the contractor have shown that the presence of these vanes results in a higher than actual total pressure loss. This was due to the geometry of the rig. The total pressure probes used to measure the augmentor inlet total pressure were located between the turbine simulator vanes. As a result, they sensed only the highest total pressure. The region behind each vane, where total pressures would be lowest, were not sampled. This bias of the inlet total pressure results in a larger than actual measured pressure drop across the swirl vanes. As reported in Reference 2, a series of tests were conducted without the turbine simulator vanes installed. The results of those tests are shown as the lower curve in figure 46. It is felt that these data better represent the total pressure losses of the augmentor due to the improvement in the inlet total pressure measurement. Also shown on figure 46 are typical nonburning pressure losses of current high-performance augmentors. As can be seen, the true swirl augmentor nonburning pressure loss represented by the lower curve is equal to that of current conventional augmentors.

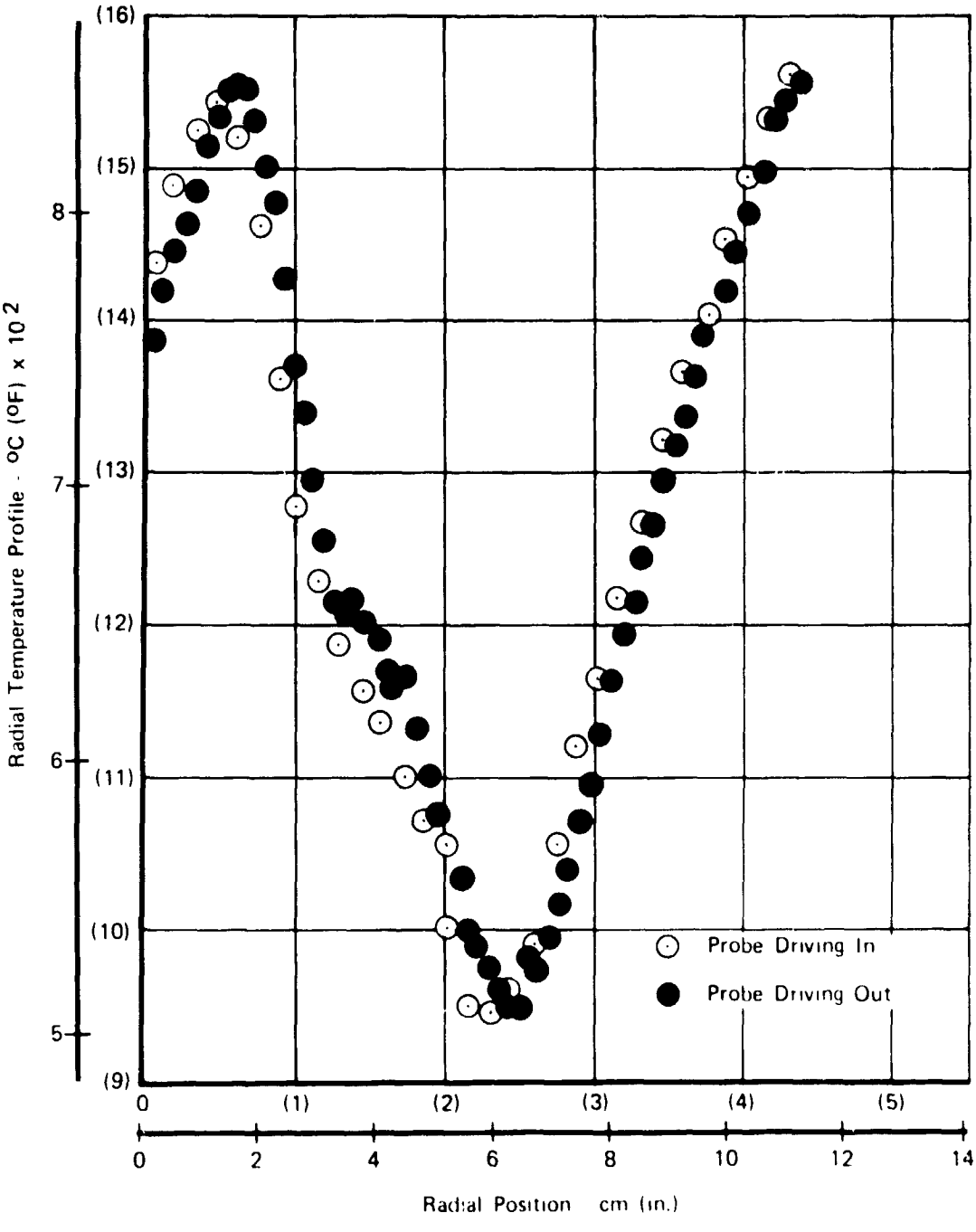

Figure 45. Combustion Chamber Temperature Traverse Probe Test No. 42.01. Augmentor Equivalence Ratio = 1.12, Axial Location 36.2 cm (14.1 in.) Downstream of Spravrings FD 95719

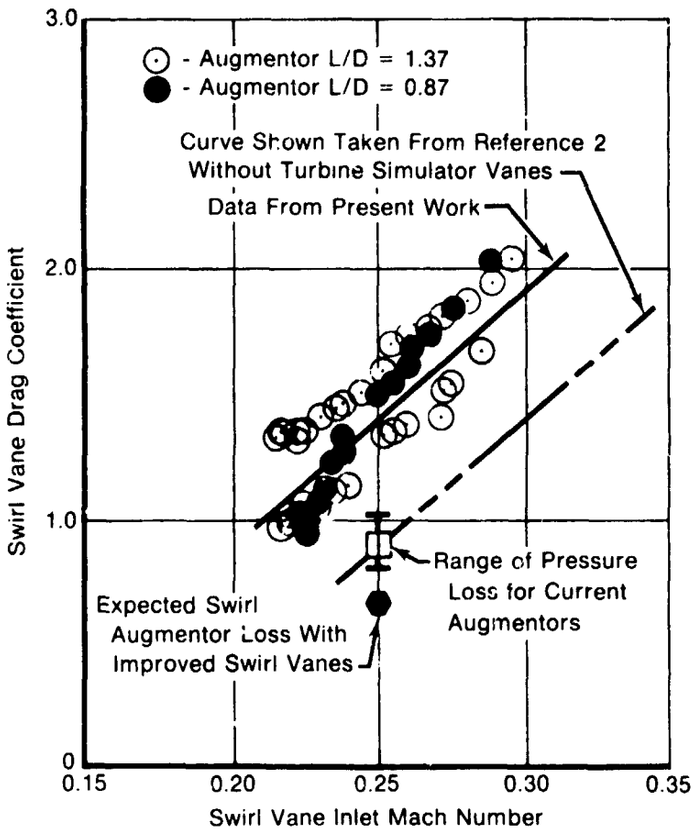

Figure 46. Augmentor Cold Flow Pressure Loss FD 99289

As mentioned in the section on Augmentor Design Features the swirl vanes were simple curved sheet-metal vanes. No attempt was made to contour the vanes to minimized vane profile losses. With well-contoured vanes, cold flow drag coefficients on the order of those shown in figure 46 may be possible.

Combustion Instabilities

In most augmentors, combustion instabilities can be a problem. In view of this, the swirling flow augmentor was equipped with high-response, pressure transducers to record any dynamic pressure oscillation that may have occurred. During the course of the test program, no instabilities occurred. Figure 47 is a typical spectrum plot obtained during the program. In previous tests with this augmentor, low-frequency pressure oscillations (rumble) occurred that could be circumvented by proper zoning of the three fuel zones. During this program, with the sprayrings used, rumble was not encountered for any zoning combination tested.

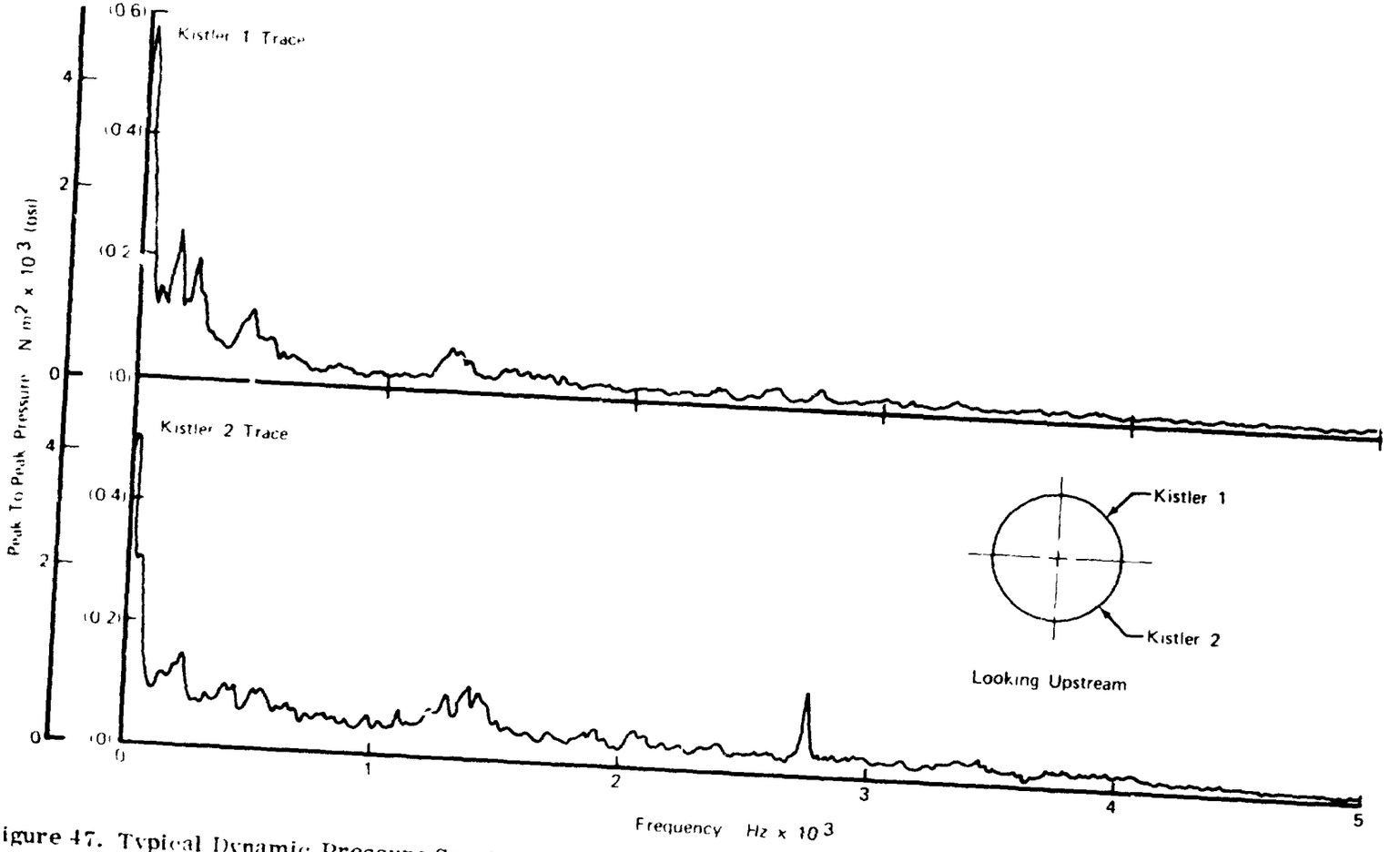

Figure 47. Typical Dynamic Pressure Spectrum Curve: Inlet Total Temperature = 683°C (1261°F); Inlet Total Pressure 2.3×10^5 N/m^2 (33.4 psia); Inlet Mach No. = 0.223; Augmentor Equivalence Ratio = 0.973; Augmentor Operating on Zones 2 and 3 Only

FD 95596

Exhaust Emissions

The exhaust emission data obtained during the program are tabulated in table 2. These data are also plotted in terms of emission indexes as a function of augmentor equivalence ratios in figures 48 through 51. Figures 48 through 50 are plots of the emission indexes of CO_2, CO, and UHC for the three augmentor tests. Figure 51 plots the NO_x emissions for all three tests. The CO emission indexes plotted are based on measured concentrations of CO. In calculating the combustion efficiency from the exhaust emission data, the equilibrium value of CO was subtracted from the measured value of CO. The equilibrium concentration of CO as a function of overall rig equivalence ratio was supplied by NASA and is shown in figure 52.

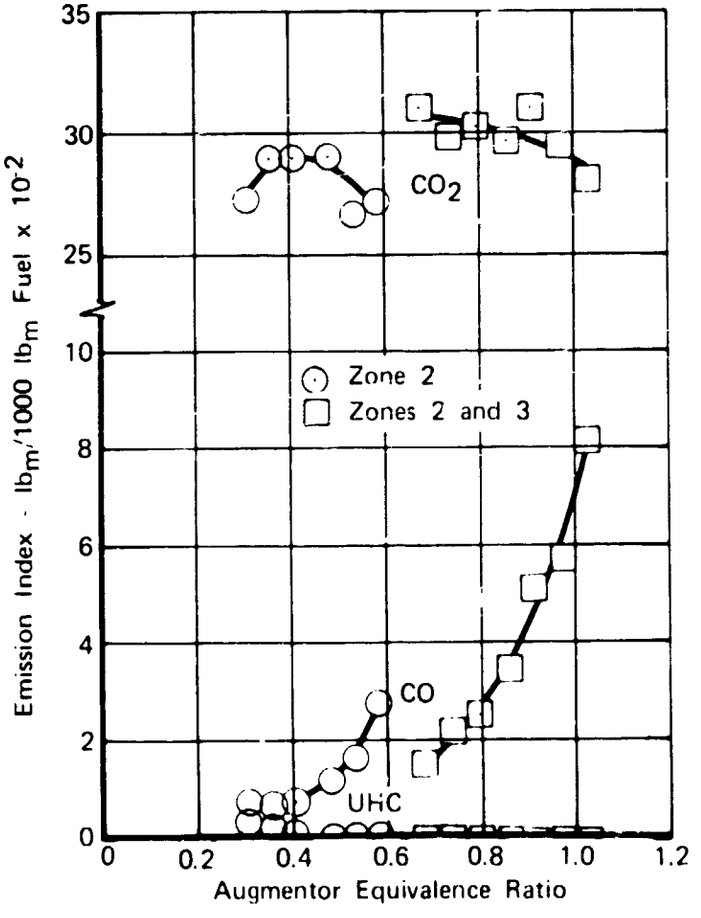

Figure 48. Gas Sample Data; Run 40.02 Augmentor L/D 1.37 Zones 2 and 3 Only FD 97550

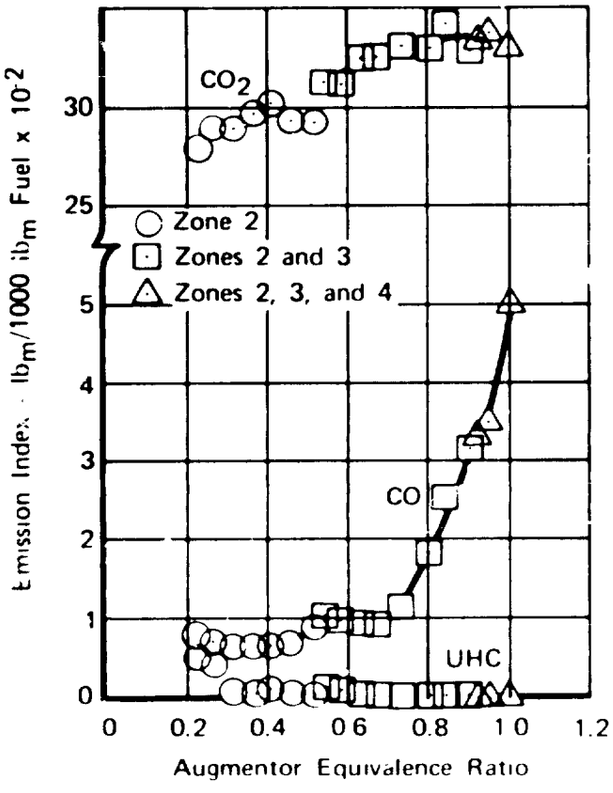

Figure 49. Gas Sample Data; Run 42.01, Augmentor L/D = 1.37, Zones 2, 3, and 4 FD 97551

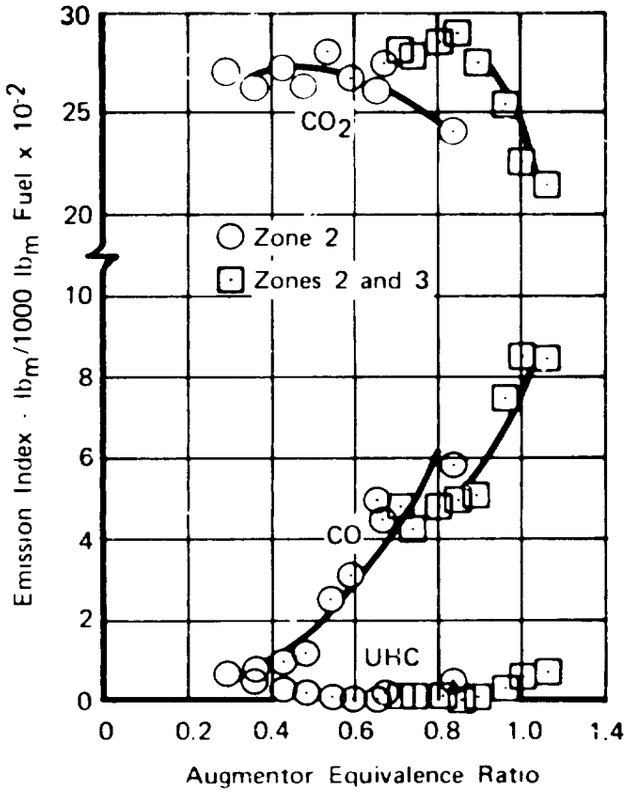

Figure 50. Gas Sample Data; Run 41.01, Augmentor L/D = 0.87, Zones 2 and 3 Only FD 97552

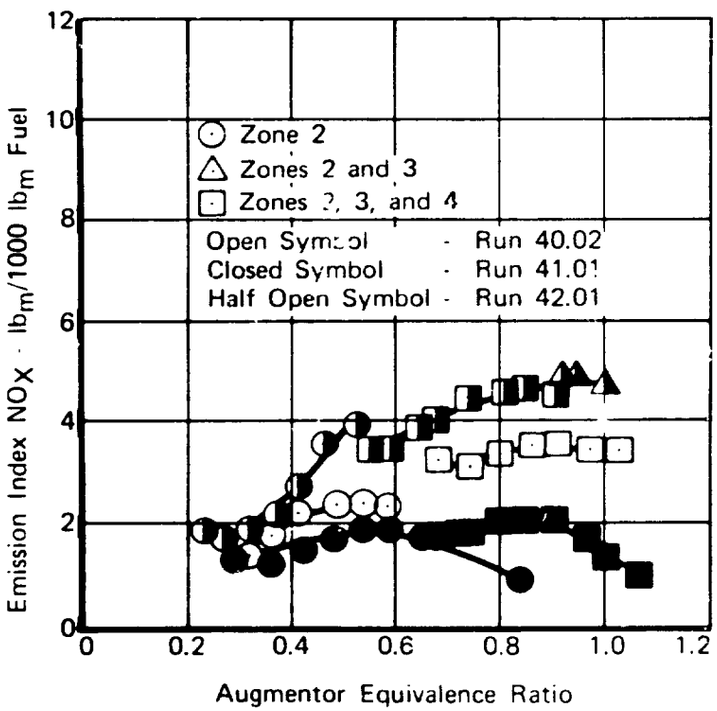

Figure 51. Emission Level of NO_X Obtained With Both Augmentor L/D's of 0.87 and 1.37 FD 97553

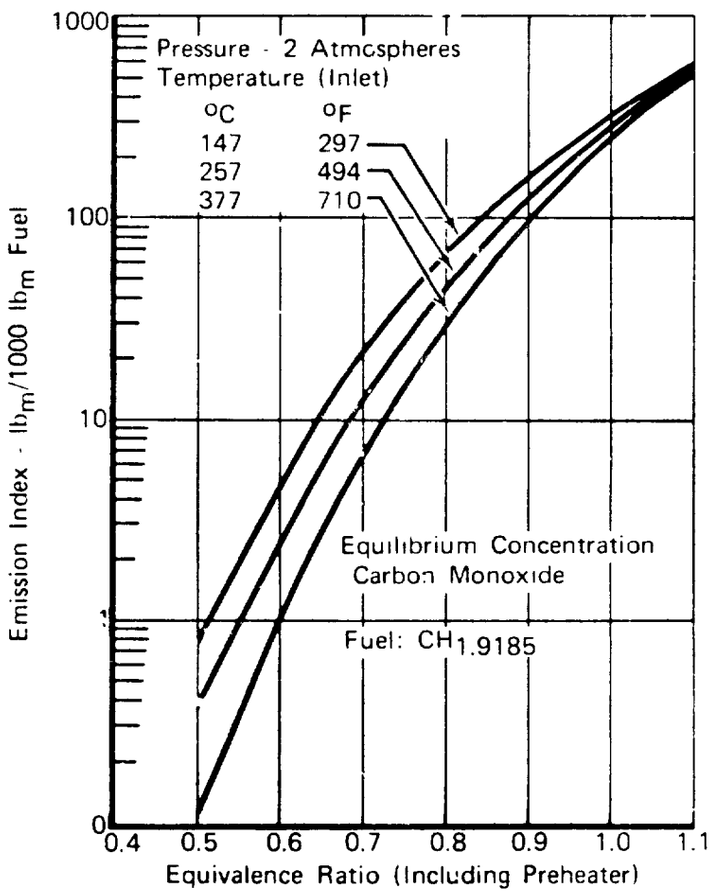

Figure 52. Equilibrium Concentration of Carbon Monoxide FD 97554

With an augmentor L/D of 1.37, the UHC emissions were extremely low at equivalence ratios above 0.4. However, the CO emissions were high. It is the high CO emissions that result in the observed inefficiencies. Quite likely a better fuel distribution than that obtained with the sprayrings used in this program would result in reduced levels of CO emissions. This is evidenced by the 39% decrease in CO emissions obtained at an equivalence ratio of 1.0 by using three fuel zones instead of two. Use of four fuel zones instead of three, for example, would yield a more uniform radial distribution of fuel than that obtained with the current sprayrings. This would result in more intimate mixing of the fuel and air, which would reduce the CO emissions.

The exhaust emissions obtained with the shorter duct (L/D = 0.87, figure 50) contained substantial amounts of UHC. A portion of this was obviously due to a very poor fuel distribution brought about by the use of zones 2 and 3 only. However, the UHC emissions obtained with the shorter duct using zone 2 only were higher than those obtained with the longer duct using zone 2 only. The emissions differ by a factor as high as 3.5 at an equivalence ratio of 0.3. There was evidently just not enough length to completely consume the UHC within the confines of the shorter duct. An improved fuel distribution would obviously improve the performance of the shorter duct, but it would probably still fall short of the performance achieved with the longer duct.

SUMMARY OF RESULTS

A test program was conducted in which the performance of a swirling flow augmentor using sprayrings designed on the basis of measured fuel dispersion data was evaluated. The tests were conducted at 649°C (1200°F) inlet air temperature. Significant test results are as follows:

1. At the inlet temperatures used, the swirling flowfield was found to have no effect on the radial movement of the fuel spray.

2. The circumferential movement of the fuel spray was found to be a simple helical motion, the helix angle of which was related to the swirl vane angle by ($\pi/2$ - swirl vane angle).

3. Combustion efficiencies of 95% were demonstrated over most of the operating range, which extended from an equivalence ratio of 0.2 to over 1.0. This result was obtained with an augmentor L/D of 1.37. Using an L/D of 0.87, the combustion efficiencies obtained were greater than 80% at all equivalence ratios.

4. The lean blowout of the pilot burner and, hence, the augmentor was found to occur at an overall augmentor fuel-air ratio of 0.0018.

5. The measured nonburning total pressure losses were greater than those of current conventional augmentors. However, test results from other programs show that these high losses were due to poor measurements of the inlet total pressure. The actual pressure losses were found to be equal to those of current conventional augmentors. Experience also indicates that with well-designed turning vanes, the nonburning pressure losses could be made lower than that of current conventional augmentors.

6. During the course of the program no combustion instabilities, either rumble or screech, were encountered at any of the test points investigated.

APPENDIX A
REVISED NOZZLE DISCHARGE COEFFICIENT CALIBRATION

In order to calculate combustion efficiency using the choked nozzle method, an accurate nozzle discharge coefficient, C_d, is required to determine the effective choked area. In swirling flow the discharge coefficient is a complex function of total pressure-to-ambient pressure ratio and the swirl intensity at the nozzle discharge plane. This necessitates a complete calibration throughout the range of pressure ratios and swirl parameters if accurate and reliable combustion efficiencies are to be calculated. For instance, a 4% error in C_d will result in a 8% error in exhaust temperature, which will result in a 12% error in combustion efficiency near an augmentor equivalence ratio of 1.0.

In previous swirl augmentor testing, two fixed area nozzles were used, one of 21.9-cm (8.62-inch) diameter and one of 27.2-cm (10.69 inch) diameter. A limited amount of calibration testing was performed on the 21.9-cm nozzle and the results provided discharge coefficient curves vs pressure ratio and nozzle tangential Mach number. The larger, 27.2-cm nozzle could not be calibrated as completely because of stand limitations on airflow and pressure. Only one calibration point was obtained at a pressure ratio of 2.1 and tangential Mach number of 0.255. This correlated exactly with the 21.9-cm nozzle at that point. The data also showed little effect of pressure ratio on the discharge coefficient. Therefore, for the 27.2-cm nozzle, the discharge coefficient used in the "choked nozzle" efficiency calculation was the same as that of the 21.9-cm nozzle at a pressure ratio of 2.1. The calibration curve is shown in figure 53. Two obvious errors result from using this calibration. First, pressure ratio effects are neglected, and second, the effect of contraction area ratio is neglected. The first error was neglected since pressure ratio variations were small during the testing. The second error was not obvious at the time but became obvious when reviewing recent in-house data on the effects of swirl on nozzle performance. That program was designed to assess the effect of pressure ratio, nozzle contraction ratio, and swirl intensity on the nozzle discharge coefficient.

All testing accomplished under the current contract used the 27.2-cm diameter nozzle. When the data were reduced using the old calibration curve, combustion efficiencies over 125% were calculated. Also, efficiency trends failed to correlate with gas sample efficiency trends. Upon analysis it became apparent that by correcting the discharge coefficient for pressure ratio, using the in-house data mentioned above, the efficiency trends correlated reasonably well with gas sample efficiency trends, but the level of combustion efficiency was still around 125%. One apparent difference from previous testing with the large nozzle that might effect the C_d was the insertion of four gas sample probes within 1/2-inch of the nozzle geometric discharge plane. As the effect of these probes was unknown, a new calibration was required if accurate efficiency calculations were to be made. Testing was complete at this time, and the calibration capability of the facility was very limited, so a review of the acquired data produced one calibration point at a pressure ratio of 1.5 and a nozzle tangential Mach number of 0.243. Using in-house data, a discharge coefficient for pressure ratios down to 1.5 was calculated. The nozzle contraction area and contraction angle used in the in-house data was matched to the 27.2-cm diameter nozzle used in this program. The revised nozzle discharge coefficient calibration is presented in figure 54. It can be seen that the one calibration point obtained under the current contract matches the revised calibration. Therefore, the revised calibration was used to reduce the data in this program.

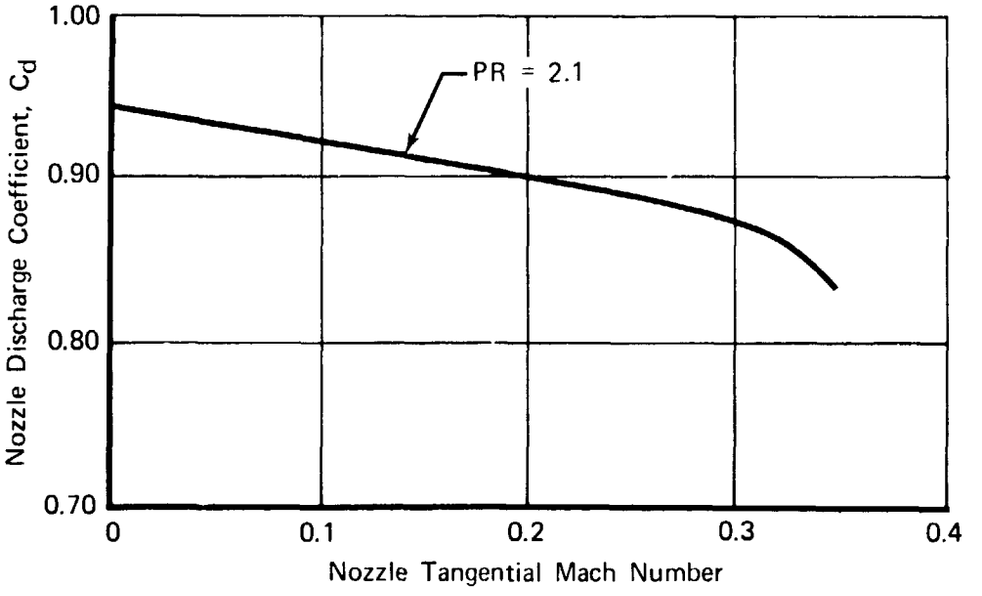

Figure 53. Initial Nozzle Discharge Coefficient Curve for 27.2-cm (10.60-in.) Diameter Exhaust Nozzle FD 95696

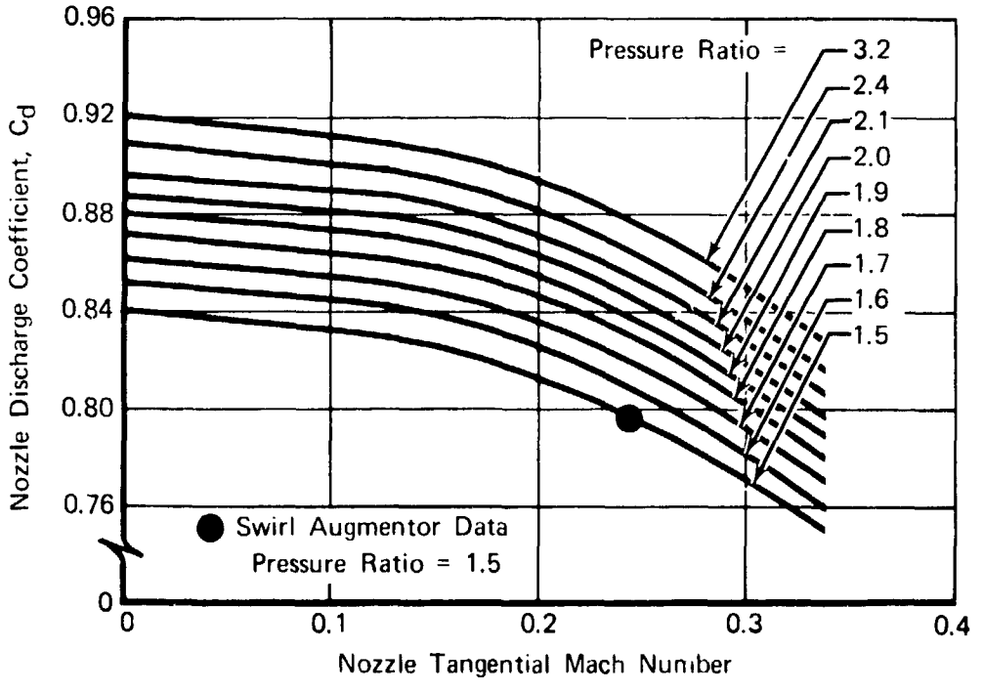

Figure 54. Revised Nozzle Discharge Coefficient Curve for 27.2-cm (10.69-in.) Diameter Exhaust Nozzle FD 95697

REFERENCES

1. Lewis, G. D., "Centrifugal Force Effects on Combustion," Proceedings of the XIVth Smposium on Combustion, Pennsylvania State University, 1972.

2. Clements, T. R., "Effect of Swirling Flow on Augmentor Performance," NASA CR-134639, 1974.

3. Lewis, G. D., and C. E. Smith, "Investigation of Centrifugal Force and Reynolds Number Effects on Combustion Processes," AFOSR-TR-75-1167, 1975.